Nanoparticles enhanced fibre-reinforced polymer composites used in marine environment

by

Wei Han

Thesis
Submitted to Flinders University
for the degree of

Doctor of Philosophy

College of Science and Engineering

28th June 2018

Table of Contents

Table of Contents 1

Abstract 1

Thesis declaration statement by author 3

Acknowledgments 4

Chapter 1: Introduction 5

1.1 Significance of the project 5

1.2 Research objectives 5

1.3 Thesis outline 6

1.4 logical arrangement of the subsequent research chapters diagram 7

1.5 References 7

Chapter 2: Literature review 10

2.1 Introduction 10

2.2 Carbon fibre-reinforced polymer laminates with nanofiller-enhanced multifunctionality 10

2.3 The marine environmental impact on the fibre reinforced polymers 13

Chapter 3: Nano-halloysite concentration effects on fracture toughness of diverse epoxy nanocomposites 20

3.1 Introduction and significance 20

3.2 Nano-halloysite concentration effects on fracture toughness of diverse epoxy nanocomposites 20

Chapter 4: Functionalised silica/epoxy nanocomposites with enhanced fracture toughness for large-scale applications 34

4.1 Introduction and significance 34

4.2 Functionalised silica/epoxy nanocomposites with enhanced fracture toughness for large-scale applications 34

Chapter 5: Fracture toughness and wear properties of nanosilica/epoxy composites under marine environment 44

5.1 Introduction and significance 44

5.2 Fracture toughness and wear properties of nanosilica/epoxy composites under marine environment 44

Chapter 6: Polydopamine as sizing on carbon fibre surfaces for enhancement of epoxy laminated composites 54

6.1 Introduction and significance 54

6.2 Polydopamine as sizing on carbon fibre surfaces for enhancement of epoxy laminated composites 54
Chapter 7: Synergistic effects of coupling agent and nanoparticle on enhancing glass fibre/ polystyrene laminates for harsh environment applications 62
7.1 Introduction and significance 62
7.2 Synergistic effects of coupling agent and nanoparticle on enhancing glass fibre/ polystyrene laminates for harsh environment applications 62
Chapter 8: Hybrid enhancements by polydopamine and nanosilica on carbon fibre reinforced polymer laminates under marine environment 108
8.1 Introduction and significance 108
8.2 Hybrid enhancements by polydopamine and nanosilica on carbon fibre reinforced polymer laminates under marine environment 108
Chapter 9: Conclusions and perspectives 116
9.1 Conclusions 116
9.2 Perspectives 117
Appendix: Publications during Ph.D 119
Refereed book chapter publication 119
Refereed journal publications 119
Refereed conference publications 120
Bibliography 121

Abstract

Fibre reinforced polymer (FRP) composites have been used in maritime engineering for more than 50 years, however, many facts such as aqueous corrosion, UV aging and tidal movements deteriorate the performance of composites and limit the applications under marine environment. Recently, the demands of more reliable, economy, environment friendly composites have prompted an industry-wide investigation of advanced materials. Nanotechnology is an advanced medium to improve the properties and expand the applications of composites. The benefits include enhancing mechanical behaviours: such as Young's modulus, toughness, impaction and fatigue, and enabling multifunctional behaviours: such as thermal conductivities, electrical conductivities and electromagnetic wave absorb. Therefore, using nanoparticles is a desirable technology to develop cost-effective, large-scale, and durable FRP composites. This thesis aims to use feasible methods by using nanoparticles (such as functionalised nanosilica, halloysite nanotubes, so-gel nanosilica) to reinforce FRP composites to extenuate harsh environment effects with the large scale manufacturing possibilities.

The first part of the thesis focuses on investigation concentration effects of nanoparticles (halloysite nanotubes, nanosilica) on the mechanical performance, especially on fracture toughness and processibility, particularly on viscosities of nanoparticle filled matrices. In addition, the toughen mechanisms of two kinds of functionalised nanosilica/ epoxy composites have been studied and revealed that nanosilica can reduce the corrosion rate and fraction coefficient under marine environment, thus providing a new pathway to improve the marine composite performance.

The second part of thesis reports that the bio-material, i.e. dopamine acting as a sizing and polymerising on carbon fibre surfaces to form polydopamine. The new method to reinforce the interlaminar shear strength of CFRP composites has been explored. Furthermore, combining coupling agent and halloysite nanotubes to develop synergistic effects on enhancing the mechanical properties of GFRP composite under simulated marine environment was studied.

The third part of thesis aims to design a new strategy to reinforce composites by two ways, i.e., using the so-gel nanosilica to reinforce the matrix and using polydopamine to enhance the interfaces of carbon fibres and matrix. Excellent performances have been achieved, especially under the simulated marine environment. The proposed enhancement mechanism has also been proposed.

In conclusion, this thesis tries to explore nanoparticle enhanced fibre reinforced composites used in marine environment, and aims to fabricate low-cost, large-scale and durable nanoparticle reinforced composites as an alternative choice for maritime engineering applications.

Thesis declaration statement by author

'I certify that this thesis does not incorporate without acknowledgment any material previously submitted for a degree or diploma in any university; and that to the best of my knowledge and belief it does not contain any material previously published or written by another person except where due reference is made in the text.

Name of Candidate:

Wei Han

Signature:

Date:

Acknowledgments

First and foremost, I would like to express my sincere gratitude to my principle supervisor – A/Prof. Youhong Tang for his valuable guidance, support and encouragement throughout my PhD study. His suggestions continuously motivate me in both scientific research and logical reasoning in my life. I also want to thank my co-supervisor: Prof. David Lewis and A/Prof. Karl Sammut who gave me lots support during my research.

Furthermore, I would like to express my deepest appreciation to my fiancée – Miss Qian Zhang who stays with me and encourages me during my PhD study. I also appreciate several collaborators help on training advanced material characterization techniques. They are Dr. Sheng Chen, Dr. Jingjing Duan and Prof. Shi Zhang Qiao from the University of Adelaide, Dr Yang Yu and A/Prof. Martin Johnston from Flinders University, A/Prof. Xiaojun Zhang from Beijing University of Technology, A/Prof. Liming Fang from South China University of Technology and Prof Lin Ye from the University of Sydney. My research has been greatly solidified by their efforts.

I want to extend my sincere thanks to all the group members from A/Prof. Tang's group in Flinders University for their technological assistance and useful discussion. They are Dr. Yang Yu, Mr Rengui Peng, Dr. Nazila Dehbari, A/Prof. Jinchao Zhao, A/Prof. Leping. Huang, Mr Ang Qiu, A/Prof. Xiaojun Zhang, Dr. Xiaoyuan Pei and A/Prof. Hongping Zhang.

Special thanks go to Mr Geoff Cottrell, Mr Richard Stanley, Mr Mark Walford, Mr Damian Kleiss, Mr Wes Penney and Mr Tim Hodge from engineering services of Flinders University. Dr. Christopher Gibson, Dr. Cameron Shearer, Mr Ashley Slattery from Australian Microscopy and Microanalysis Research Facility. Dr Jonathan Campbell from Materials Characterisation Facility of Flinders University, for their kindly training, technical supports and helps during the study.

I would also like to acknowledge the Flinders University Research Scholarship, which has financially supported my Ph. D research, and the Australian Nanotechnology Network, which gave travel and accommodation support for my conference and workshop.

Last but not least, I give my thankful and love to my parents and all my friends in China and Australia to help enjoy my Ph.D.

Chapter 1: Introduction

1.1 Significance of the project

The market of marine composite was worth 900 million US dollars in 2011 and expected reach to $ 1500 million US dollars in 2018, with a 7% annual growth rate [1]. The safety, recycling, new resin and fibre, and multi-functionality are the future trends of the marine composite [2]. However, the innate characters of FRPs such as brittleness of the matrix or poor adhesive between fibre and matrix, determined the limitations of composites applications. In addition, composites used in the marine environment have more challenges such as deteriorate performance by aqueous corrosion, degradation, moisture uptake, etc.[3-6] Meanwhile, the large-scale fabrication nanocomposites for industrial application, especially in maritime engineering fields is also a challenge [7- 18]. For these reasons, it is momentous but challenging to develop cost-effective, reliable and multifunctional marine composite as metal alternatives to promote the sustainable marine applications.

1.2 Research objectives

The major goals of this thesis are to explore and understand nanoparticle enhanced fibre reinforced polymer composites used in marine environment, and aim to develop low-cost, large-scale and durable nanoparticle reinforced composites as an alternative for the metal parts. Specifically, the objectives of this thesis are:

- ***Investigating*** commercial nanoparticles (halloysite nanotubes, nanosilica) concentration effects on mechanical and machinability of diverse epoxy nanocomposites;
- ***Understanding*** the role of functional groups toughen the interface between nanoparticles and epoxy by study two kinds of functionalised nanosilica/ epoxy composites;
- ***Revealing*** the salt water deteriorate mechanical properties of composite with time, the nanosilica effects on reducing the corrosion rate and friction coefficient of epoxy under marine environment, and thus providing a new pathway to improve the marine composite performances;

- ***Tuning*** dopamine as sizing by in situ polymerization on carbon fibre surface to enhance interfaces between fibre and matrix, providing a new convenient method to further toughing the FRPs composites;
- ***Combining*** matrix toughening by nanoparticles (such as halloysite nanotubes, nanosilica) and interface enhancing by introduction of polydopamine to develop synergistic effects on enhancing the mechanical performances of composites used in simulated marine environment.

1.3 Thesis outline

This thesis is the outcomes of my PhD research presented in the form of journal publications. The chapters in this thesis are presented in the following sequence:

- ***Chapter 1*** introduces the significance of the thesis and outlines the objectives and key contributions to the field of research;
- ***Chapter 2*** reviews the literatures to overview various nanofillers enhance mechanical and multifunctional behaviours of carbon fibre reinforce polymer (CFRP) composites;
- ***Chapter 3*** presents halloysite nanotube concentration effects on fracture toughness of diverse epoxy nanocomposites;
- ***Chapter 4*** investigates two kind of functionalised nanosilica/epoxy nanocomposites with enhanced fracture toughness;
- ***Chapter 5*** investigates fracture toughness and wear properties of nanosilica/epoxy composites under marine environment;
- ***Chapter 6*** develops polydopamine as sizing on carbon fibre surfaces for enhancement of epoxy laminated composites;
- ***Chapter 7*** designs and fabricates coupling agent and nano halloysite synergistic enhancing glass fibre/ polystyrene laminates under harsh environment applications;
- ***Chapter 8*** devotes to hybrid enhancement by polydopamine and nanosilica on carbon fibre reinforced polymer laminates under marine environment;
- ***Chapter 9*** presents conclusions and perspectives for future work;

1.4 Logical arrangement of the subsequent research chapters diagram

This section explains the logic structure of the thesis. First, the literature review gives a general idea of the nanoparticles used in the fibre reinforced polymer composites (FRPs) and the environmental impacts on the FRPs. Second, explains my research in details. Third, concludes my current study and prospects the further work. A diagram of overall flow and logical arrangement of the subsequent research chapters shown in Fig. 1.

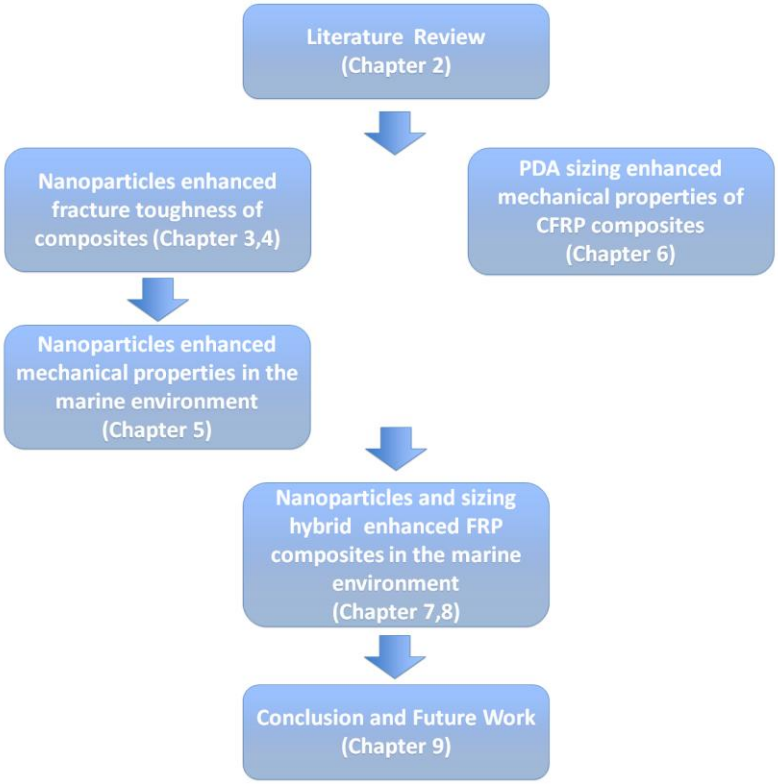

Fig. 1. Overall flow and logical arrangement of the subsequent research chapters

1.5 References

1. Neser G. Polymer based composites in marine use: history and future trends： 10th International Conference on Marine Technology. Procedia Engineering 2017; 194: 19 – 24.

2. Mouritz AP, Gellert E, Burchill P, Challis K. Review of advanced composite structures for naval ships and submarines. Compos Struct 2001; 53: 21-41.

3. Tang Y, Ye L, Deng S, Yang C, Yuan W. Influences of processing methods and chemical treatments on fracture toughness of halloysite-epoxy composites. Mater Des 2012; 42: 471-77.

4. Le Gac PY, Le Saux V, Paris M, Marco Y. Ageing mechanism and mechanical degradation behavior of polychloroprene rubber in a marine environment: Comparison of accelerated ageing and long term exposure. Polym Degrad Stabil 2012; 97: 288-96.

5. Deng SQ, Ye L, Friedrich K. Fracture behaviours of epoxy nanocomposites with nano-silica at low and elevated temperatures. J Mater Sci 2007; 42: 2766-74.

6. Hsieh TH, Kinloch AJ, Masania K, Taylor AC, Sprenger S. The mechanisms and mechanics of the toughening of epoxy polymers modified with silica nanoparticles. Polymer 2010; 51: 6284-94.

7. Sprenger S. Fiber-reinforced composites based on epoxy resins modified with elastomers and surface-modified silica nanoparticles. J Mater Sci 2014; 49: 2391-2402.

8. Tang Y, Ye L, Zhang Z, Friedrich K. Interlaminar fracture toughness and CAI strength of fibre-reinforced composites with nanoparticles-A review. Compos Sci Technol 2013; 86: 26-37.

9. Akbarinezhada E, Ebrahimib M, Sharifb F, Ghanbarzadeha A. Evaluating protection performance of zinc rich epoxy paints modified with polyaniline and polyaniline-clay nanocomposite. Prog Org Coat 2014; 77:1299-1308.

10. Shen Z, Simon GP, Cheng YB. Comparison of solution intercalation and melt intercalation of polymer–clay nanocomposites. Polymer 2002; 43: 4251-60.

11. Mouritz AP, Geliert E, Burchill P, Challis K. Review of advanced composite structure for naval ships and submarines. Compos Struct 2001; 53: 21-41.

12. Gellert EP, Turley DM. Seawater immersion ageing of glass-fibre reinforced polymer laminates for marine applications. Compos Part A 1999; 30: 1259-65.

13. Rahman IA, Padavettan V. Synthesis of silica nanoparticles by sol-gel: size-dependent properties, surface modification and applications in silica-polymer nanocomposites-a review. J Nano Mat 2012; 2012: 132424.

14. Han W, Yang Y, Fang L, Johnston MR, Qiao SZ, Tang Y. Functionalised silica/epoxy nanocomposites with enhanced fracture toughness for large-scale applications. J Compos Mater 2015; 49: 1439-47.

15. Qian H, Greenhalgh ES, Shaffer MSP, Bismarck A. Carbon nanotube-based hierarchical composites: a review. J Mater Chem 2010; 20: 4751-62.

16. Sprenger S. Epoxy resins modified with elastomers and surface-modified silica nanoparticles. Polymer 2013; 54: 4790-97.

17. Dalina W.A.D.W., Mariatti M., Ramlee R., Ishak Z.A.M., Mohamed A.R. Comparison on the properties of glass fiber/MWCNT/epoxy and carbon fiber/MWCNT/epoxy composites Adv Mater Res 2014; 858: 32-39.

18. Ma P.C., Siddiquia N.A., Maromb G., Kima J.K. Dispersion and functionalization of carbon nanotubes for polymer-based nanocomposites: a review. Compos Part A 2010; 41 (10): 1345-67.

Chapter 2: Literature review

2.1 Introduction

This chapter gives a concise appraisal on nanofillers enhanced fibre reinforced polymer (FRP) laminates, including mechanical properties, electrical conductivity, and thermomechanical properties. Especially, the mechanical properties have been reviewed in details in section 2.2, such as interlaminar fracture toughness, compression-after-impact strength and interlaminar shear strength toughed by different nanofillers, such as carbon nanotubes, nanofibers, organoclay, nanosilica and/or rubber, et al.

In addition, FRP laminates suffer environmental impacts when those parts are exposed to harsh environments for the period of service. Particularly in the marine environment, the mechanical performances of laminates degrade due to cyclic variation of temperature and hygrothermal conditions – creating the high risk of accidentally creating fracture. In section 2.3 reviews some current research carried on environmental impacts on FRP composites, such as thermal fatigue, moisture and hygrothermal impacts.

2.2 Carbon fibre-reinforced polymer laminates with nanofiller-enhanced multifunctionality

This section is included as it appears as a book chapter published by **Wei Han**, Youhong Tang, Lin Ye. Chapter 8: Carbon fiber-reinforced polymer laminates with nanofiller-enhanced multifunctionality. In: Beaumont PWR et al, editors. The structural integrity of carbon fibre composites. Switzerland: Springer, 2017, 171-189. It provides an overview of with various nano-fillers to (1) enhance mechanical behaviours the structural materials, including interlaminar strength and toughness, impaction, fatigue performances, and (2) enable/enhance multifunctional behaviours, including thermal conductivities, electrical conductivities, and other performances. Overall, this discussion gives a broad overview and technical viable routes to obtain a particular combination of various mechanical and functional behaviours of CFRP with nano-fillers included.

Carbon Fibre-Reinforced Polymer Laminates with Nanofiller-Enhanced Multifunctionality

Wei Han, Youhong Tang, and Lin Ye

8.1 Introduction

Fibre-reinforced polymers (FRPs) are prime choice materials in various structural and high-performance applications. Their unique properties make them superior to their metallic counterparts. A carbon fibre-reinforced polymer (CFRP) is a composite in which at least one of the fillers is carbon fibre, either short or continuous, unidirectional (UD) or multidirectional or woven or nonwoven. The matrix is usually a polymer, a metal, a ceramic or a combination of different materials. Except for sandwich composites, the matrix is three-dimensionally continuous, whereas carbon fibre (CF) fillers are usually three-dimensionally discontinuous, unless the fibres are three-dimensionally interconnected by weaving or by the use of a binder such as carbon. The high strength and modulus of CFs make them useful as reinforcement for various matrices, even though they are brittle. Effective reinforcement requires good bonding between the fibres and the matrix. Meanwhile, CFs are electrically and thermally conductive, in contrast to the non-conductive nature of polymer matrices. Therefore, CFs can serve not only as reinforcement but also as additives to enhance electrical and/or thermal conductivity. Furthermore, CFs have a near-zero coefficient of thermal expansion. The combination of high thermal conductivity and low thermal expansion makes CFRP useful for heat

W. Han • Y. Tang (✉)
Centre for NanoScale Science and Technology, Centre for Maritime Engineering, Control and Imaging, School of Computer Science, Engineering and Mathematics, Flinders University, Tonsley, SA 5042, Australia
e-mail: youhong.tang@flinders.edu.au

L. Ye (✉)
Centre for Advanced Materials Technology, School of Aerospace, Mechanical and Mechatronic Engineering, The University of Sydney, Sydney, NSW 2006, Australia
e-mail: lin.ye@sydney.edu.au

P.W.R. Beaumont et al. (eds.), *The Structural Integrity of Carbon Fiber Composites*,
DOI 10.1007/978-3-319-46120-5_8

Figure (text/chart/diagram etc) has been removed due to copyright restrictions.

2.3 The marine environmental impact on the fibre reinforced polymers

2.3.1 Introduction

The superior properties of FRPs such as excellent strength, lightweight, chemical resistance, and good mechanical performance supported they are widely used in many fields. Their applications include various components in automobiles, aerospace, navigation, offshore platforms and also in structures [1]. Those parts are exposed to the environment for the period of service. The environmental impacts include temperatures, humidity, and UV light exposure. Especially in the marine condition, the cyclic variation of hygrothermal environment may degrade the properties and performances of FRP composites – making the high possibility of accidentally generating fracture. Bastioli et al. reported water aging may strongly affect the matrix behaviour, by producing changes in its chemical and physical nature by itself or in conjunction with other chemical or physical agents such as heat and ultraviolet light [2, 3]. In additional, a hydrolysis reaction can degraded interface of the fibre/matrix caused by unsaturated groups within the matrix of FRP composites in the marine environment.

FRP laminated composites are vulnerable to suffer impact in the environment. The performances of the composites are determined by the adhesion strength of the interface between the fibre and matrix. However, in the high temperature condition the thermal expansion of matrix and fibre are different which can affect the interface in result of detriment interlaminar shear strength of the laminators. On the other hand, at low temperature most polymers become brittle and more vulnerable to the stress concentration or relaxation of residual stresses. Moisture is very common in our environment. However, the FRP laminated composites absorb moisture that can reduce the interfacial adhesion strength at the interface. Despite FRP composites having lots

of outstanding performance as structures and components, they still need reinforcement to against the harsh environment.

This review highlights the environmental impact on the FRP laminated composites. Discussed the deleterious effects on the matrix and the interfacial strength of fibre and matrix caused the different environmental conditions. Reveal the degradation in the interface between fibre and matrix may occur to a significant variation in the property and performance of FRPs.

2.3.2 Thermal fatigue impact on the FRP composites

FRP laminated composites suffer temperature variations. This kind cyclic variation of temperature induces thermal stresses in composites because of the different thermal expansion coefficients between the fibres and resins [4]. This kind of reciprocating stress variation in the composites is considered as a fatigue and which can induce various types of damage, like matrix fracture, debonding and delamination. Moreover, Hiemstra observed micro-cracks at the interface between fibre and polymer due to the temperature variations [4]. In an oxidative environment, the temperature variations may cause resins oxidation. Some researches on found that the oxidation in epoxy resin can cause mass loss and volume shrink of the epoxy resin, which may result of composites delamination [5–6].

2.3.3 Exposure to moisture impact on FRP composites

When FRPs laminated composites exposure in the wet environment, the moisture can be absorbed into the composites. The moisture diffusion observes in the composites as a result of capillary action reported by Scheirs. In the study, water wicking is principal in the composites as defective wetting of the fibre [7]. Other researches on moisture transport behaviour report that voids in the matrix and the interface of fibre-matrix have a significant effect on the diffusivity of

FRPs laminated composites [8, 9]. Moreover, moisture can cause matrix plasticization, chemical degradation and mechanical degradation when moisture long time situated in a FRP laminated composite [10]. Weitsman and Morii report water diffusion may in form of interfacial micro-cracks in FRP composites [11, 12]. Furthermore, the moisture exposure time also significantly affects the performance of the FRP composites. For example, uncoated fibre/polylactide composites in saturated water vapour condition at 70 ℃ for 24 h, the tensile strength decreases 15 % compared with that without ageing specimens. And in the same condition after 72 h, it decreases 30% compared with that without ageing specimens [13]. Long-term moisture immersion can cause the detrimental effects of mechanical performances of the composites which can potentially decrease the service period [14–17]. Phifer et al. study E-glass/vinyl ester lamented composites, the reduction of stiffness and strength are 10 % and 60 % after 24 months immersed in water, respectively [15]. Yang et al. reported glass fibre modified by coating nano-silica can be slow the moisture uptake and enhanced the mechanical performances of GF/pCBT composites [18].

2.3.4 Hygrothermal impact on FRP composites

Hygrothermal ageing is most common conditions in the marine environment, and it is the synergetic effects in the temperature and moisture environment which has the deleterious effects on the polymer [19]. Moreover, Ray et al. reported that temperature can further accelerate the diffusion of moisture in FRPs [20]. Some researchers have studied the FRP composites in a hygrothermal environment [21–24]. For example, Aditya et al. studied the symmetric and antisymmetric GFRP laminates in hygrothermal condition, and they reported reduction rates in flexural stiffness were 54% and 27% respectively in the condition of a saturation humid condition for 2000 h [25]. A study of unidirectional glass fibre/epoxy composite degraded by

humidity absorption / desorption is shown by [26], reduction rates of the static bearing strength were at a range of 8% to 22% for woven laminates. Li et al. studied three kinds of sizing on carbon fibre (T300, CF-1, CF-2), the interfacial fracture engineer decreased after 3days hygrothermal treated by 45%, 69% and 40%, respectively. They said the sizing play an important role in the mechanical performances of CFRP composites in the hygrothermal conditions [27]. Buehler et al. studied moisture sorption and desorption on solvent treated glass fibre and carbon fibre reinforced composite laminates. The final moisture uptake rate was 4–5 wt % at 70 ℃ for 1200 h moisture exposure and the moisture uptake rates was 3 wt% after 450 h dry out [28]. The moisture in composites can degrade the interfacial adhesion and the matrix in that way detriment the properties and performances.

2.3.4 Conclusions

Applications of FRP laminated composites have developed rapidly during the last few decades. A rising concern on the environmental impact affects the bonded and durable interfaces of FRPs. The delamination has been known as the most harmful phenomenon on the mechanical performances of FRPs. The marine environments, such as cyclic variation of temperature and hygrothermal, are having detrimental effects on fibre-matrix interface of FRPs. The nano technology and sizing techniques are efficiently methods to reduce the detrimental effects by the harsh environment. However, currently little research has been carried out to study the hybrid enhancement of FRP in harsh environments by nanoparticles and sizing. This present review highlights the interfacial vulnerability to environmental impacts and the damaging effects on interfaces between fibre and matrix. The micro degradation at the interface between fibre and matrix may occur to a significant variation in the property and performance of FRPs.

Reference

[1] Hollaway LC. A review of the present and future utilization of FRP composites in the civil infrastructure with reinforce to their important in-service properties. Constr Build Mater 2010; 24:2419-2445.

[2] Bastioli C, Casciola M and Romano G. Role of the interface in composite materials during water ageing. In: Proceedings of the third international conference on composite interfaces, Cleveland, OH, 21–24 May 1990, pp. 569–581.

[3] Blaga A. Water sorption characteristics of GRP composite: effect of outdoor weathering. Polym Compos 1981; 2(1): 13–17.

[4] Hiemstra DL, Sottos NR. Thermally induced interfacial micro-cracking in polymer matrix composites. J Compos Mater 1993; 27:1030-1051.

[5] Lafarie-Frenot MC and Rouquie S. Influence of oxidative environments on damage in c/epoxy laminates subjected to thermal cycling. Compos Sci Technol 2004; 64:1725-1735.

[6] Madhukar MS, Bowles K, Papadopoulos DS. Thermo-oxidative stability and fiber surface modification effects on the inplane shear properties of graphite/PMR-15 composites. J Compos Mater 1997; 31: 596-618.

[7] Scheirs J. Compositional and failure analysis of polymers — a practical approach. New York: Wiley; 2000.

[8] Miettinen VM, Narva KK, Vallittu PK. Water sorption, solubility and effect of post-curing of glass fibre reinforced polymers. Biomaterials 1999; 20:1187-1194.

[9] Woo M, Piggott MR. Water absorption of resins and composites: IV. Water transport in fiber reinforced plastics. J Compos Technol Res 1988; 10:20-24.

[10] Shen C-H, Springer GS. Environmental effects in the elastic moduli of *composite* materials. J Compos Mater 1977; 11: 250-264.

[11] Weitsman YJ, Guo Y-J. A correlation between fluid-induced damage and anomalous fluid sorption in polymeric composites. Compos Sci Technol 2002; 62: 889-908.

[12] Morii T, Ikuta N, Kiyosumi K, Hamada H. Weight-change analysis of the interphase in hygrothermally aged FRP: Consideration of debonding. Compos Sci Technol 1997; 57: 985-990.

[13] Hu RH, Sun MY, Lim JK. Moisture absorption, tensile strength and microstructure evolution of short jute fiber/polylactide composite in hygrothermal environment. Mater Des 2010; 31: 3167-3173.

[14] Roy S, Xu WX, Park SJ, Liechti KM. Anomalous Moisture Diffusion in Viscoelastic Polymers: Modeling and Testing. J Appl Mech 2000; 67: 391-396.

[15] Phifer SP. Hygrothermal evaluation of pultruded polymer composite laminates — experimentation, analysis, and prediction. Blacksburg: VA: Virginia Tech; 2003.

[16] Doxsee LE, Janssens W, Verpoest I, Demeester P. Strength of Aramid-Epoxy Composites during Moisture Absorption. J Reinf Plast Compos 1991; 10: 645-655.

[17] Shen CH, Springer GS. Moisture absorption and desorption of composite materials, environmental effects on composite materials. Westport, CT: Technomic Publishing Company; 1981.

[18]. Yang B, Zhang J, Zhou L, Lu M, et al. Effect of fiber surface modification on water absorption and hydrothermal aging behavious of GF/pCBT composites. Compos B 2015; 82: 84-91.

[19] Davies P, Mazeas F, Casari P. Sea Water Aging of Glass Reinforced Composites: Shear Behaviour and Damage Modelling, J Compos Mater 2001; 35: 1343-1372.

[20] Ray BC. Temperature effect during humid ageing on interfaces of glass and carbon fibers reinforced epoxy composites. J Colloid Interface Sci 2006; 298: 111-117.

[21] Pauchard V, Grosjean F, Campion-Boulharts H, Chateauminois A. Application of a stress-corrosion-cracking model to an analysis of the durability of glass/epoxy composites in wet environments. Compos Sci Technol 2002; 62: 493-498.

[22] Whitaker G, Darby MI, Wostenholm GH, Yates B, Collins MH, et al. Influence of temperature and hydrostatic pressure on moisture absorption in polymer resins. Mater Sci 1991; 26:49-55.

[23] Neumann S, Marom G. Prediction of Moisture Diffusion Parameters in Composite Materials Under Stress. J Compos Mater 1987; 21:68-80.

[24] Wan YZ, WangYL HuangY, He BM, Han KY. Hygrothermal aging behaviour of VARTMed three-dimensional braided carbon-epoxy composites under external stresses. Compos A 2005; 36:1102-1109.

[25] Aditya PK, Sinha PK. Diffusion Coefficients of Polymeric Composites Subjected to Periodic Hygrothermal Exposure. J Reinf Plast Compos 1992; 11: 1035-1047.

[26] Chateauminois A, Vincent L, Chabert B, Soulier JP. Study of the interfacial degradation of a glass-epoxy composite during hygrothermal ageing using water diffusion measurements and dynamic mechanical thermal analysis. Polymer 1994; 35: 4766-4774.

[27] M. Li, H. Liu, Y. Gu, Y. Li and Z. Zhang, Effects of carbon fiber surface characteristics on interfacial bonding ofepoxy resin composite subjected to hygrothermal treatments. Appl Surf Sci 2014; 288: 666-672.

[28] Buehler FU, Seferis JC. Effect of reinforcement and solvent content on moisture absorption in epoxy composite materials. Compos A 2000; 31: 741-748.

Chapter 3: Nano-halloysite concentration effects on fracture toughness of diverse epoxy nanocomposites

3.1 Introduction and significance

In this chapter, we reported the concentration effects of halloysite nanotubes (HNTs) on thermal and mechanical properties of as-received and phenylphosphonic-acid (PPA)-treated HNTs prepared by mechanical mixing or ball-milling homogenization. It was found that with HNTs added in the region of 0.0–10.0 wt. %, significantly reinforced fracture toughness of the epoxy composites. The highlights in this work include:

1. We have firstly reported that ball-milling homogenization has much more uniform HNTs size and dispersion in epoxy matrix than those prepared by simple mechanical mixing.

2. We have the first time investigated the morphology of (PPA)-treated HNTs changing from nanotubes to nanoplatelets; as a result, with a substantial increase in the total contact areas between HNTs and epoxy, enhanced fracture toughness of epoxy composites has been reported.

3. Higher HNTs concentration, higher fracture toughness was achieved for various epoxy composites. However, the optimal concentration of HNTs was 5.0 wt. % in this study. The addition of further HNTs achieved only marginal fracture toughness enhancement and more negative effects appear, such as HNTs concentration gradient in cured epoxy composites, high potential decrease in glass transition temperature (Tg), and potential immature tensile failure.

This section is included as it appears as a journal paper published by Wei Han, Yang Yu, Youhong Tang, Karl Sammut. Nano-halloysite concentration effects on fracture toughness of diverse epoxy nanocomposites, ASTM Mater Performance Charact 2014, 3(3): 506-518.

3.2 Nano-halloysite concentration effects on fracture toughness of diverse epoxy nanocomposites

Materials Performance and Characterization

doi:10.1520/MPC20130032 / Vol. 3 / No. 3 / 2014 / available online at www.astm.org

Wei Han,[1] Yang Yu,[2] Youhong Tang,[3] and Karl Sammut[4]

Nano-Halloysite Concentration Effects on Fracture Toughness of Diverse Epoxy Nanocomposites

Manuscript received August 23, 2013; accepted for publication November 25, 2013; published online January 17, 2014.

[1] Centre for Nanoscale Science and Technology; and Centre for Maritime Engineering, Control and Imaging, School of Computer Science, Engineering and Mathematics, Flinders Univ.South Australia 5042, Australia.

[2] Centre for Nanoscale Science and Technology, School of Computer Science, Engineering and Mathematics; and Centre for Nanoscale Science and Technology, School of Chemical and Physical Sciences, Flinders Univ., South Australia 5042, Australia.

[3] Centre for Nanoscale Science and Technology; and Centre for Maritime Engineering, Control and Imaging, School of Computer Science, Engineering and Mathematics, Flinders Univ.South Australia 5042, Australia (Corresponding author), e-mail: youhong.tang@flinders.edu.au

[4] Centre for Maritime Engineering, Control and Imaging, School of Computer Science, Engineering and Mathematics, Flinders Univ., South Australia 5042, Australia

[5] This paper is a contribution to a Special Issue of *Materials Performance and Characterization* on "Fracture Toughness," Guest Editors, Bojan Podgornik and Votjeh Leskovsek, Institute of Metals and Technology, Ljubljana, Slovenia.

Reference

Han, Wei, Yu, Yang, Tang, Youhong, and Sammut, Karl, "Nano-Halloysite Concentration Effects on Fracture Toughness of Diverse Epoxy Nanocomposites," *Materials Performance and Characterization*, Vol. 3, No. 3, 2014, pp. 506–518, doi:10.1520/MPC20130032. ISSN 2165-3992[5]

ABSTRACT

We experimentally report material design of halloysite nanotube (HNT)/epoxy composites, focusing on the effects of HNT concentration on thermal and mechanical properties, especially fracture toughness, of diverse epoxy composites with as-received and phenylphosphonic-acid (PPA)-treated HNTs prepared by mechanical mixing or ball-milling homogenization. It is demonstrated that, with HNT added in the region of 0.0–10.0 wt. %, significantly reinforced fracture toughness of the epoxy composites can be achieved. The epoxy composites prepared by ball-milling homogenization have much more uniform HNT size and dispersion than those prepared by simple mechanical mixing, enhancing their fracture toughness. The morphology of treated HNTs changes from nanotubes to nanoplatelets; as a result, with a substantial increase in the total contact area between HNT and epoxy and enhancing the fracture toughness of epoxy composites. This higher HNT concentration and the higher fracture toughness are achieved for various epoxy composites. However, the optimal concentration of HNT is 5.0 wt. % in this study. The addition of further HNT achieves only marginal fracture toughness enhancement and more negative effects appear, such as HNT concentration gradient in cured epoxy composites, high potential decrease in glass transition temperature (T_g), and potential immature tensile failure.

Keywords
halloysite, epoxy, fracture toughness, concentration, nanocomposites

Introduction

Organic/inorganic composites are widely used to overcome the limitations of organic polymer properties. In particular, because of the nature of the thermoset cross-link structure, the nature of the bonding, and the embrittlement compared to thermoplastics, the applications of thermosets/inorganic nanoparticles composites have gradually increased. Because of their favorable mechanical properties, low cost, low density, and ease of processing, they are used in different industrial sectors, such as marine construction, offshore applications, coatings, adhesives, casting, potting, composites, laminates, encapsulation of semiconductor devices, etc. [1,2].

Among organic/inorganic composites, a focus of much current research interest is the halloysite nanotube/epoxy (HNT/EP) system [3–9]. HNT is a naturally occurring aluminosilicate, $Al_2Si_2O_5(OH)_4 \cdot 2H_2O$, which varies mainly in its crystal morphology. The most common form of HNT is an elongated hollow tubular structure with a large aspect ratio, similar to that of carbon nanotubes (CNTs) [10]. Recently, HNT particles have been investigated as an alternative type of additive for polymers because they are more easily obtainable and cheaper than other nanoparticles such as CNTs [3–9]. Moreover, because of their similarity to other layered clay minerals such as montmorillonite (MMT) [11], HNTs have the potential to be further intercalated or exfoliated chemically or physically [12].

Preliminary results have demonstrated that blending epoxies with a certain amount of HNT can noticeably increase their fracture toughness, strength, and modulus, without sacrificing their thermal and mechanical properties such as glass transition temperature (T_g) [3–9]. Recently, we reported that phenylphosphonic acid (PPA) was successfully used to unfold and intercalate HNT, resulting in an increase of basal spacing, accompanied by the morphological change of most particles from nanotubes to nanoplatelets [6,7]. It was found that better dispersion in the epoxy was achieved using the unfolded and intercalated HNT than using as-received HNT (AR HNT). There was a significant increase in fracture toughness of epoxy composites with 10 wt. % PPA-treated HNT ("treated HNT") particles, without sacrificing other properties. The fracture toughness of the HNT/EP composites was markedly increased with an increase in the intercalation levels. We also reported that the ball mill homogenization method was effective in achieving homogeneous mixtures of 10 wt. % HNT with epoxies [5,6]. Large-sized particle clusters that occur during the mechanical mixing process can be significantly decreased by the ball-milling method.

A few research groups have briefly reported mechanical behaviors with different concentrations of AR HNT. Ye et al. [3] reported that the highest impact strength was achieved by using 2.3 wt. % AR HNT in epoxy by direct mixing, compared with 0.0 wt. %, 0.8 wt. %, and 1.6 wt. % HNT in epoxy matrix. We also reported 0.0 wt. %, 5.0 wt. %, 10 wt. %, and 20 wt. % AR HNT/EP composites, and the highest critical stress intensity factor (K_{IC}) was achieved with 10 wt. % HNT in epoxy.

Following the above studies, we investigated the effects of HNT nanofiller concentration, especially treated HNT, on the properties of epoxy composites. Composites of epoxies with different concentrations of AR or treated HNT particles were prepared by either mechanical mixing or ball milling. The effects of concentration on mechanical behaviors and thermal properties of the composites are reported here, with further investigation of the optimal HNT concentration for enhanced thermal and mechanical properties of the epoxy, especially the fracture toughness of the composites.

Experimental Details

MATERIALS

The halloysite particles used in this study were purchased from Sigma-Aldrich, Australia. The chemical treatment of the HNT particles by PPA (analytical grade, Sigma-Aldrich, Australia) has been reported by us previously [6]. The AR HNT particles are geometrically similar to multi-walled CNTs with a length of 100–2000 nm and a diameter of 50–150 nm. After treatment, the HNT morphology changes from nanotubes to nanoplatelets form.

The AR and treated HNT particles were separately combined with a diglycidyl ether of bisphenol A (DGEBA) epoxy resin, Araldite-F (Ciba-Geigy, Australia) to form composites. Both the AR and the treated HNT particles with concentrations of 2–10 wt. % were separately added into the epoxy resin by means of mechanical mixing or ball milling. With mechanical mixing, the mixture was stirred at 100°C on a hotplate stirrer (IKA C-Mag HS7) for 5 h to obtain a homogeneous mixture. With ball-milling homogenization, a planetary ball mill, Pulverisette 5 (Fritsch, Germany), was used to mix AR or treated HNTs with epoxies to obtain a homogeneous mixture [5–7]. The mixtures were then degassed in a vacuum oven (about 100 kPa) for at least 30 min. After that, a hardener, piperidine (Sigma-Aldrich, Australia), was added to the mixtures in a ratio of 100:5 by weight, while stirring slowly. Following further degassing for 10 min, the vacuum was released and the liquid mixtures were cast into specimen cavities of preheated silicon rubber molds and cured at 120°C for 16 h. For the designated mechanical tests, rubber molds were prepared to produce tensile test and compact tension (CT) specimens. When the specimens had been cooled and removed from the molds, they were milled using a surface grinder on both top and bottom surfaces to ensure flatness of specimens and, most importantly, to remove possible oversized halloysite particle aggregates, which could sink to the bottom surfaces during curing, as reported previously [4].

CHARACTERIZATION

A universal material testing machine (Instron, Mode 5567) was used for all mechanical property tests. All mechanical tests were conducted at room temperature. Tensile tests were conducted to measure the basic material properties of the cured neat epoxy and diverse HNT/EP composites. Tensile specimens had a dog-bone shape as required by ASTM D638 [13], with a constant cross section of 13 mm × 5 mm at the gauge length region. An extensometer with a gauge length of 50 mm was attached to the surface of the tensile specimen to determine the axial strain. A loading rate of

1 mm/min was selected for all tensile tests. At least five specimens were successfully tested for each group.

The fracture toughness of the cured neat epoxy and diverse HNT/EP composites was measured using CT specimens according to ASTM D5045 [14]. A CT specimen has a nominal dimension of 48 mm × 48 mm × 10 mm. To minimize the effects of residual stress and residual plastic deformation around the pre-crack tip, a sharp pre-crack was introduced to each CT specimen by inserting a fresh razor blade at the tip of the machined crack and tapping gently with a light hammer [15]. A loading rate of 2 mm/min was adopted for all fracture tests, as recommended by ASTM D5045. As there are strict requirements for specimen geometry and crack length for the accurate measurement of fracture toughness using CT tests according to the ASTM criteria, only those specimens that fulfilled the condition $a/W = 0.45–0.55$ (a is the pre-crack length and W is the distance from the center of the loading pin to the edge of the CT specimen) were used to calculate the K_{1C}. At least eight CT specimens were successfully tested for each group of materials.

The glass transition temperature (T_g) of the cured neat epoxy and the HNT/EP composites were determined by a dynamic mechanical analyzer (DMA 2980, TA Instruments, New Castle, DE) with temperature scanning from ambient temperature to 150°C at a heating rate of 3°C/min. A three-point bending fixture was used for the DMA measurements. A displacement amplitude of 10 μm was alternately applied with a frequency of 1 Hz for all DMA measurements. At least three specimens were tested for each group. The average value of T_g determined from the peak of the tan δ versus temperature curves was obtained.

A scanning electron microscope (SEM) (Philips XL30 SEM, the Netherlands and Zeiss ULTRA Plus Field Emission SEM, Germany) was utilized to identify the homogeneity of HNT particles in the epoxy nanocomposites and fracture surfaces of the CT fracture specimens.

Thermal stability analysis was performed using a Hi-Res TGA 2950 thermogravimetric analysis apparatus (TA instruments, New Castle, DE). The tests were carried out in air with a heating rate of 20.0°C/min from 50.0°C to 600.0°C, followed by isotherm for 15 min at 600.0°C before cooling.

Results and Discussion

TENSILE PROPERTIES

The tensile properties of the HNT/EP composites with a concentration of 0.0 wt. %, 2.0 wt. %, 5.0 wt. %, and 10.0 wt. % HNT are shown in **Figs. 1(*a*)** and **1(*b*)**. **Figure 1(*a*)** shows that the measured modulus increased with the HNT content. For example, the tensile modulus of 2.9 GPa was obtained for the neat epoxy. This increased to 3.1 wt. % GPa with 2 wt. % HNT and continued increasing to 3.3 GPa with 5 wt. % HNT, which was almost 14 % higher than the value measured of the neat epoxy. A marginal increase to 3.4 GPa was obtained for the epoxy with 10.0 wt. % of HNT for the treated HNT/EP composite prepared by ball mill homogenization.

In general, the tensile properties of the epoxies modified with HNT particles did not change greatly. The tensile strength of pure epoxy is 62 MPa. It increased only slightly (<5 %) with the HNT loading of 2 wt. %. However, after further addition of HNT, all the tensile strengths reduced marginally, as shown in **Fig. 1(*b*)**. In the cured

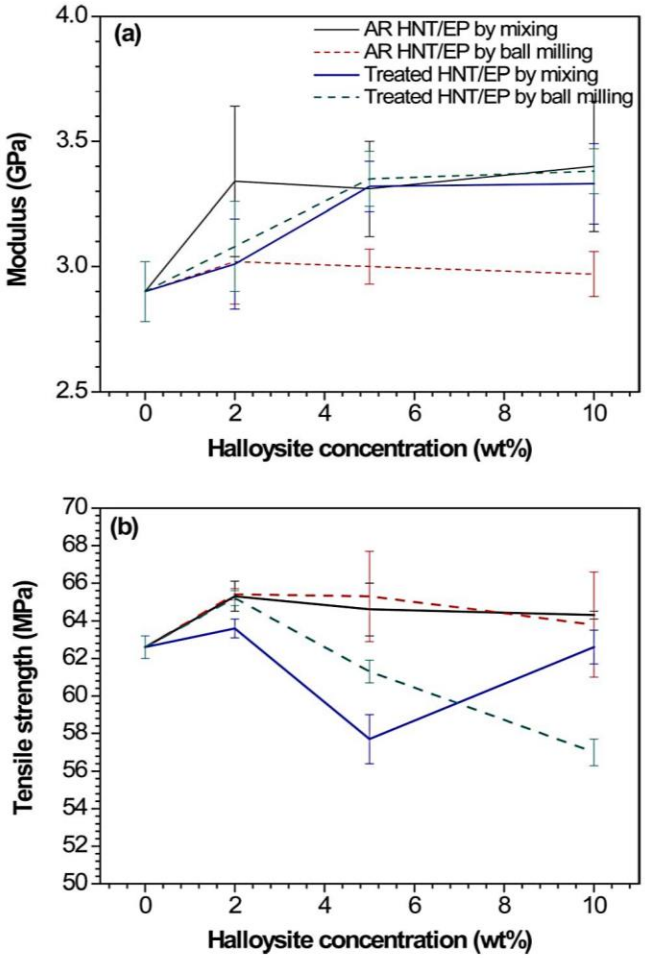

FIG. 1
Tensile modulus (a), and tensile strength (b) of HNT/EP composites with different concentrations of HNT.

neat epoxy, failure of the tensile specimen began from a defect on the specimen surface or inside the specimen, and the specimen underwent substantial permanent deformation before final failure. However, for the HNT/epoxy composites, the stresses at which cracks began to grow were obviously higher because of the strengthening effect of HNTs, although the cracks also initiated from defects somewhere on the specimen surface or within the specimen. With an increased concentration of HNT, micro-sized aggregates were unavoidable even with ball mill homogenization, and those aggregates acted as potential defects for tensile failure. A similar phenomenon has been reported previously by us [5], where premature brittle failure occurred in all specimens because of the presence of massive particle clusters for 20.0 wt.% AR HNT/EP composites.

GLASS TRANSITION TEMPERATURE

The glass transition temperatures of the neat epoxy and HNT/EP composite samples were defined from the tan δ peaks in DMA results and the average values are also

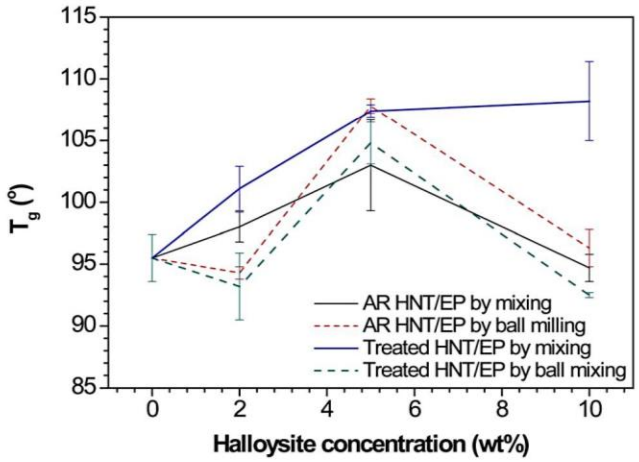

FIG. 2
Glass transition temperature (T_g) of HNT/EP composites with different HNT concentrations.

shown in **Fig. 2**. It has been reported that in the sulfonated PS/alumina composite system, the addition of rigid fillers in matrix made it difficult to move the polymer chain and therefore damping decreased and the T_g was shifted higher [16]. In **Fig. 2**, the T_g gradually increased until the HNT concentration reached 5 wt. %. But further introduction of HNT into this cross-link resin exhibited a clear decrease in T_g, which could be a result of severe aggregation of the fillers. The average value of cross-link density υ_e of pure epoxy was introduced using the formula [17] $\upsilon_e = G'/RT$, where G' is the shear storage modulus of an epoxy system above the glass-transition temperature, R is a universal gas constant (8.314472 J/K mol), and T is the absolute temperature in which the experimental modulus was determined. The cross-link density of pure epoxy cured by piperidine hardener is $(5.27 \pm 0.54) \times 10^{-3}$ mol/cm^3.

FRACTURE TOUGHNESS

Figure 3 shows the K_{IC} of diverse HNT/EP composites. Generally, the K_{IC} of the modified epoxies improved significantly after HNT particles were incorporated [3–9]. With the same HNT concentration and morphology, the composites prepared by ball-milling homogenization had higher K_{IC} values than those prepared by direct mechanical mixing [7]. With the same HNT concentration and fabrication method, the composites with treated HNT had much higher K_{IC} values than those with AR HNT [6].

The improvements in fracture toughness of the AR HNT/EP composites can be attributed to mechanisms such as the ability of HNT particle clusters to interact with a crack, bridging the crack as it passes through, resisting the advance of the crack or several broken HNTs with obvious separations from the matrix (debonding), or pull-out of HNTs from the matrix and hallows left in the matrix thus resulting in an increase in fracture toughness [3–5]. The improvements in fracture toughness of the treated HNT/EP composite can be attributed to further improved dispersion because of the changed morphology. The fracture toughness mechanisms are different from those of the AR HNT/EP composites but similar to intercalated or exfoliated organoclay in epoxy matrices, which promote the formation of a large

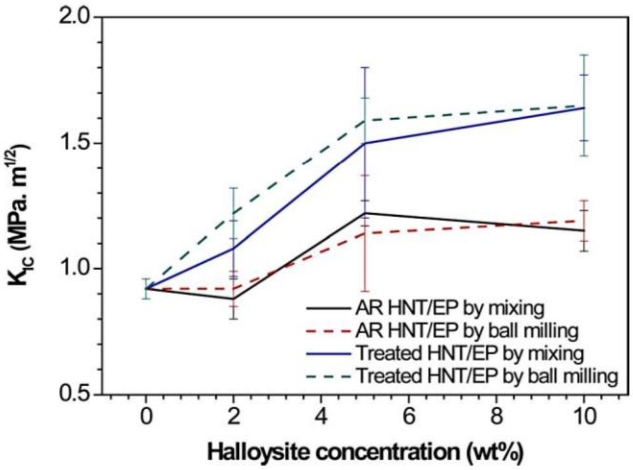

FIG. 3
Plane-strain fracture toughness of different HNT/EP nanocomposites with different concentrations.

number of microcracks and fracture energy absorptions in the intercalated HNT/EP interfaces, resulting in a further enhancement of fracture toughness [6,7].

With an increase in HNT content, the K_{IC} values of HNT/EP composites also increased but the increment was not linear and did not fit the rule of mixtures well. Specifically, when a small amount of HNT (2.0 wt. %) was added into the epoxies, the performance differed with regard to K_{IC} values. AR HNT/EP composites showed no increment in K_{IC}, even a slight decrease in the composite prepared by direct mixing. However, the treated HNT/EP composites had much higher fracture toughness values, with 17.4 % and 32.6 % increments for composites prepared by mixing and ball milling, respectively. **Figure 4** shows SEM micrographs of the fracture surfaces of CT specimens of 2.0 wt. % HNT/EP composites with different HNTs and preparation methods. From **Fig. 4**, it can be seen that even with the same amount of HNT added into the epoxy, the fracture surfaces of the CT specimens were different. There were mainly isolated particle clusters of relatively large size, up to 10 μm, in the composite with AR HNT prepared by simple mechanical mixing, which may be the reason for the marginally decreasing K_{IC} values, as shown in **Fig. 3**. After ball milling, the HNT aggregate size was much smaller, as shown in **Fig. 4(*f*)**. The fracture surfaces of the composites with treated HNT were much rougher than those of the AR HNT/EP composites. Meanwhile, there was a substantial increase in the total contact area between HNT and epoxy, as a result of which the morphology changed from nanotubes to nanoplatelets with almost double the surface area (specific surface area of 21.22 m^2/g and 41.13 m^2/g for AR and treated HNTs) [6]. In addition, the treated HNT nanoparticles achieved an improved dispersion in the epoxy matrix with ball milling, resulting in further improvement in fracture toughness.

When 5.0 wt. % HNT particles were added into the epoxy matrix, significant enhancement of epoxy fracture toughness was achieved, with 32.6 %, 23.9 %, 63.0 %, and 72.8 % increments, respectively, for AR HNT/EP prepared by mixing, ball milling, and for treated HNT/EP prepared by mixing and ball milling, as shown in **Fig. 3**. Compared with the fracture toughness values for composites containing 2.0 wt. % HNT, the increment in K_{IC} values was nonlinear and much higher for

FIG. 4

SEM micrographs of fracture surfaces of CT specimens of (a,b) pure epoxy, and (c–j) 2.0 wt. % HNT/EP composites, where (c,d) AR HNT/EP prepared by mixing, (e,f) AR HNT/EP prepared by ball milling, (g,h) treated HNT/EP prepared by mixing, and (i,j) treated HNT/EP prepared by ball milling.

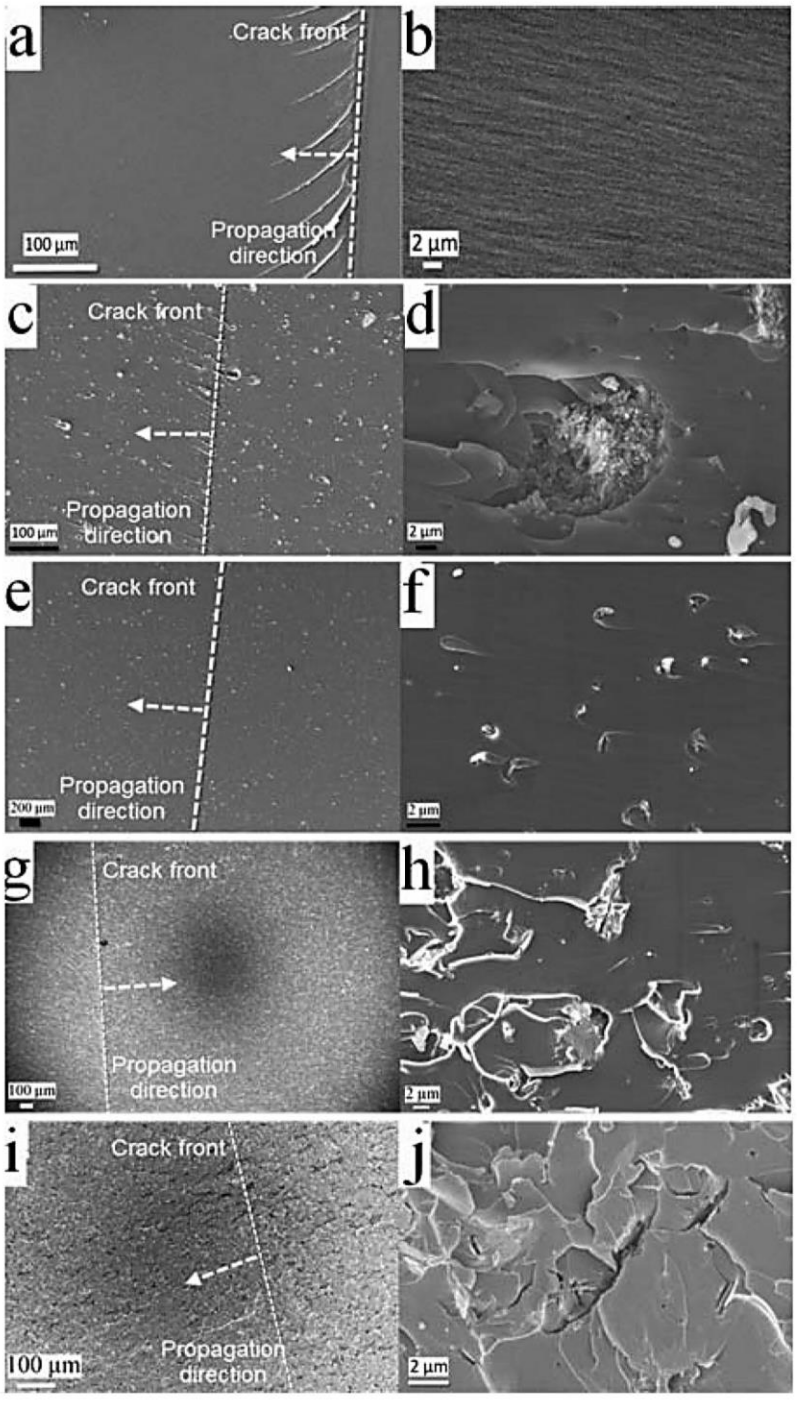

FIG. 5

SEM micrographs of fracture surfaces of CT specimens of (a,b) pure epoxy, and (c–j) 5.0 wt. % HNT/EP composites, where (c,d) AR HNT/EP prepared by mixing, (e,f) AR HNT/EP prepared by ball milling, (g,h) treated HNT/EP prepared by mixing, and (i,j) treated HNT/EP prepared by ball milling.

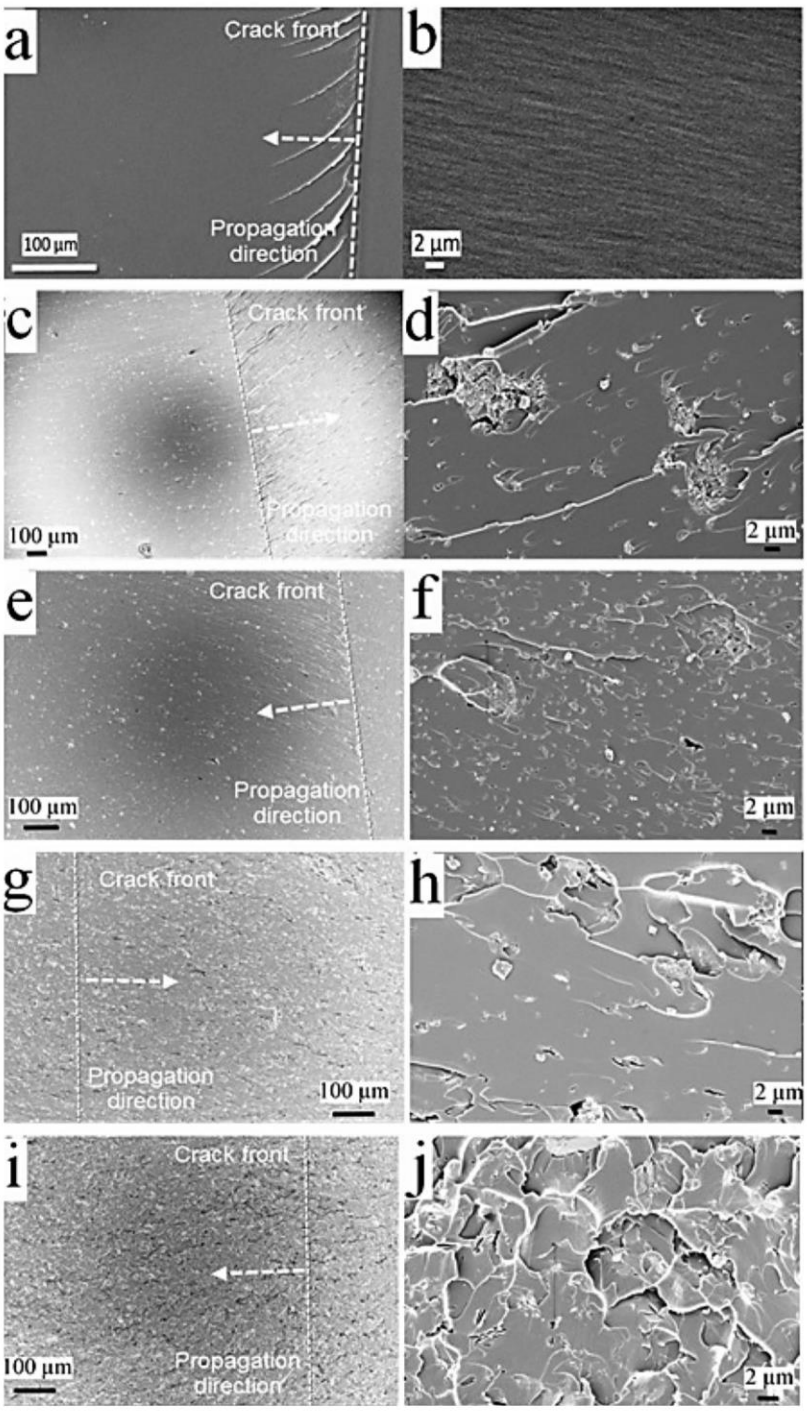

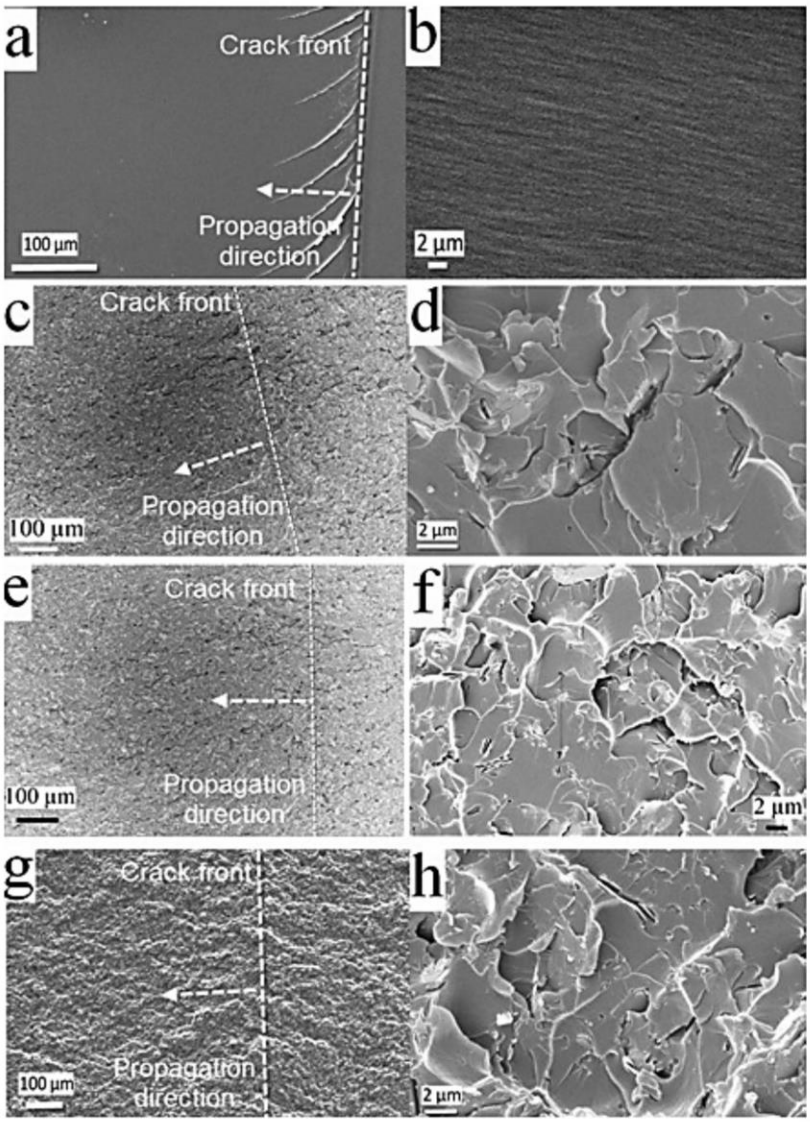

FIG. 6
SEM micrographs of fracture surfaces of CT specimens of (a,b) pure epoxy, (c,d) 2.0 wt. %, (e,f) 5.0 wt. %, and (g,h) 10.0 wt. % treated HNT/EP composites prepared by ball milling.

composites containing 5.0 wt. % HNT. **Figure 5** shows SEM images of fracture surfaces of CT specimens of 5.0 wt. % HNT/EP composites. All of the fracture surfaces were much rougher than the corresponding fracture surfaces of the 2.0 wt. % HNT/EP composite shown in **Fig. 4**. With simple mixing, some micro-size aggregates still existed in the composites, as shown in **Figs. 5(*d*)** and **5(*h*)**. The use of ball mill homogenization greatly reduced the size of the HNT particle clusters and resulted in more uniform distribution of HNTs at this concentration, as shown in **Figs. 5(*f*)** and **5(*j*)**.

When the HNT concentration was further increased to 10.0 wt. %, the K_{IC} values increased marginally compared with values of the 5.0 wt. % HNT/EP composites,

with only – 5.7 %, 4.4 %, 9.3 %, and 3.8 % increases for corresponding composites, respectively. **Figure 6** shows SEM images of fracture surfaces of treated HNT/EP composite CT specimens with 0.0 wt. %, 2.0 wt. %, 5.0 wt. %, and 10.0 wt. % HNT. In **Fig. 6**, the fracture surface of the neat epoxy is very smooth except for some river-line marks near the crack-initiation site, as shown in **Figs. 6(*a*)** and **6(*b*)**. The featureless crack surface indicates the absence of significant plastic shear deformation, highlighting a typical feature of brittle fracture behavior and accounting for the low fracture toughness of the unfilled epoxy. Compared to the neat epoxy, the fracture surfaces of the HNT/EP composites had a much rougher surface and very different morphologies of crack propagation at different HNT concentrations. The increased surface roughness implies that the cracking path was deflected by the presence of the rigid particles, making crack propagation more difficult. Phenomenologically, compared with the fracture surfaces of the 2.0 wt. % HNT/EP composite (**Fig. 6(*d*)**) and the 5.0 wt. % HNT/EP composite (**Fig. 6(*f*)**), the 5.0 wt. % HNT/EP composite shows higher surface roughness, but the surface roughnesses of the 5.0 wt. % HNT/EP composite (**Fig. 6(*f*)**) and the 10.0 wt. % HNT/EP composite (**Fig. 6(*h*)**) are similar.

With a further increase in HNT concentration in the epoxy matrix from 5.0 wt. % to 10.0 wt. %, the fracture toughness increased marginally but suffered the disadvantage of the high potential T_g decrease shown in **Fig. 2**, non-homogeneity of the cured composites with high concentration in the bottle of the cured composites [7], and much more immature tensile failure caused by the micro-size HNT aggregates [5]. Meanwhile, **Fig. 7** shows the thermal stability of the neat epoxy and 10.0 wt. % HNT/EP composites. From the curves, it is clearly shown that the HNT could effectively enhance thermal stability of the epoxy matrix, especially in the high-temperature region (>450°C). However, the final weights for the 10.0 wt. % HNT/EP composite are clearly less than that of the 10.0 wt. % inorganic HNT (see *inset* in **Fig. 7**). The weight difference comes from the losing of organic molecules such as PPA in HNT, but is mainly caused by the concentration gradient existing in the 10.0 wt. % HNT/EP composite. The TGA specimens were milled using a surface grinder on both upper and lower surfaces to ensure flatness of specimens and, most importantly, to remove possible oversized halloysite particle agglomerates, which

FIG. 7

TGA data in air for neat epoxy, 10.0 wt. % AR HNT/EP and 10.0 wt. % treated HNT/EP prepared by mechanical mixing.

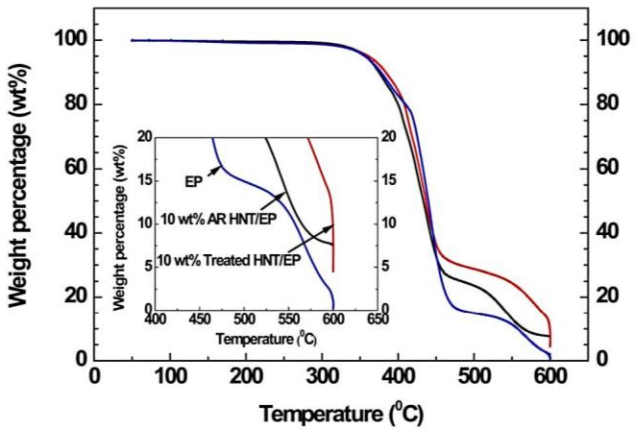

can sink to the bottom during curing. During the smoothing process, the high concentration HNT bottle layer was removed, which caused the lower concentration reported in the TGA experiment and further proved that the concentration gradient existed in the HNT/EP composites, especially at high HNT concentration.

Considering the K_{IC} values of the HNT/EP composites reported in **Fig. 3** together with the SEM images of fracture surface in **Figs. 4–6**, as well as with the TGA results in **Fig. 7**, it is evident from the reported experiments that the 5.0 wt. % HNT is the optimal concentration for the reinforced epoxy.

Conclusions

The effects of HNT concentration on the mechanical and thermal properties of diverse epoxy composites are reported in this study. The tensile properties, glass transition temperature (T_g), and especially the fracture toughness of epoxy composites with different concentrations of AR or treated HNTs prepared by mechanical mixing or ball mill homogenization were experimentally characterized. Increases in the concentration of HNT particles in the region of 0.0–10.0 wt. % significantly reinforced the fracture toughness of the epoxy composites. For the mechanical and thermal properties of the diverse epoxy composites in this research, 5.0 wt. % HNT was an optimal concentration. A much higher concentration (10.0 wt. %) of HNT achieved only marginal enhancement of fracture toughness but had the negative effects of lowering T_g, clear HNT concentration gradient in cured HNT/EP composites, and potential immature tension failure caused by inhomogeneous micro-size aggregates.

ACKNOWLEDGMENTS

W.H. and Y.T. are grateful for the support of a research internship at the Centre for Maritime Engineering, Control and Imaging of Flinders University and to the Australian Research Council for a Discovery Early Career Research Award (DECRA) for research work, respectively.

References

[1] Barbero, E. J., *Introduction to Composite Materials Design*, Taylor and Francis, London, 2011.

[2] Tang, Y. H., Ye, L., Zhang, Z., and Friedrich, K., "Interlaminar Fracture Toughness and CAI Strength of Fiber-Reinforced Composites With Nanoparticles—A Review," *Compos. Sci. Technol.*, Vol. 86, 2013, pp. 26–37.

[3] Ye, Y. P., Chen, H. B., Wu, J. S., and Ye, L., "High Impact Strength Epoxy Nanocomposites With Natural Nanotubes," *Polymer*, Vol. 48, 2007, pp. 6426–6433.

[4] Deng, S. Q., Zhang, J. N., Ye, L., and Wu, J. S., "Toughening Epoxies With Halloysite Nanotubes," *Polymer*, Vol. 49, 2008, pp. 5119–5127.

[5] Deng, S. Q., Zhang, J. N., and Ye, L., "Halloysite-Epoxy Nanocomposites With Improved Particle Dispersion through Ball Mill Homegenisation and Chemical Treatments," *Compos. Sci. Technol.*, Vol. 69, 2009, pp. 2497–2505.

[6] Tang, Y. H., Deng, S. Q., Ye, L., Yang, C., Yuan, Q., Zhang, J. N., and Zhao, C. B., "Effects of Unfolded and Intercalated Halloysites on Mechanical

Properties of Halloysite–Epoxy Nanocomposites," *Compos. Part A: Appl. S.*, Vol. 42, 2011, pp. 345–354.

[7] Tang, Y. H., Ye, L., Deng, S. Q., Yang, C., and Yuan, W. Z., "Influences of Processing Methods and Chemical Treatments on Fracture Toughness of Halloysite–Epoxy Composites," *Mater. Des.*, Vol. 42, 2012, pp. 471–477.

[8] Alamri, H. and Low, I. M., "Microstructural, Mechanical, and Thermal Characteristics of Recycled Cellulose Fiber-Halloysite-Epoxy Hybrid Nanocomposites," *Polym. Compos.*, Vol. 33, 2012, pp. 589–600.

[9] Alamri, H. and Low, I. M., "Effect of Water Absorption on the Mechanical Properties of Nano-Filler Reinforced Epoxy Nanocomposites," *Mater. Des.*, Vol. 42, 2012, pp. 214–222.

[10] Joussein, E., Petit, S., Churchman, J., Theng, B., Righi, D., and Delvaux, B., "Halloysite Clay Minerals—A Review," *Clay Miner.*, Vol. 40, 2005, pp. 383–426.

[11] Balakrishnan, H., Hassan, A., Wahit, M. U., Yussuf, A. A., and Razak, S. B. A., "Novel Toughened Polylactic Acid Nanocomposite: Mechanical, Thermal and Morphological Properties," *Mater. Des.*, Vol. 31, 2010, pp. 3289–3298.

[12] Horvath, E., Kristof, J., Frost, R. L., Redey, A., Vagvolgvi, V., and Cseh, T., "Hydrazine-Hydrate Intercalated Halloysite Under Controlled-Rate Thermal Analysis Conditions," *J. Therm. Anal. Calorim.*, Vol. 71, 2003, pp. 707–714.

[13] ASTM D638: Standard Test Method for Tensile Properties of Plastics, *Annual Book of ASTM Standards*, ASTM International, West Conshohocken, PA, 2010.

[14] ASTM D5045: Standard Test Methods for Plane-Strain Fracture Toughness and Strain Energy Release Rate of Plastic Materials, *Annual Book of ASTM Standards*, ASTM International, West Conshohocken, PA, 2007.

[15] Xiao, K. Q., Ye, L., and Kwok, Y. S., "Effects of Pre-Cracking Methods on Fracture Behaviour of an Araldite-F Epoxy and Its Rubber-Modified Systems," *J. Mater. Sci.*, Vol. 33, 1998, pp. 2831–2836.

[16] Cousin, P. and Smith, P., "Dynamic Mechanical Properties of Sulfonated Polystyrene/Alumina Composites," *J. Polym. Sci. Polym. Phys.*, Vol. 32, 1994, pp. 459–468.

[17] Hill, L. W., "Dynamic Mechanical and Tensile Properties," *Paint and Coating Testing Manual*, 15th ed., J. V. Koleske, Ed., ASTM International, West Conshohocken, PA, 2012, pp. 624–636.

Chapter 4: Functionalised silica/epoxy nanocomposites with enhanced fracture toughness for large-scale applications

4.1 Introduction and significance

In this chapter, we reported that nanosilica with amino and epoxide groups (RNS-A and RNS-E) can enhance fracture toughness of epoxy by mechanical mixing homogenization. It was found that the functional groups in nanosilica provided better resin-wettability, suppress nanosilica aggregation. The highlights in this work include:

1. We have reported that with 2 wt% of amino and epoxide functionalised nanosilica significant enhanced the fracture toughness of epoxy by 25.0% and 35.9%, respectively.

2. We found that the viscosity of those functional groups modified nanosilica/epoxy was similar with that of pure epoxy, which means no change needed for processing and fabrication.

3. We found that the specific surface area (SSA) of RNS-E was 4.5 times higher than that of RNS-A, which improved the interfaces between nanosilica and epoxy, then enhanced the fracture toughness of epoxy composites.

This section is included as it appears as a journal paper published by **Wei Han**, Yang Yu, Liming Fang, Martin Johnston, Youhong Tang. Functionalized silica/epoxy nanocomposites with enhanced fracture toughness for large-scale applications. ***J Compos Mater*** 2015; 49(12):1439-47.

4.2 Functionalised silica/epoxy nanocomposites with enhanced fracture toughness for large-scale applications

Article

JOURNAL OF COMPOSITE MATERIALS

Journal of Composite Materials
2015, Vol. 49(12) 1439–1447

DOI: 10.1177/0021998314534867
jcm.sagepub.com
SAGE

Functionalised silica/epoxy nanocomposites with enhanced fracture toughness for large-scale applications

Wei Han[1], Yang Yu[1,2], Liming Fang[3], Martin R Johnston[2], Shi Zhang Qiao[4] and Youhong Tang[1]

Abstract

A small amount of commercial functional nanosilica was mechanically mixed with epoxy to enhance the composite fracture toughness. Nanosilicas with amino and epoxide functional groups show strong interfaces with epoxy, which suppress large aggregations and enhance resin-wettability, hence enhancing the fracture toughness of epoxy composites. Compared with other reports, less nanosilica content was needed to achieve the same fracture toughness values or similar enhancement ratio. Due to their commercial availability, the low-cost of the raw material and simple fabrication method, those nanocomposites have the potential for large-scale applications.

Keywords

Functionalised nanosilica, particle-reinforcement, fracture toughness, epoxy

Introduction

As widely used thermosetting polymers in various industrial applications, particularly as adhesives for bonding and as matrix resins for producing high-performance fibre-reinforced composites, epoxy resins have several unique characteristics, including high adhesive strength, high strength and hardness, excellent chemical and heat resistance. However, most cured epoxy systems exhibit low fracture toughness, poor resistance to crack initiation and propagation and inferior impact strength. For example, the delamination and poor impact resistance of fibre-reinforced epoxy composites is often attributed to the low fracture toughness of the epoxy matrix. Many attempts have been made in recent decades to improve the fracture toughness of epoxies by modifying the epoxy resins with additives. Research has shown that nanoparticles such as nanosilica, halloysite, nanoclay and nanotube can enhance the fracture toughness of the epoxy.[1–6] When nanoparticles are used as modifiers in epoxies, a homogeneous dispersion is required in order to achieve the nanophase structure. As particles tend to agglomerate, special techniques have had to be devised and used to achieve homogeneous particle distribution, including mechanical mixing using high shear forces, ultrasonic vibration and chemical methods such as sol–gel process to obtain nanosized particles.[1,2,7]

Due to the difficulties of large-scale production and adequate dispersion of nanofillers into epoxy, commercial nanofiller-modified epoxy is rare. One commercial and popularly used nanosilica-modified epoxy is called Nanoresins, Germany[1,2,7–14] with a concentration of 40 wt.% nanosilica in diglycidyl ether of bisphenol A (DGEBA) epoxy resin. The average particle size of the silica nanoparticles is ~20 nm, with a narrow range of particle size distribution. The silica nanoparticles are synthesised in situ by a sol–gel manufacturing process,

[1]School of Computer Science, Engineering and Mathematics, Flinders University, South Australia, Australia
[2]School of Chemical and Physical Sciences, Flinders University, South Australia, Australia
[3]School of Materials Science and Engineering, South China University of Technology, Guangdong, China
[4]School of Chemical Engineering, University of Adelaide, South Australia, Australia

Corresponding author:
Youhong Tang, Centre for NanoScale Science and Technology & Centre for Maritime Engineering, Control and Imaging, School of Computer Science, Engineering and Mathematics, Flinders University, South Australia 5042, Australia.
Email: youhong.tang@flinders.edu.au; s.qiao@adelaide.edu.au

whereby the particle size and excellent dispersion of these particles remains unchanged during any further mixing and/or blending operations. It has been reported that nanosilica can significantly improve the mechanical properties of polymers, e.g. their strength, fracture toughness and scratch/creep resistance. In particular, despite the relatively high silica content of 40 wt.%, the epoxy resin still has comparatively low viscosity due to the agglomerate-free colloidal dispersion of the silica nanoparticles in the epoxy resin. However, with other nanofillers such as agglomerated carbon nanotube (CNT) and nanoclay, uniform dispersal with a high weight/volume fraction in epoxy resins while achieving comparatively low viscosity has been a challenge. Viscous resin systems cannot easily impregnate continuous fibres or fibre fabrics when fabrication methods based on resin infusion have been used, and filtering of dense fibre bundles against agglomerated nanofillers can lead to severe segregation and depletion of nanofiller in the matrices. In such cases, fabrication methods including 'brushing and rolling' with hand-layup have been adopted for incorporating the modified epoxy resins into fibres or fibre fabrics. These methods can hardly produce continuous fibre composite laminates with consistent high quality, in particular for laminates with a fibre volume fraction of over 60%.[14,15]

Here, we report a feasible method of fabricating epoxy/silica composites by a simple melt-mixing with reasonable dispersion. With a small amount of functionalised nanosilica added (2 wt.%), the epoxy composites can achieve the requisite high fracture toughness with a higher concentration of nanosilica reported by other researchers.[8–13] The epoxy and nanosilica are commercially available, making these composites potentially suitable for large-scale applications.

Experimental

Sample preparation

The raw epoxy resin used was Araldite-F, DGEBA resin, produced by Ciba-Geigy, Australia. The sample was prepared as follows. First, the epoxy resin was placed in a glass beaker on a hotplate (Thermo Scientific, Australia) at 120°C under a fast and stable mixing using a laboratory homogeniser (Laboratory equipment, Australia). Two types of commercial silica nanoparticles denoted as RNS-A and RNS-E (Wangwu nanoscience Inc., China) were used as modifiers to toughen a DGEBA epoxy resin. Both RNS-A and RNS-E nanosilica particles at given concentrations (2 wt.% or 5 wt.%) were separately added in the epoxy resin, and stirred at 3000 r/min for 20 min to obtain homogeneous mixture. Second, piperidine (Sigma–Aldrich, Australia) hardener was added at a ratio of 100:5 by weight while stirring slowly. The mixture was then cast into the specimen cavities of preheated silicon rubber moulds and cured at 120°C for 16 h. The specimens in the oven were cooled gradually to room temperature (RT) before removal from the moulds. As controls for evaluation, pure epoxy and Nanopox F400 resin diluted by DGEBA epoxy to form 2 wt.% nanosilica/epoxy composites specimens were prepared separately.

Characterisation

A Fourier transform infrared spectrometer (Nicolet iN10 MX FTIR Microscope, Thermo Scientific, USA) was used in absorption mode to identify the functional group on the commercial nanosilica surface. Spectral resolution of the FTIR was maintained at 2 cm^{-1}. Dry nitrogen gas was used to purge the sample compartment to reduce interference of water and carbon dioxide in the spectrum. The sample was made into a potassium bromide (KBr) thin pellet using dry KBr at a 1:100 ratio (sample:KBr). Thermal stability analysis was carried out using a Hi-Res TGA 2950 thermogravimetric analysis apparatus (TA instruments, USA). The tests were carried out in N_2 with a heating rate of 10.0°C/min from RT to 700.0°C for the nanosilica. The silica particles were vacuum-dried for 2 days at RT before TGA characterisation. An XPS spectrometer (Specs, Germany) equipped with an Al Ka source (1486.6 eV) was used to investigate the chemical elements of the functionalised nanosilica. Transmission electron microscopy (TEM) images of silica nanoparticles were obtained using a transmission electron microscope (Philips CM200, the Netherlands) at 200 kV. For the preparation of the TEM specimens, silica nanoparticles were dispersed in acetone and sonicated by an ultrasonication pin (SKL-950IIDN, Ningbo Haishu Sklon Electronic Instrument Ltd., China) for 5 min, and the solution was dropped onto carbon-coated Cu grids for TEM observation after evaporation of the solvent. Nitrogen-sorption isotherms were collected by a TriStar II 3020 Micrometrics apparatus. Prior to measurement, samples were degassed at 120°C for at least 10 h. The Brunauer–Emmett–Teller (BET) specific surface area (SSA) was calculated using a BEL Sorp Max (Japan) with N_2 gas at 77 K.

Rheological dynamic strain sweep measurements of the uncured pure epoxy and nanosilica/epoxy composites were performed on an Anton Paar Physica MCR301 rheometer at 25°C and 120°C respectively, and frequency was set to 10 rad/s for each test.

The phase transition temperatures of the cured pure epoxy and its nanocomposites were determined by a differential scanning calorimeter (DSC) (PYRIS

diamond DSC, Perkin–Elmer Instruments, USA), using indium as the calibration standard, with both heating and cooling rates of 10.0°C/min under nitrogen atmosphere. The cured nanosilica/epoxy composites were ultramicrotomed using glass knives on an ultra-cut microtome (Leica ultracut-R ultramicrotomed, Germany) to produce thin sections with a nominal thickness of 100 nm. The sections were transferred onto Cu grids for TEM observation (Philips CM200, the Netherlands). All fracture toughness tests were conducted on a universal material testing machine (Instron, Mode 5969, USA) at RT. The fracture toughness of the cured epoxies was measured using the compact tension (CT) specimens according to ASTM D5045. The CT specimens have nominal dimensions of 48 mm × 48 mm × 10 mm. To minimise the effects of residual stress and residual plastic deformation around the pre-crack tip, a sharp pre-crack was introduced to the sample by razor blade tapping, using a specially designed clip holding a fresh razor blade at the tip of the machined crack and tapping gently with a light hammer. All fracture tests were conducted a loading rate of 2 mm/min. Only those specimens which fulfilled the condition of $a/W = 0.45$–0.55 (a: the pre-crack length; W: the distance from the centre of the loading pin to the edge of the CT specimen) were used to calculate the critical stress intensity factor (K_{IC}). At least 6 CT specimens were tested for each group of epoxies. Scanning electron microscopes (CAMScan MX2500 SEM, the Netherlands) were employed to study the fracture surfaces of the CT specimens.

Results and discussion

Functionalised nanosilica

Figure 1 shows the FTIR spectra of the as-received nanosilica with different functional groups. The characteristic peaks appearing at 1490 cm^{-1} and 1550 cm^{-1} for the RNS-A nanosilica are ascribed to N–H stretching[16] and bending vibrations,[17] providing evidence that amino groups reside on the RNS-A nanosilica surfaces. Meanwhile, the RNS-E nanosilica obviously has a C–O–C stretching and a C–O stretching vibrations at 846 cm^{-1} and 909 cm^{-1}, respectively, indicating that epoxide groups reside on the RNS-E nanosilica surfaces. The XPS survey curves in Figure 2 also clearly show that an element of nitrogen exists in the RNS-A surface, which should be contributed from the amino groups.

The results of TGA are shown in Figure 3 for the functionalised nanosilica samples. It can be seen that the RNS-A nanosilica is relatively unstable. The first obvious weight loss (~6.7 wt.%) after 100°C represents the removal of the entrapped water and a weight loss of

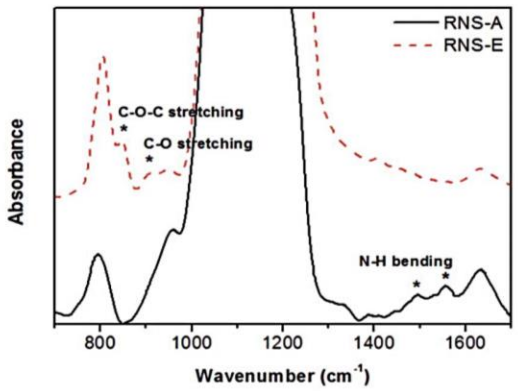

Figure 1. FTIR spectra of silica nanoparticles with different functional groups (* shows the typical peaks for the functional groups in nanosilica).

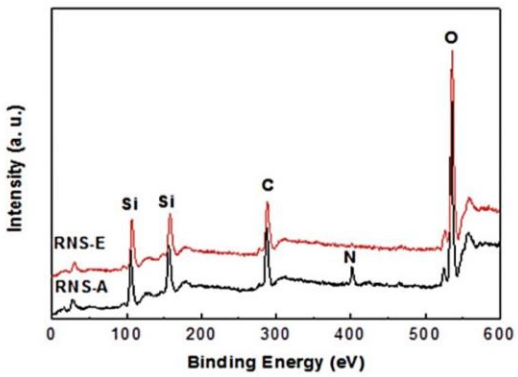

Figure 2. XPS survey of silica nanoparticles of RNS-A and RNS-E (the individual elements are marked in the curve).

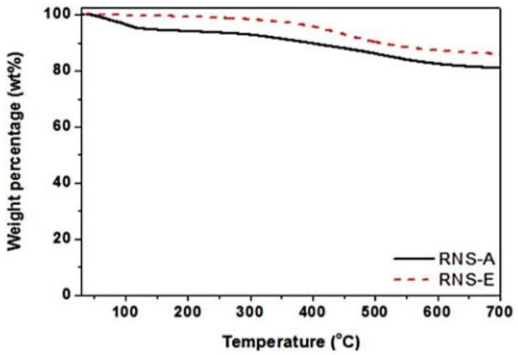

Figure 3. TGA curves of nanosilica RNS-A and RNS-E in N_2.

18.6 wt.% occurs when the temperature reaches 700°C. There is comparatively less weight loss (~4.8 wt.%) for the RNS-E nanosilica sample during the heating process up to 250°C, probably due to the presence of less entrapped water in the RNS-E nanosilica sample. The total weight loss is approximately 13.3 wt.% when the temperature reaches 700°C. Thus there is at least 11.9 wt.% of functionalised amino and 8.5 wt.% of functionalised epoxide material on the RNS-A and RNS-E surfaces, respectively.

Figure 4 shows typical TEM images of the two kinds of functionalised nanosilica. The nanosilica showed a preference for aggregation even after sufficient ultrasonication. The primary particle size of the nanosilica is quite uniform, and with a much greater primary particle size of the RNS-A (~20 nm) than that of the RNS-E (~10 nm). The standard BET model was used to calculate the SSA with RNS-A and RNS-E of 62.54 m^2/g and 283.12 m^2/g, respectively. The RNS-E has a significantly higher SSA (about 4.5 times) than that of the RNS-A.

Processability of nanosilica/epoxy composites

The viscosity of the uncured neat epoxy and nanosilica-modified epoxies at room and evaluated temperatures is shown in Figure 5. With the addition of nanosilica, the viscosity of the nanosilica-modified epoxies clearly increases. The neat epoxy has a viscosity of about 20.0 Pa·s at RT. With 2 wt.% RNS-A and RNS-E nanosilica in the epoxy, the viscosity increases slightly to 23.9 Pa·s and 23.8 Pa·s, respectively. Meanwhile, the viscosity decreases dramatically with the increase of temperature. At the temperature of the vacuum-assisted resin infusion moulding (VARIM) process of the fibre-reinforced laminate (90°C), the viscosities of the neat epoxy, 2 wt.% RNS-A and RNS-E nanosilica-modified epoxies have similar low values of 0.85 Pa·s. With such low values, silica-modified epoxy resins can easily impregnate carbon fibre layers as the neat epoxy does in the VARIM process.

Fracture toughness

Figure 6 shows exemplarily load–crack opening displacement (COD) curves obtained from CT tests at RT for each material. It is observed that both neat and reinforced epoxy specimens undergo fracture in a brittle manner when the maximum load is reached, and the maximum loads for the modified epoxies are obviously higher than that of the pure counterpart. The values of critical stress intensity factor (K_{IC}) obtained are shown in Table 1 for both pure and modified specimens. For 2 wt.% F400/epoxy composite, the K_{IC} value increases by 16.3% from 0.92 MPa $m^{1/2}$ (pure) to 1.07 MPa $m^{1/2}$, while the 2 wt.% RNS-A/epoxy K_{IC} values improves to 25% (1.15 MPa $m^{1/2}$) and 2 wt.% RNS-E/epoxy reaches 35.9% at 1.25 MPa $m^{1/2}$.

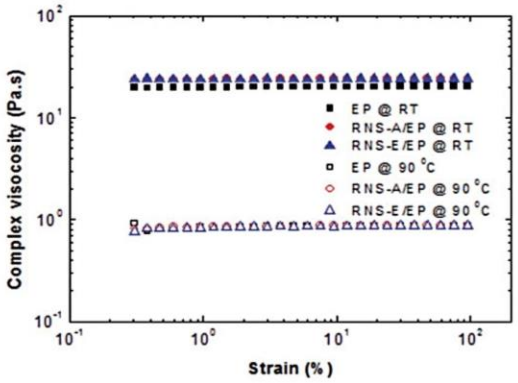

Figure 5. Dynamic strain sweep of neat epoxy and 2 wt% nanosilica/epoxy composites before curing at room temperature (RT) and evaluated temperature of 90°C.

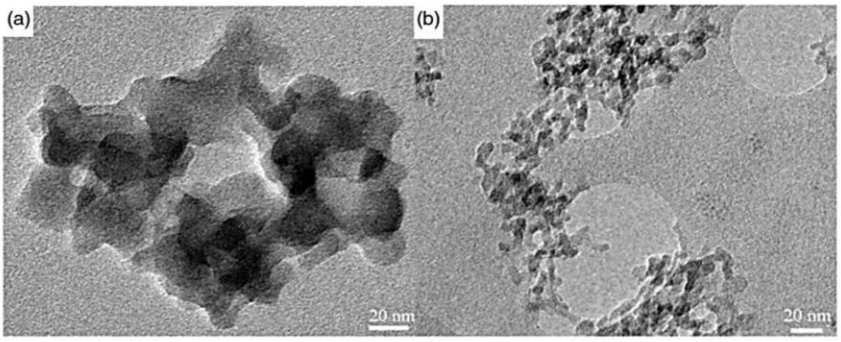

Figure 4. TEM images of nanosilica particles of (a) RNS-A and (b) RNS-E.

Thus, with the same silica concentration in epoxy and same preparation procedure for silica/epoxy composites, simply mixing commercial nanosilica and epoxy together can achieve higher fracture toughness than that of the commercial nanosilica-modified epoxy produced by sol-gel methods. The K_{IC} values of the 5 wt.% RNS-A/epoxy and the 5 wt.% RNS-E/epoxy composites are also reported in Table 1, where no further increase but a slight decrease of K_{IC} values (5.2–12.0%) was found, compared with the 2 wt.% silica/epoxy composites. This may be due to the significant aggregation of the RNS-A or RNS-E nanosilica particles in epoxy composites which limits the penetrating ability of epoxy into the nanosilica clusters and causes incomplete wetting of the silica aggregates.

The glass transition temperatures of the neat epoxy and silica–epoxy composite (2 wt.% RNS-A/epoxy, 2 wt.% RNS-E/epoxy and 2 wt.% F400/epoxy) samples were obtained from the DSC results. Typical second heating curves for the samples are shown in Figure 7, indicating that the addition of silica nanoparticles to

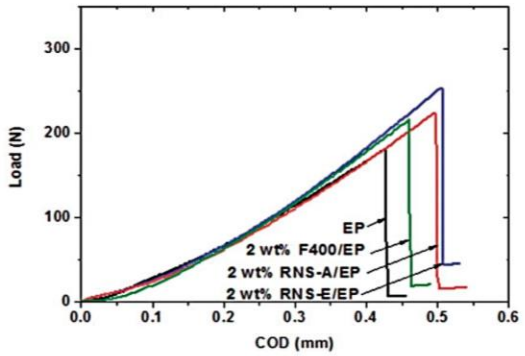

Figure 6. Typical load vs. COD curves of the neat epoxy and nanosilica/epoxy composites (CT specimens with initial crack length of about 20 mm).

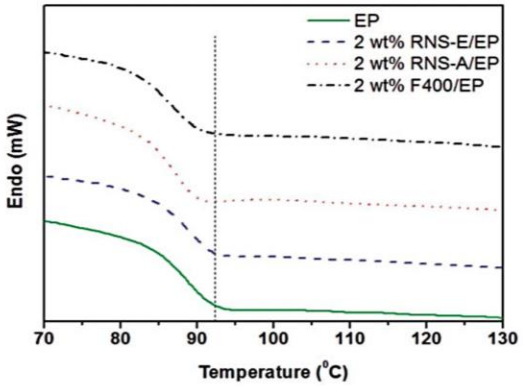

Figure 7. DSC second-heating curves for pure epoxy and its nanocomposites.

Table 1. Critical stress intensity factor (K_{IC}) of the neat epoxy and the nanosilica/epoxy composites.

Samples	Silica content (wt.%)	K_{IC} (MPa $m^{1/2}$)	Increment (%)	Reference
Araldite-F/piperidine	0	0.92 ± 0.04	0	
Araldite-F/piperidine/RNS-A nanosilica	2	1.15 ± 0.04	25.0	
Araldite-F/piperidine/RNS-A nanosilica	5	1.09 ± 0.04	18.5	
Araldite-F/piperidine/RNS-E nanosilica	2	1.25 ± 0.05	35.9	
Araldite-F/piperidine/RNS-E nanosilica	5	1.10 ± 0.05	19.6	
Araldite-F/piperidine/nanopox F 400	2	1.07 ± 0.05	16.3	
Araldite-F/piperidine/nanopox F 400	0	0.95 ± 0.03	0	8,9
	4	1.14 ± 0.06	20.0	
	6	1.26 ± 0.04	32.6	
Bisphenol-A/Albidur HE600/Nanopox F520	0	0.64 ± 0.07	0	10
	3.2 (1.8 vol %)	0.78 ± 0.04	21.9	
	6.1 (3.5 vol %)	0.85 ± 0.02	32.8	
Araldite-F/DDS/Nanopox F 400	0	0.5 ± 0.04	0	11
	10	0.69 ± 0.02	38	
Bisphenol-A/Albidur HE600/Nanopox F 400	0	0.51	0	12,13
	4	0.64	25.5	

the epoxy did not result in any significant change in the glass transition temperature of the composites.

Table 1 also lists the K_{IC} values of the epoxies with silica nanoparticles. All the experimental data show that K_{IC} value increases with an amount of nanosilica added in the epoxy matrix, regardless of epoxy type, curing agent type, nanosilica type and fabrication method. Few reports can be found for comparison after excluding the dissimilarity in epoxy and curing agent type, epoxy and curing agent ratio, and processing method. Liu et al.[8,9] showed that 4 wt.% (1.14 MPa $m^{1/2}$) and 6 wt.% (1.26 MPa $m^{1/2}$) or more Nanopox F400 nanoparticles were needed to reach similar values of fracture toughness K_{IC} to those obtained by using 2 wt.% RNS-A (1.15 MPa $m^{1/2}$) and RNS-E (1.25 MPa $m^{1/2}$) nanosilica particles reinforced epoxies, respectively. Meanwhile, compared with the present research results, to achieve similar K_{IC} incremental ratios to those of the RNS-A/epoxy (25%) and RNS-E/epoxy (35.9%) composites, a bisphenol-A/albidur HE600 system with 4 wt.% Nanopox F400 particles was needed to achieve a 25% (0.64 MPa $m^{1/2}$) improvement in fracture toughness,[12,13] and an araldite-F/DDS system with 10 wt.% Nanopox F400 particles was needed to obtain 38% (0.69 MPa $m^{1/2}$) more performance of the K_{IC}.[11] When bisphenol-A/albidur HE600 and Nanopox F520 were used, 3.2 wt.% (1.8 vol.% silica) and 6.1 wt.% (3.5 vol.% silica) were needed to achieve similar incremental ratios (K_{IC} from 0.64 MPa $m^{1/2}$ to 0.78 MPa $m^{1/2}$ and 0.85 MPa $m^{1/2}$).

Fracture toughness mechanism

The fracture surfaces of the neat and the modified epoxies were compared using SEM, and some typical micrographs are shown in Figure 8. The fracture surface of the neat epoxy specimen was flat, with intensive river-line marks near the crack initiation site, as in Figure 8(a). This is a typical feature of brittle fracture behaviour and accounts for the low-fracture toughness of the pure epoxy.[18] In 2 wt.% RNS-A and RNS-E nanosilica modified epoxies fracture surfaces, the somewhat roughened fracture surfaces near the crack tip indicated considerably different morphologies, which could be attributed to the deflection of the cracking path because of the presence of the rigid particles, making crack propagation more difficult. Further SEM investigation of fractured surfaces is shown in Figure 9. The dispersion of nanosilica particles in the epoxy matrix is generally uniform, though most are in the form of particle clusters of different sizes. There are mostly isolated particle clusters of relatively large size, up to several or even more than 10 μm. Nanosilica particle clusters can interact with a crack, bridging the crack when it passes through, resisting the advance of the crack and thus resulting in an increase in fracture toughness. As shown in Figure 9, uneven facades and deformations can be clearly seen around these silica particle clusters of different sizes. Therefore, plastic deformation of the epoxy around particle clusters and crack deflection through the clusters may be the dominant toughening mechanisms for those composites. Although the nanosilica particle clusters are not in nanoscale, they consist of numerous nanosized particles. The epoxy resin indeed can penetrate into the clusters and wet the nanoparticles, as shown in the higher magnification images of Figure 9, which is somewhat similar to intercalated montmorillonite (MMT)[19] and Halloysite nanotube (HNT) particles.[4]

From the high-magnification TEM images of the nanosilica particles in epoxy matrix (Figure 10), it is evident that the morphologies of the nanosilica clusters differ. In the RNS-A/epoxy composite (Figure 10(a)), the morphology is similar to that of RNS-A particles dispersed in acetone (Figure 4(a)) with many nanosilica particles aggregating together and forming clusters. These clusters mostly are not isolated but are connected together. In contrast, the aggregation size of RNS-E in the epoxy matrix is much smaller than that of RNS-A, and the clusters are mostly isolated, as shown in Figure 10(c). Meanwhile, the higher enhanced epoxy fracture toughness of the RNS-E epoxy matrix is

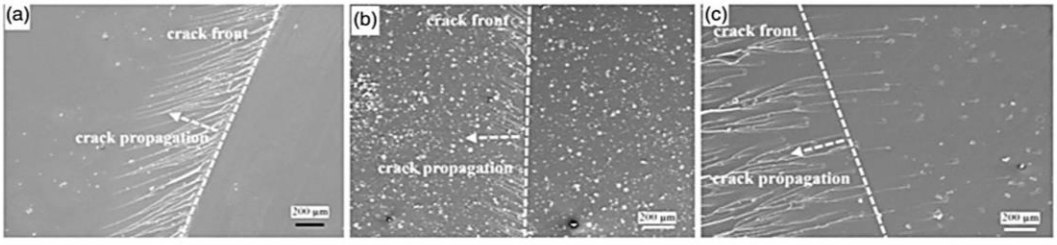

Figure 8. SEM micrographs of fracture surfaces of CT specimens of neat epoxy and nanosilica/epoxy composites: (a) pure epoxy; (b) 2 wt.% RNS-A/epoxy and (c) 2 wt.% RNS-E/epoxy.

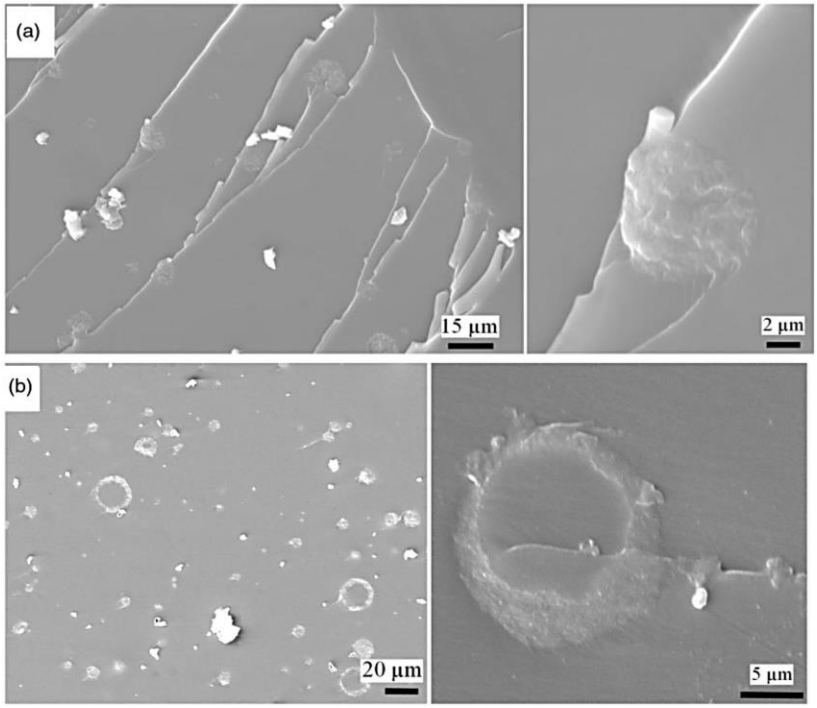

Figure 9. High-magnification SEM of fracture surfaces of CT specimens of nanosilica/epoxy composites with nanofillers of (a) RNS-A and (b) RNS-E.

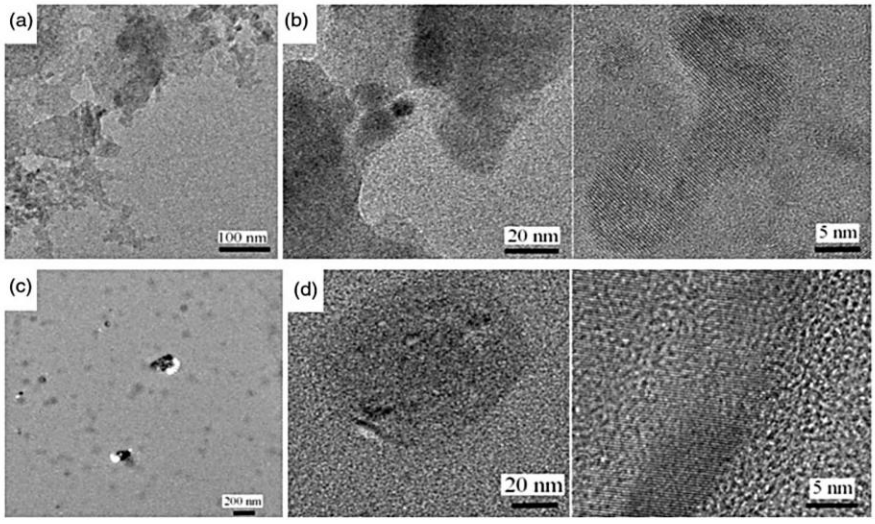

Figure 10. TEM images of 2 wt.% nanosilica/epoxy composite after curing with different magnifications (a) (b) RNS-A and (c) (d) RNS-E.

probably attributable to the fact that the RNS-E silica particles have a much greater effective surface area in contact with the epoxy matrix, compared to the RNS-A silica particles. This speculation is confirmed by the standard BET test, in which the RNS-A silica particle had a SSA of 62.54 m^2/g, whereas the RNS-E silica particle had a SSA of 283.12 m^2/g. The SSA of the RNS-E silica was almost 4.5 times higher than that of the RNS-A silica. The increased surface area provided more surfaces to interact with the epoxy polymer chains to further enhance the fracture toughness of the composite. The interfacial strength between the silica and epoxy can be observed clearly in the TEM characterisations. Chemically reactable silica particles such as –epoxide or $–NH_2$ groups show strong interfaces in epoxy composites, as shown in Figure 10(b) and (d). There are no clear interfaces between the particle(s) and the epoxy matrix. Particles containing $–NH_2$ and –epoxide may have a strong interface in epoxy composites because they react chemically with the epoxy or the curing agent. Silica with epoxide groups has been mixed with a curing agent to ascertain reactability.[20] Due to the excellent compatibility of the functionalised nanosilica particles with the epoxy matrix, even nanosilica clusters can be effective reinforcers for epoxy matrix, enhancing the fracture toughness of the matrix at low reinforcer loading levels.

Conclusion

We have reported a new nanosilica/epoxy system with a small amount of commercially available functionalised nanosilica particles and significantly enhanced fracture toughness of epoxy matrix. Through simple melt mixing, nanosilica particles were homogeneously dispersed in epoxy matrix with similar low viscosity, a procedure which is feasible for processing and fabrication. High-fracture toughness can be achieved with a small amount of nanosilica loading. In contrast, high nanosilica content is needed for the same fracture toughness values or incremental ratios to be achieved using other kinds of nanosilica particles, as reported by other researchers. The functional groups on the nanosilica surfaces and the SSAs of the nanosilica play critical roles in improving the interface between particle(s) and matrix and increasing the interaction areas between silica and epoxy chains, further enhancing the high fracture toughness with a small amount of nanosilica in epoxy composites.

Acknowledgements

We thank Dr JF Zhou of the University of South Australia for providing the commercial nanosilicas. Y Tang is grateful to ARC-DECRA for financial support on the research (DE120102784).

Funding

This research received no specific grant from any funding agency in the public, commercial, or not-for-profit sectors.

Conflict of interest

None declared.

References

1. Deng SQ, Ye L and Friedrich K. Fracture behaviours of epoxy nanocomposites with nano-silica at low and elevated temperatures. *J Mater Sci* 2007; 42(8): 2766–2774.
2. Tang YH, Ye L, Zhang DH, et al. Characterization of transverse tensile, interlaminar shear and interlaminate fracture in CF/EP laminates with 10 wt% and 20 wt% silica nanoparticles in matrix resins. *Compos Part A-Appl S* 2011; 42: 1943–1950.
3. Deng SQ, Zhang JN, Ye L, et al. Toughening epoxies with halloysite nanotubes. *Polymer* 2008; 49: 5119–5127.
4. Tang YH, Deng SQ, Ye L, et al. Effects of unfolded and intercalated halloysites on mechanical properties of halloysite-epoxy nanocomposites. *Compos Part A-Appl S* 2011; 42: 345–354.
5. Lan T and Pinnavaia TJ. Clay-reinforced epoxy nanocomposites. *Chem Mater* 1994; 6: 2216–2219.
6. Xie XL, Mai YW and Zhou XP. Dispersion and alignment of carbon nanotubes in polymer matrix: a review. *Mater Sci Eng R-Rep* 2005; 49: 89–112.
7. Kinloch AJ, Mohammed RD, Taylor AC, et al. The interlaminar toughness of carbon-fibre reinforced plastic composites using "hybrid-toughened" matrices. *J Mater Sci* 2006; 41: 5043–5046.
8. Liu HY, Wang GT and Mai YW. Cyclic fatigue crack propagation of nanoparticle modified epoxy. *Compos Sci Technol* 2012; 72: 1530–1538.
9. Liu HY, Wang GT, Mai YW, et al. On fracture toughness of nano-particle modified epoxy. *Compos Part B-Eng* 2011; 42: 2170–2175.
10. Zhang H, Tang LC, Zhang Z, et al. Fracture behaviours of in situ silica nanoparticle-filled epoxy at different temperatures. *Polymer* 2008; 49: 3816–3825.
11. Ma J, Mo MS, Du XS, et al. Effect of inorganic nanoparticles on mechanical property, fracture toughness and toughening mechanism of two epoxy systems. *Polymer* 2008; 49: 3510–3523.
12. Hsieh TH, Kinloch AJ, Taylor AC, et al. The toughness of epoxy polymers and fibre composites modified with rubber microparticles and silica nanoparticles. *J Mater Sci* 2010; 45: 1193–1210.
13. Blackman BRK, Kinloch AJ, Sohn Lee J, et al. The fracture and fatigue behaviour of nano-modified epoxy Polymers. *J Mater Sci* 2007; 42: 7049–7051.
14. Tang YH, Ye L, Zhang Z, et al. Interlaminar fracture toughness and CAI strength of fibre-reinforced composites with nanoparticles – a review. *Compos Sci Technol* 2013; 86: 26–37.
15. Qian H, Hreenhalgh ES, Shaffer MSP, et al. Carbon nanotube-based hierarchical composites: a review. *J Mater Chem* 2010; 20: 4751–4762.

16. Yu Y, Shapter JG, Popelka-Filcoff R, et al. Copper removal using bio-inspired polydopamine coated natural zeolites. *J Hazard Mater* 2014; 273: 174–182.
17. Jellali S, Wahab MA, Anane M, et al. Biosorption characteristics of ammonium from aqueous solutions onto *Posidonia oceanica* (L.) fibers. *Desalination* 2011; 270: 40–49.
18. Hull D. *Fractography*. London: Cambridge University Press, 1999, p.91.
19. Wang K, Chen L, Wu JS, et al. Epoxy nanocomposites with highly exfoliated clay: mechanical properties and fracture mechanisms. *Macromolecules* 2005; 38: 788–800.
20. Kang S, Hong SII, Choe CR, et al. Preparation and characterization of epoxy composites filled with functionalized nanosilica particles obtained via sol-gel process. *Polymer* 2001; 42: 879–887.

Chapter 5: Fracture toughness and wear properties of nanosilica/epoxy composites under marine environment

5.1 Introduction and significance

In this chapter, we reported that commercially available nanosilica (Nanopox-F400) with 2 wt% concentration can enhance fracture toughness and wear properties of epoxy composites under marine environment. It was found that fracture toughness was weakened with salt water immersion. However, the fracture toughness of nanosilica reinforced composite after immersion was comparable to that of the neat epoxy without immersion. The highlights in this work include:

1. We reported that the friction coefficient of neat epoxy increased with salt water immersion time and rotation speed increasing. By contrast, the friction coefficient of nanosilica reinforced epoxy decreased with salt water immersion time increasing.

2. We found that fracture toughness of the neat epoxy and the nanosilica reinforced epoxy were both deleteriously affected by salt water immersion. However, increment of the fracture toughness by nanosilica adding was able to complement the fracture toughness loss due to salt water immersion.

This section is included as it appears as a journal paper published by **Wei Han**, Sheng Chen, Jonathan Campbell, Xiaojun Zhang and Youhong Tang. Nanosilica enhanced fracture toughness and wear properties of epoxy under marine environment. ***Mater Chem Phy*** 2016; 177: 147-155.

5.2 Fracture toughness and wear properties of nanosilica/epoxy composites under marine environment

Materials Chemistry and Physics 177 (2016) 147–155

Contents lists available at ScienceDirect

Materials Chemistry and Physics

journal homepage: www.elsevier.com/locate/matchemphys

Fracture toughness and wear properties of nanosilica/epoxy composites under marine environment

Wei Han [a], Sheng Chen [b], Jonathan Campbell [c], Xiaojun Zhang [d, **], Youhong Tang [a, *]

[a] Centre for NanoScale Science and Technology, Centre for Maritime Engineering, Control and Imaging, School of Computer Science, Engineering and Mathematics, Flinders University, South Australia 5042, Australia
[b] School of Chemical Engineering, The University of Adelaide, South Australia 5005, Australia
[c] Centre for NanoScale Science and Technology, School of Chemical and Physics Sciences, Flinders University, South Australia 5042, Australia
[d] College of Mechanical Engineering and Applied Electronics Technology, Beijing University of Technology, Beijing 100124, China

HIGHLIGHTS

- Saltwater immersion deteriorates fracture toughness of epoxy and nanosilica composites.
- Nanosilica enhances fracture toughness of epoxy.
- Nanosilica enhances corrosion resistance of epoxy.
- Increasing saltwater immersion decreases friction coefficient of silica composites.

ARTICLE INFO

Article history:
Received 13 July 2015
Received in revised form
1 March 2016
Accepted 1 April 2016
Available online 8 April 2016

Keywords:
A: Composite materials
C: Tribology and wear
D: Corrosion
D: Fracture

ABSTRACT

In this research, we report the use of a commercial epoxy based nanocomposite with 2 wt % nanosilica to enhance the fracture toughness and wear performance of neat epoxy under marine environment. The mechanical behaviours of neat epoxy and the nanosilica enhanced epoxy composite are characterised after different periods of immersion in sea water (0 day, 7 days and 30 days). The experimental results indicate that sea water immersion does not greatly affect the tensile behaviours of the epoxy or the nanosilica enhanced epoxy nanocomposite. However, the fracture toughness of the neat epoxy is weakened by the sea water immersion with an 18.5% decrease after 7 days immersion and no further decrease after 30 days immersion. The fracture toughness of the nanocomposite also decreases after immersion, but the final value after immersion is comparable to that of the neat epoxy without immersion. The friction coefficient of the neat epoxy increases but that of the nanocomposite decreases with increasing immersion in sea water. The proposed mechanisms are also discussed here.

1. Introduction

Thermosetting polymers are used in various industrial applications. Most pure epoxy systems show low fracture toughness and poor resistance to crack initiation and propagation. The use of nanoparticles in various polymers to improve performance has been evaluated in many studies [1–16]. In the marine environment, complex conditions such as high salinity, high pressure, high humidity and alkaline corrosion accelerate the degradation of polymer and greatly reduce the reliability of the material. Wave scouring, impact with floating debris and bacteria in the sea mud can lead to corrosion of marine vehicles, equipment, and oil exploration platforms to different degrees [17–19]. Mouritz et al. [20] showed that the flexural strength of a glass/unsaturated polyester composite decreased as the composite was exposed to sea water. Geliert et al. [21] demonstrated that the flexural strength of glass fibre reinforced composites with polyester, phenol, and vinyl ester also decreased in the presence of sea water.

Many researchers have reported that nanoparticles can successfully enhance the fracture toughness of epoxy [22–24]. When nanoparticles are used as modifiers in epoxies, homogeneous dispersion is necessary to achieve the nanophase structure. As particles tend to agglomerate, special techniques have had to be

* Corresponding author.
** Corresponding author.
E-mail addresses: xjzhang@bjut.edu.cn (X. Zhang), youhong.tang@flinders.edu.au (Y. Tang).

http://dx.doi.org/10.1016/j.matchemphys.2016.04.008
0254-0584/

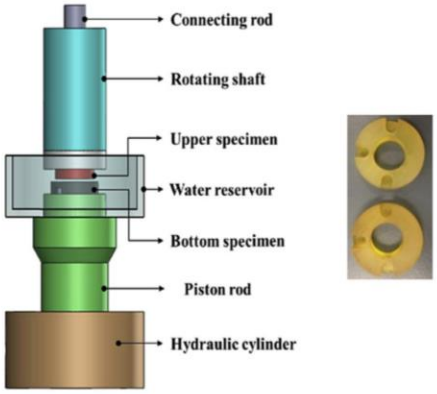

Fig. 1. Principal scheme of the test rig and images of test samples of the epoxy and the nanosilica enhanced epoxy composite [20].

devised and used to achieve homogeneous particle distribution, including mechanical mixing using high shear forces, ultrasonic vibration [25–27], and chemical methods such as a sol-gel process, to obtain nanosilica particles [4,28]. New techniques to break down clusters or agglomerates have been investigated extensively by many research groups, and among these, a sol-gel technique introducing nanoparticles into pre-polymers by chemical reaction has proved very effective [22–29].

Due to the difficulty of large-scale production and adequate dispersion of nanofillers into epoxy, commercial nanofiller-modified epoxy is rare. However, several commercial and popularly used nanosilica-modified epoxies are available. One such is Nanopox F400, from Germany, with a concentration of 40 wt.% nanosilica in diglycidyl ether of bisphenol A (DGEBA) epoxy resin [29]. The average particle size of the silica nanoparticles is 20 nm, with a narrow range of particle size distribution. The silica nanoparticles are synthesised in situ by a sol-gel manufacturing process, whereby the particle size and excellent dispersion of these particles remain unchanged during any further mixing and/or blending operations. It has been reported that nanosilica can significantly improve the mechanical properties of polymers, e.g. strength, fracture toughness and scratch/creep resistance [29]. In particular, despite the relatively high silica content of 40 wt.%, the Nanopox F400 epoxy resin retains comparatively low viscosity due to the agglomerate-free colloidal dispersion of the silica nanoparticles in the epoxy resin.

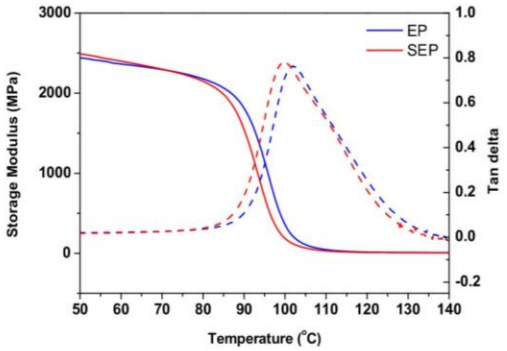

Fig. 2. Storage modulus and loss tangent of neat epoxy (EP) and nanosilica enhanced epoxy composite (SEP) as a function of temperature.

Table 1
Mechanical properties of epoxy (EP) and nanosilica enhanced epoxy composite (SEP) after different periods of salt water immersion.

	Tensile strength (MPa)	Strain at break (%)	Modulus (GPa)
EP-0 days	73.60 ± 0.46	3.74 ± 0.09	3.38 ± 0.08
EP-7 days	72.57 ± 1.35	3.77 ± 0.06	3.47 ± 0.03
EP-30 days	74.09 ± 0.47	3.72 ± 0.08	3.37 ± 0.02
SEP-0 days	73.04 ± 1.19	3.53 ± 0.17	3.43 ± 0.10
SEP-7 days	72.63 ± 1.67	3.90 ± 0.19	3.56 ± 0.13
SEP-30 days	73.97 ± 0.88	3.85 ± 0.03	3.51 ± 0.03

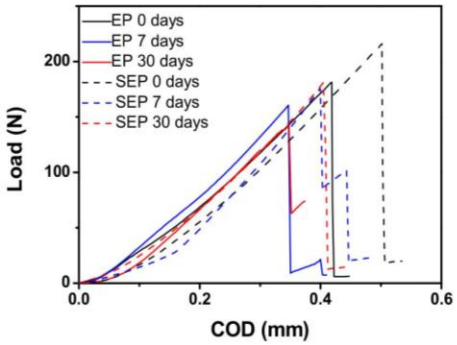

Fig. 3. Typical load-crack opening displacement (COD) curves for neat epoxy (EP) and nanosilica enhanced epoxy composite (SEP) with different periods of immersion of 0, 7 and 30 days.

In this study, further exploration of this commercial nanosilica enhanced epoxy composite with 2 wt.% nanosilica was conducted in a simulated marine environment. The mechanical behaviours, including tensile properties, fracture toughness, corrosion resistance and wearing properties, after different periods of immersion in sea water were carefully characterised and the potential enhancement mechanisms are also discussed.

2. Materials and experiment

2.1. Materials

Nanocomposites were prepared by diluting the commercialised Nanopox F400 resin with a diglycidyl ether of bisphenol A (DGEBA) epoxy resin, Araldite-F (Ciba-Geigy, Australia). The sample was prepared as follows. First, the epoxy resin was placed in a glass

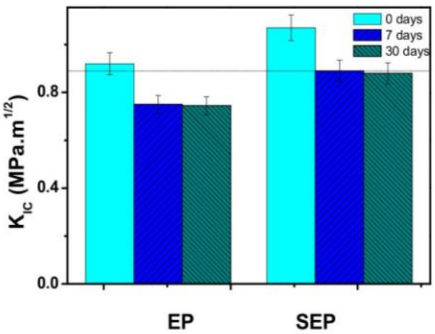

Fig. 4. The critical stress intensity factor K_{IC} of neat epoxy (EP) and nanosilica reinforced epoxy composite (SEP).

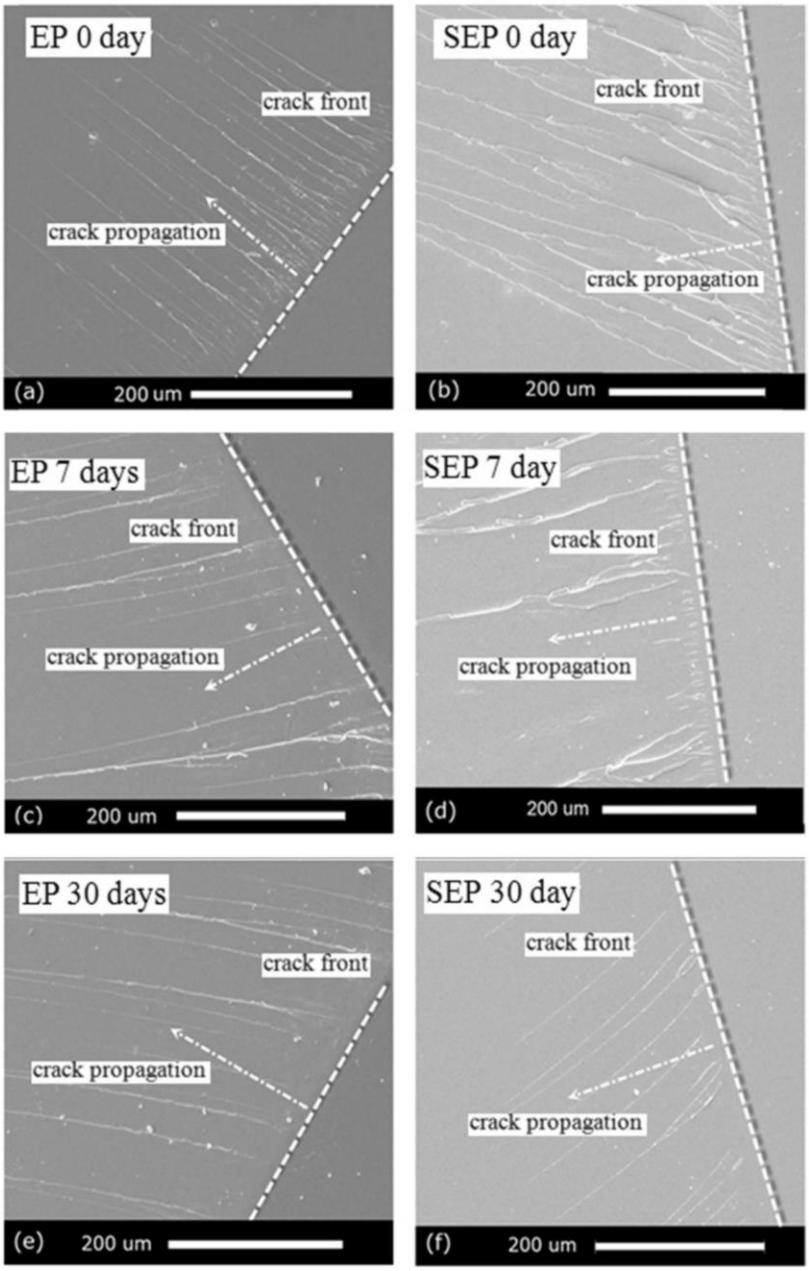

Fig. 5. SEM images of fracture surfaces of (a), (c) and (e) neat epoxy (EP) and (b), (d) and (f) nanosilica reinforced epoxy composite (SEP) after (a) and (b) 0 days, (c) and (d) 7 days, (e) and (f) 30 days of salt water immersion.

beaker on a hotplate (Thermo Scientific, Australia) at 120 °C,and an epoxy based nanocomposite, "Nanopox F400" (Evonik Hanse, Germany), used as a modifier, was added to achieve 2 wt.% nanosilica in the final epoxy matrix under fast and stable mixing using a laboratory homogeniser (Laboratory equipment, Australia). Then, the resin was stirred at 3000 rpm for 20 min to obtain a homogeneous mixture. Second, a piperidine (Sigma-Aldrich, Australia) hardener was added at a ratio of 100: 5 by weight while stirring slowly. The mixture was then cast into the specimen cavities of preheated silicon rubber moulds and cured at 120 °C for 16 h. The specimens in the oven were cooled gradually to room temperature before removal from the moulds. As controls for evaluation, neat epoxy was prepared separately. The steel coupons of Cor-ten B type (UNS number K11430) with a surface area of 1 cm^2 were used as the epoxy coating substrate for corrosion mechanism understanding.

2.2. Characterisations

5 wt.% NaCl solvent was used to simulate marine water. Samples were put under salt spray for periods of 0, 7 and 30 days

Table 2
Corrosion rate of epoxy (EP) and nanosilica-epoxy composite (SEP) after different periods of salt water immersion.

Corrosion rate (μm/year)	0 day	7days	30 days
EP	5.00 ± 0.25	34.50 ± 1.73	70.10 ± 3.50
SEP	0.80 ± 0.04	2.70 ± 0.14	3.00 ± 0.15

respectively, according to ASTM b117 standard [30]. Mechanical tensile tests were performed on a universal material testing machine (Instron, Model 5969, USA) at room temperature, in accordance with ASTM D638. The samples were stretched at a crosshead speed rate of 5.0 mm/min until failure; at least 5 specimens were tested for each sample. All fracture toughness tests were conducted on the Instron at room temperature. The fracture toughness of the cured epoxies was measured using the compact tension (CT) specimens according to ASTM D5045. The CT specimens had nominal dimensions of 48 mm × 48 mm × 10 mm. To minimize the effects of residual stress and residual plastic deformation around the pre-crack tip, a sharp pre-crack was introduced to the sample by razor blade tapping, using a specially designed clip to hold a fresh razor blade at the tip of the machined crack and tapping gently with a light hammer. All fracture tests were conducted a loading rate of 2 mm/min. Only those specimens which fulfilled the condition of a/W = 0.45–0.55 (a: the pre-crack length; W: the distance from the centre of the loading pin to the edge of the CT specimen) were used to calculate the critical stress intensity factor (K_{IC}). At least 6 CT specimens were tested for each group of epoxies. Scanning electron microscopes (CAMScan MX2500 SEM, the Netherlands) were employed to study the fracture surfaces of the CT specimens. Dynamic mechanical analysis (DMA) was performed on a TA Q800 dynamic mechanical analyzer, scanning from ambient temperature to 180 °C at a heating rate of 3 °C/min. Amplitude of 10 mm with a frequency of 1.0 Hz were chosen for all DMA measurements. The peak on the Tanδ curve was selected as the glass transition temperature (Tg) of the samples.

In order to apply a uniform thin barrier coating on the surface of steel, both resin and its hardener were diluted separately by acetone with a 1:1 weight ratio. Then put the steel on a spin coater (WS-400B-6NPP/LITE 150 mm, Laurell Technologies Corporation) at a rate of 1000 rpm for 15 s. Electrochemical measurements were conducted using a three-electrode system. The epoxy-coated steel coupon served as the working electrode, while the counter electrode and the reference electrode used were a platinum grid and a saturated calomel electrode (SCE) respectively. The corrosive solution was prepared by 5 wt.% aqueous NaCl solution. Two methods were used to test the anticorrosive capacity of epoxy-coated steel: electrochemical impedance spectroscopy (EIS) and potentiodynamic weak polarization. The EIS measurement was carried out periodically using a CH Instruments 1650D electrochemical analyzer. The steel was polarized at +10 mV around its open circuit potential (OCP) by an alternating current (AC) signal with its frequency ranging from 0.1 Hz to 1 mHz.

Analysis of the wearing properties of the specimens under a marine environment was conducted on a MCF-10 ring-on-ring rig with a sea water tank [31]. The principal scheme of the test rig is shown in Fig. 1. The upper ring specimens with geometry of about Φ28 × 20 × 7 mm were made from the test materials, while the lower ring specimens with geometry of Φ34 × 16 × 8 mm were made of AISI630 stainless steel. To improve the hardness and wear resistance of the stainless steel, the specimens were all processed by Quench-Polish-Quench (QPQ) [32]. The upper ring specimen rotated with the shaft of the electric motor, and the rotation speed could be controlled by a servo integration speed control system. The load applied on the lower ring specimen could be modified by regulating the oil pressure of the piston cylinder. A small submersible pump created a circulating water condition in the sea water reservoir. The friction coefficient f was calculated using the equation (1):

$$f = \frac{DF}{dN} \tag{1}$$

where F is friction force, N is load, D is nominal diameter of friction torque, d is actual diameter of friction torque. Tests were conducted for 20 min under a 5 wt.% salted water condition. The friction coefficient values given in this research were the mean values of data from five experiments. The worn surfaces of the specimens were observed by means of a SEM.

3. Results and discussion

3.1. Dynamic mechanical behaviour

Dynamic mechanical behaviour of the neat epoxy and the nanocomposite has been performed. Storage modulus and tanδ as a function of temperature are shown in Fig. 2. The glass transition temperature (T_g) of a specimen can be determined at the temperature where the tanδ rises up to its maximum value. From Fig. 2, it can be seen that with the adding of nanosilica, the T_g values are very close with 102 °C for the epoxy and 100 °C for the nanocomposite, suggesting that the nanocomposite have similar network characteristics as the epoxy [33]. The dynamic mechanical behaviours of epoxy were marginally affected by the addition of nanosilica and temperature, the storage modulus of the nanocomposite has a slight higher value than that of the epoxy at the same temperature, for example at 50 °C, the storage modulus of the epoxy is 2440 MPa while the nanocomposite has a value of 2490 MPa, which is consistent with the enhancement in stiffness as shown below in Table 1. The storage modulus of both samples decreased significantly until approaching their T_gs and had the similar values when the temperature was higher than Tg. So, with the small amount of nanosilica added, the epoxy dynamic mechanical behaviours have not been affected much.

3.2. Mechanical tensile properties under marine environment

To determine the effect of the nanosilica particles on the mechanical properties of the epoxy after immersion in salt water, tensile tests were performed on the neat epoxy and nanosilica enhanced composite specimens after periods of 0, 7 and 30 days of salt water immersion, respectively. Table 1 summarises the mechanical behaviours of the neat epoxy and nanosilica enhanced epoxy composite. From the results, with the low content (2 wt.%) of nanosilica in the epoxy matrix, the tensile strength and strain at break had values similar to those of neat epoxy. Meanwhile, after 7 and 30 days of salt water immersion, both the neat epoxy and the composite showed no obvious decrease in mechanical properties.

3.3. Fracture behaviours under marine environment

To further investigate the effect of nanosilica on the epoxy resin with different periods of salt water immersion, the fracture toughness of the neat epoxy and the nanocomposite were characterised. Fig. 3 shows exemplary load-crack opening displacement (COD) curves obtained from CT tests at room temperature for each material. It is observed that both neat epoxy and composite specimens undergo fracture in a brittle manner when the maximum load is reached, and the maximum loads for the nanocomposite are

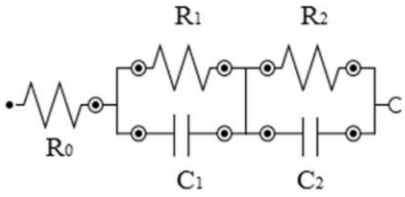

Fig. 6. A simple equivalent electric circuit model with R_0 associated with the electrolyte resistance, R_1 and C_1 of the resistance and capacitance of coating characteristic of its pore network structure, and R_2 and C_2 of the corrosion resistance of the steel and the double layer capacitance on the steel surface respectively.

Table 3
Parameters of the equivalent circuits for different materials in 5 wt.% NaCl solution.

Samples	R0	R1	R2	C1	C2
EP 0 day	233	2.11E + 05	6.38E + 05	1.86E − 09	1.77E − 06
SEP 0 day	226	1.24E + 07	9.86E + 06	5.35E − 10	1.89E − 08
EP 30 days	72	1.11E + 03	2.42E + 04	6.31E − 08	2.54E − 04
SEP 30 days	89	2.26E + 05	7.28E + 05	2.67E − 09	3.39E − 07

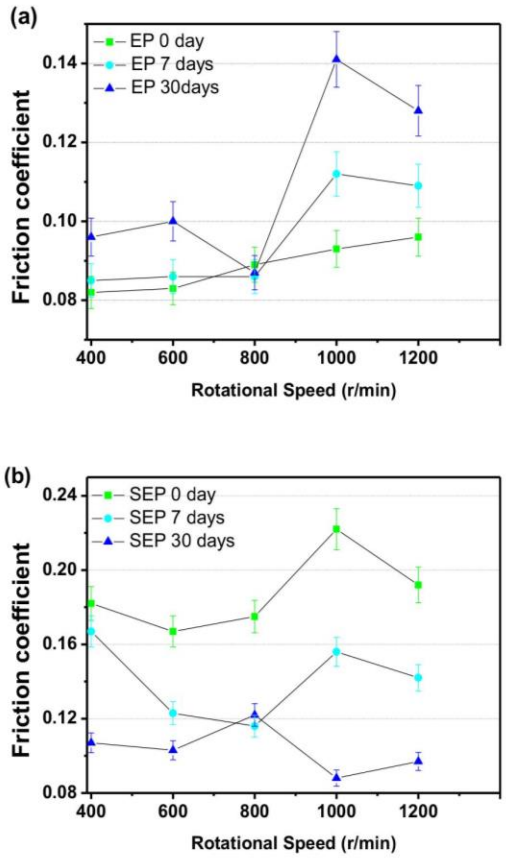

Fig. 7. Friction coefficient of (a) neat epoxy (EP) and (b) nanosilica reinforced epoxy composite (SEP) with different rotational speeds at a load of 400 N with different periods of salt water immersion.

obviously higher than those of the corresponding neat counterpart. Researchers have already found that a small amount of nanoparticle can increase the fracture toughness of epoxy resin [1–5]. In addition, after a period of salt water immersion, the maximum load decreases greatly for both neat epoxy and nanocomposite, making the fracture toughness of the specimens lower than that of the corresponding counterparts without salt water immersion.

Fig. 4 shows the critical stress intensity factor (K_{IC}) of the neat epoxy and the composite. Generally, the K_{IC} of the composite is significantly improved after nanosilica particles are incorporated [1–5]. After 7 days salt water immersion, the K_{IC} values of the neat epoxy and the nanocomposite decreased by about 18.5% and 16.8%, respectively. After 30 days salt water immersion, however, only a further 1% decrease of K_{IC} occurred in both the neat epoxy and the nanocomposite compared to the 7 days' immersion. It is clear that the sea water immersion decreased the fracture toughness in both the neat epoxy and the nanocomposite. However, the increment of fracture toughness due to the addition of nanosilica was able to complement the loss due to salt water immersion. Thus, the modified epoxy could work functionally in a marine environment, in preference to neat epoxy which would lose its functionality due to the loss of fracture toughness through salt water immersion.

Typical SEM micrographs of the fracture surfaces of the neat and the modified epoxies after salt water immersion are shown in Fig. 5. The fracture surface of the neat epoxy near the crack tip is glossy and brittle, as shown in Fig. 5(a). The fracture surfaces of the composite manifest small crack trajectories that are reflected and meander through the matrix, giving rise to the increased resistance to crack propagation, as shown in Fig. 5(b). After salt water immersion (Fig. 5(c) and (d)), many micro-cracks were generated along the crack initiation site. Meanwhile, comparing the neat epoxy without salt water immersion (Fig. 5(a)) and after immersion (Fig. 5(c) and (e)), the density of crack lines decreases in the fracture surfaces. According to previous research [34], the addition of a small amount of nanoparticles into the epoxy coating significantly reduces the rate of corrosion. The SiO_2 nanoparticles tend to occupy interspacing in the resin and serve to bridge more molecules in the interconnected matrix, leading to improve corrosion protection for the inner matrix.

3.4. Effect of nanoparticles on the corrosion resistance of coated steel

Table 2 shows the temporal evolution of instantaneous corrosion rate of steel coated by neat epoxy and the nanocomposite, at 0, 7 and 30 days immersion in 5 wt.% salt water, respectively. Without salt water immersion, the corrosion rate of neat epoxy is 6 times higher than the composite. After 7 and 30 days of immersion, its corrosion rate increased by 12 times and 23 times higher than that of the composite. The result shows the incorporation of small amount of nanosilica into the epoxy coating significantly reduced the corrosion rate of epoxy-coated steel in electrolytes.

In this research, the fitting of all EIS data was performed using a simple equivalent electric circuit model (Fig. 6) with two time constants well separated. R_0 is the solution resistance between the reference electrode and working electrode, and R_0 is not a property of the coating. Therefore it is not technically important in the analysis of coating performance. According to the EIS data in Table 3, without immersion in the 5 wt.% aqueous NaCl solutions, the adding of nanosilica increased the coating resistance R_1 by 58 times and reduced the coating capacitance C_1 by 3.5 times, indicating reducing coating porosity and improved barrier performance for corrosion protection [34]. The charge transfer resistance R_2 also increased by 15.5 times and the double layer capacitance C_2 reduced by 93.7 times, indicating enhanced corrosion resistance of steel at steel-electrolyte interface [35]. It was also observed that after 30 days immersion, the R_1 decreased and C_1 increased with R_1 dropped by 54.8 times and 190 times, and C_1 increased by 5 times

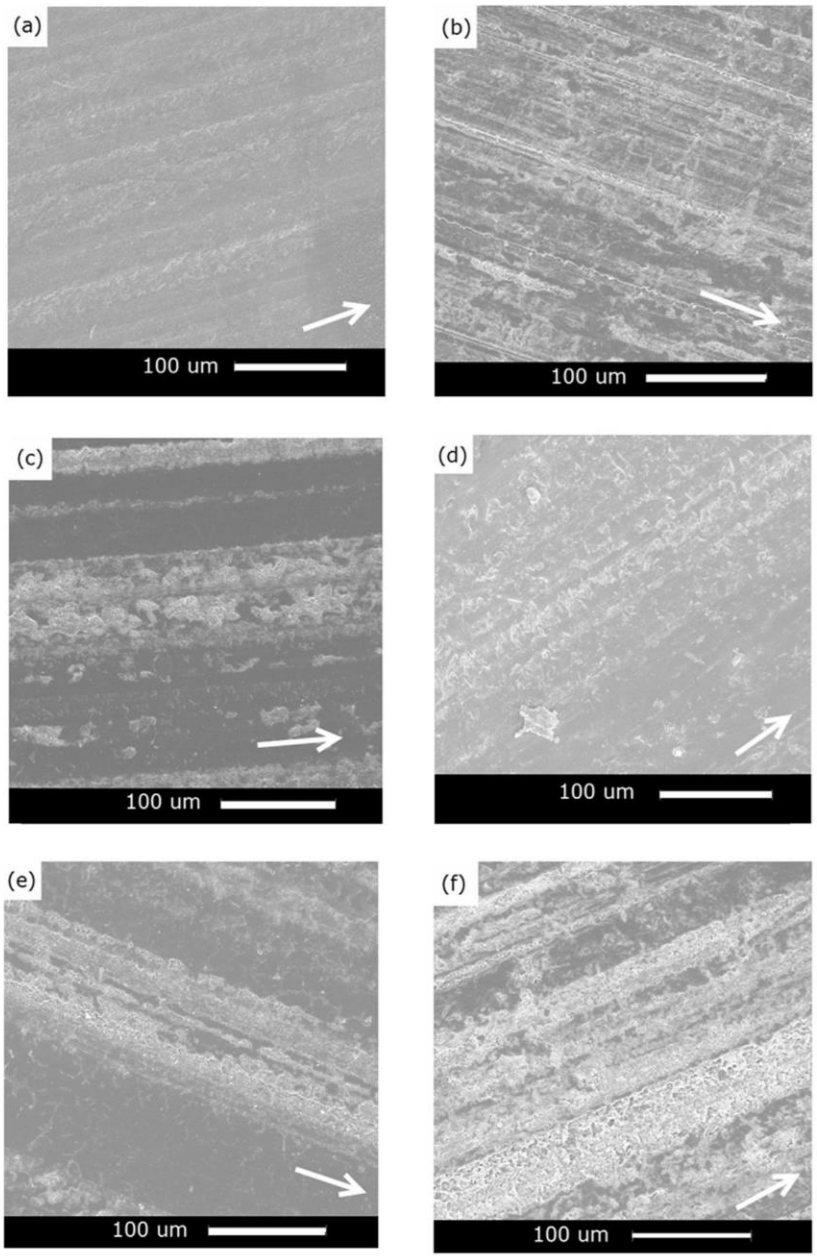

Fig. 8. SEM images of neat epoxy worn surfaces at a load of 400 N and rotation speeds of (a), (c) and (e) 600 r/min and (b), (d) and (f) 1000 r/min with (a) and (b) 0 days, (c) and (d) 7 days, and (e) and (f) 30 days of salt water immersion. The arrow in each image shows the rotation direction.

and 33.9 times for the nanosilica enhanced epoxy and the neat epoxy coatings, respectively. It indicated the entry of electrolyte into the epoxy coatings [36]. Meanwhile, after 30 days immersion, the charge transfer resistance R_2 reduced by 13.5 times and 26.3 times, and the double layer capacitance C_2 increased by 17.9 times and 143.5 times for the nanosilica enhanced epoxy and the neat epoxy coatings respectively. The nanosilica added into the epoxy signification improved barrier performance for enhanced the corrosion resistance.

3.5. Wear properties under marine environment

Fig. 7 shows the friction coefficient versus rotation speed of the neat epoxy and the nanocomposite after salt water immersion of 0, 7 and 30 days, respectively. It is observed that the friction coefficient of the neat epoxy increases continuously with the increase in wear rotation speeds at a load of 400 N applied on the specimens, as shown in Fig. 7(a). Moreover, the friction coefficient increases when the period of immersion increases. Fig. 8 shows the SEM images of neat epoxy worn surfaces with different salt water immersion periods at rotation speeds of 600 and 1000 rpm,

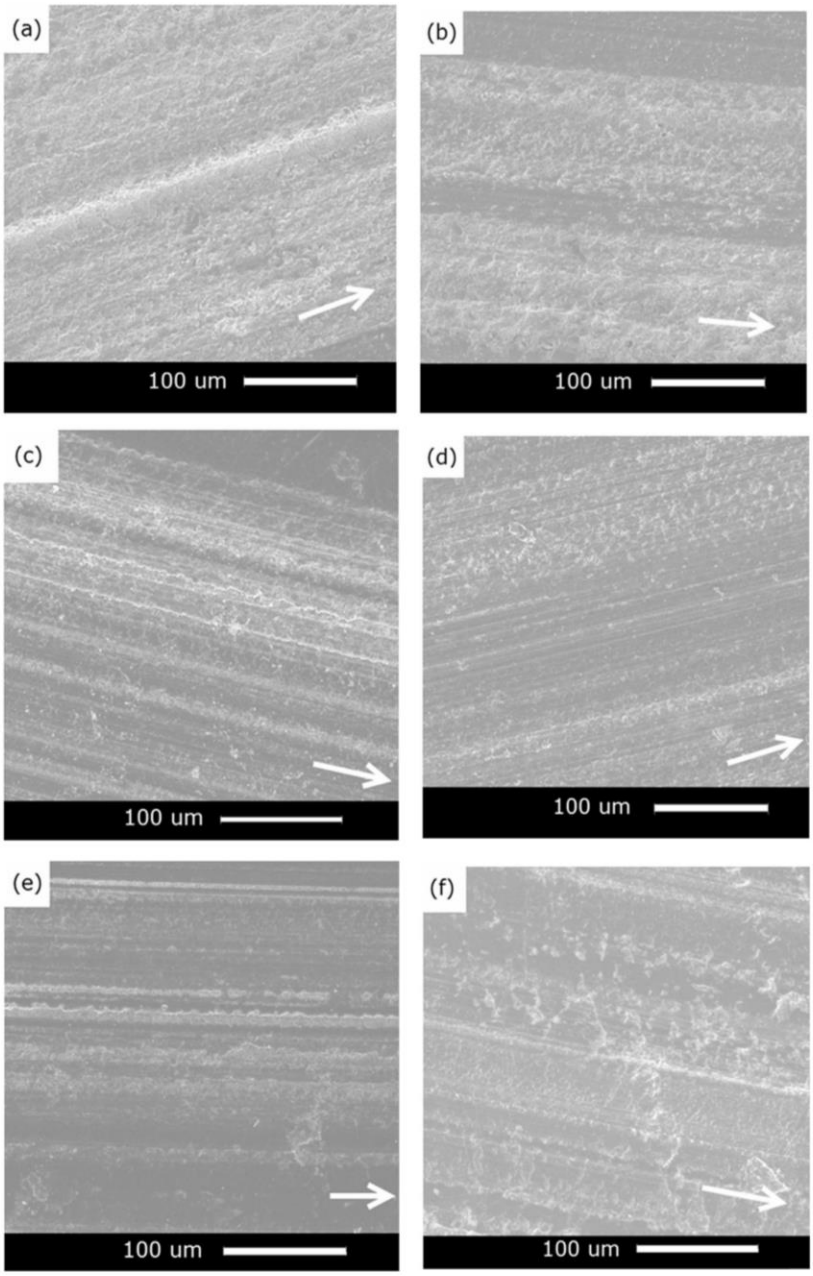

Fig. 9. SEM images of worn surfaces of nanosilica enhanced epoxy composite at a load of 400 N and rotation speeds of (a), (c) and (e) 600 r/min and (b), (d) and (f) 1000 r/min with (a) and (b) 0 days, (c) and (d) 7 days, and (e) and (f) 30 days of salt water immersion. The arrow in each image shows the rotation direction.

respectively. It is very clear that all the worn surfaces are tough. Fatigue wear has been regarded as a main mechanism responsible for the sliding of epoxy against a hard counterpart [37,38]. The model is based on the sub-surface crack nucleation and coalescence due to shear deformation of the softer surface induced by the traction of the harder asperities [39]. As shown in Fig. 8, scale-like removal of materials has left traces on the worn surface of the neat epoxy and careful examination of the wear grooves indicates that the distribution of flaws produced on the worn surfaces is in a discontinuous mode, similar to a previous report [40]. In comparisons of the low rotation speed of 600 rpm (Fig. 8(a), (c) and (e)) and the high rotation speed of 1000 rpm (Fig. 8(b), (d) and (f)), the high rotation speed generates more micro-cracks in the wear surfaces due to fatigue wear of the adhesive contact [41].

Fig. 7(b) shows the friction coefficient versus rotation speed of the composites with salt water immersion of 0, 7 and 30 days, respectively. Compared with the neat epoxy, the friction coefficient of the composite increases with nanoparticles added into the epoxy matrix from 0.082 to 0.182 before any salt water immersion under the rotational speed of 400 rpm at a load of 400 N. A more

Table 4
Tribological behaviors of different silica/epoxy nanocomposites.

Ref.	Materials/test parameters	Concentration (wt.%)		Specific wear rate ($\times 10^{-4}$ mm^3/Nm)	Friction coefficient
40	DGEBA, nano-SiO_2, SiO_2-g-PMMA (9 nm), DDS/Pin-on-ring, Load = 3 or 5 MPa, velocity = 0.4 m/s for 3 h	P = 3 MPa	0	2.05	0.58
			2.17 vol%	0.41	0.50
			2.17 vol% (g-PMMA)	0.11	0.40
		P = 5 MPa	0	9.00	0.58
			2.17 vol%	0.11	0.28
			2.17 vol% (g-PMMA)	0.02	0.25
41	DGEBA, Nanopox F400 (20 nm), Piperidine/Ball-on-plate, Load = 5 N, sliding speed = 0.1 m/s for 20 h		0	3.15	0.53
			4	5.38	0.65
			6	6.12	0.67
			8	6.72	0.69
			10	3.74	0.82
			20	2.07	0.90
Current study	DGEBA, Nanopox F400 (20 nm), Piperidine/Ring-on-ring, Load = 400 N, rotation speed = 1000 r/min for 20 min	0	0 day		0.09
			7 day		0.11
			30 day		0.14
		2	0 day		0.22
			7 day		0.16
			30 day		0.09

important observation is that after salt water immersion, the friction coefficient values of the nanocomposites are lower than those without salt water immersion and the composite with 30 days' immersion has the lowest value of 0.103. Meanwhile, the friction coefficient of the nanocomposite is not significantly increased with the increase in rotation speed compared to that of the neat epoxy. Fig. 9 shows SEM images of worn surfaces of the composite, which appear compact and rough. The friction coefficient was not increased due to uneven stress concentrations built up inside the epoxy, which might have been homogenised to some extent in the composites due to the effect of dispersion strengthening of the nanoparticles [40]. Bassaani et al. [42] suggested that the nominal pressure controls the interfacial stress between counterparts involved in such contacts, and hence the stability of transfer films. The addition of inorganic nanoparticles into polymers might increase the adhesion strength of a transfer film on the counter face [43,44]. It can be deduced that nanosilica not only acts as a load carrier in the composites but also helps to improve the bonding between the transfer film and the steel counter-face.

Table 4 listed the tribological behaviors of different nanosilica/epoxy composites. To overcome the disadvantages generated by loosened nanoparticle agglomerates dispersed in polymer composites, an irradiation grafting method has been applied to modify nanosilica by covalently bonding polyacrylamide (PAAM) onto the particles [40]. Sliding wear tests of the materials demonstrated that the frictional coefficient and the specific wear rate of nanosilica/epoxy composites were lower than those of the unfilled epoxy. Zhang et al. [41] reported that nanosilica particles did not improve the wear resistance of epoxy nanocomposites until the nanoparticle content exceeded a critical value, i.e., 10 wt.%, even though the frictional coefficient of the nanocomposites were improved with an increase in the content of nanosilica particles. Both the wear properties and mechanical properties were effectively increased. However; there was no simple correlation between the mechanical properties and wear properties of the nanocomposites [41]. Our study shows the similar trend that with the addition of nanosilica, the friction coefficient of the epoxy increased. However, with the long time salt water immersion (i.e., 30 days), the nanocomposite has a lower fraction coefficient than that of the epoxy.

4. Conclusion

We report using a commercially available epoxy composite with 2 wt.% nanosilica to enhance the mechanical behaviours of epoxy for different periods of salt water immersion. The neat epoxy and the nanocomposite were deleteriously affected by salt water immersion, with decreased fracture toughness values. However, the increment of fracture toughness due to the addition of nanosilica was able to complement the loss due to salt water immersion, rendering the modified epoxy able to work functionally in a marine environment to replace neat epoxy in terms of fracture toughness. Sea water immersion also caused an increase in the friction coefficient of epoxy with increases in immersion time and rotation speed, but the nanocomposite exhibited less variation with rotation speeds. More importantly, the friction efficient decreased with increasing immersion duration. The proposed mechanisms were also discussed.

Acknowledgments

Y Tang is grateful for the research support of a Premier's Research and Industry Fund Catalyst Research Grant (CRG 65), 2015-2016 and X Zhang is grateful for the support from Changjiang River Scientific Research Institute, Changjing Water Resources Commission, China (Grant No. CKWV2013209/KY).

References

[1] S.Q. Deng, L. Ye, K. Friedrich, Fracture behaviours of epoxy nanocomposites with nano-silica at low and elevated temperatures, J. Mater. Sci. 42 (2007) 2766–2774.
[2] T.H. Hsieh, A.J. Kinloch, K. Masania, A.C. Taylor, S. Sprenger, The mechanisms and mechanics of the toughening of epoxy polymers modified with silica nanoparticles, Polymer 51 (2010) 6284–6294.
[3] S. Sprenger, Fiber-reinforced composites based on epoxy resins modified with elastomers and surface-modified silica nanoparticles, J. Mater. Sci. 49 (2014) 2391–2402.
[4] Y. Tang, L. Ye, S. Deng, C. Yang, W. Yuan, Influences of processing methods and chemical treatments on fracture toughness of halloysite-epoxy composites, Mater. Des. 42 (2012) 471–477.
[5] Y. Tang, L. Ye, Z. Zhang, K. Friedrich, Interlaminar fracture toughness and CAI strength of fibre-reinforced composites with nanoparticles-a review, Compos. Sci. Technol. 86 (2013) 26–37.
[6] M. Hassan, K.R. Reddy, E. Haque, A.I. Minett, V.G. Gomes, High-yield aqueous phase exfoliation of graphene for facile nanocomposite synthesis via emulsion polymerization, J. Colloid Interface Sci. 410 (2013) 43–51.

[7] S.J. Han, H. Lee, H.M. Jeong, B.K. Kim, A.V. Raghu, K.R. Reddyd, Graphene modified lipophilically by stearic acid and its composite with low density polyethylene, J. Macromol. Sci. Part B Phys. 53 (2014) 1193–1204.
[8] K.R. Reddy, M. Hassan, V.G. Gomes, Hybrid nanostructures based on titanium dioxide for enhanced photocatalysis, Appl. Catal. A Gen. 489 (2015) 1–16.
[9] K.R. Reddy, B.C. Sin, K.S. Ryu, J.C. Kim, H. Chung, Y. Lee, Conducting polymer functionalized multi-walled carbon nanotubes with noble metal nanoparticles: synthesis, morphological characteristics and electrical properties, Synth. Met. 159 (2009) 595–603.
[10] R.S. Andre, A. Pavinatto, L.A. Mercante, E.C. Paris, L.H.C. Mattoso, D.S. Correa, Improving the electrochemical properties of polyamide 6/polyaniline electrospun nanofibers by surface modification with ZnO nanoparticles, RSC Adv. 5 (2015) 73875–73881.
[11] S.H. Choi, D.H. Kim, A.V. Raghu, K.R. Reddy, H. Lee, K.S. Yoon, H.M. Jeong, B.K. Kim, Properties of graphene/waterborne polyurethane nanocomposites cast from colloidal dispersion mixtures, J. Macromol. Sci. Part B Phys. 51 (2012) 197–207.
[12] K.R. Reddy, K.P. Lee, G.A. Iyenger, Self-assembly directed synthesis of poly (ortho-toluidine)-metal (gold and palladium) composite nanospheres, J. Nanosci. Nanotechnol. 7 (2007) 3117–3125.
[13] M. Hassan, K.R. Reddya, E. Haque, S.N. Faisal, S. Ghasemi, A.I. Minett, V.G. Gomes, Hierarchical assembly of graphene/polyaniline nanostructures to synthesize free-standing supercapacitor electrode, Compos. Sci. Technol. 98 (2014) 1–8.
[14] K.R. Reddy, B.C. Sin, C.H. Yoo, D. Sohn, Y. Lee, Coating of multiwalled carbon nanotubes with polymer nanospheres through microemulsion polymerization, J. Colloid Interface Sci. 340 (2009) 160–165.
[15] Y.P. Zhang, S.H. Lee, K.R. Reddy, A.I. Gopalan, K.P. Lee, Synthesis and characterization of core-shell SiO2 nanoparticles/poly(3-aminophenylboronic acid) composites, J. Appl. Polym. Sci. 104 (2007) 2743–2750.
[16] Y.R. Lee, S.C. Kim, H. Lee, H.M. Jeong, A.V. Raghu, K.R. Reddy, B.K. Kim, Graphite oxides as effective fire retardants of epoxy resin, Macromol. Res. 19 (2011) 66–71.
[17] E. Akbarinezhada, M. Ebrahimib, F. Sharifb, A. Ghanbarzadeha, Evaluating protection performance of zinc rich epoxy paints modified with polyaniline and polyaniline-clay nanocomposite, Prog. Org. Coat. 77 (2014) 1299–1308.
[18] Z. Shen, G.P. Simon, Y.B. Cheng, Comparison of solution intercalation and melt intercalation of polymer–clay nanocomposites, Polymer 43 (2002) 4251–4260.
[19] P.Y. Le Gac, V. Le Saux, M. Paris, Y. Marco, Ageing mechanism and mechanical degradation behavior of polychloroprene rubber in a marine environment: comparison of accelerated ageing and long term exposure, Polym. Degrad. Stabil. 97 (2012) 288–296.
[20] A.P. Mouritz, E. Geliert, P. Burchill, K. Challis, Review of advanced composite structure for naval ships and submarines, Compos. Struct. 53 (2001) 21–41.
[21] E.P. Gellert, D.M. Turley, Seawater immersion ageing of glass–fiber reinforced polymer laminates for marine applications, Compos. Part A 30 (1999) 1259–1265.
[22] J. Jin, J.J. Lee, B.S. Bae, S.J. Park, S. Yoo, K. Jung, Silica nanoparticle-embedded sol-gel organic/inorganic hybrid nanocomposites for transparent OLED encapsulation, Org. Electron 13 (2012) 53–57.
[23] I.A. Rahman, V. Padavettan, Synthesis of silica nanoparticles by sol-gel: size-dependent properties, surface modification and applications in silica-polymer nanocomposites-a review, J. Nano. Mat. 2012 (2012) 132424.
[24] W. Han, Y. Yu, L. Fang, M.R. Johnston, S.Z. Qiao, Y. Tang, Functionalised silica/epoxy nanocomposites with enhanced fracture toughness for large-scale applications, J. Compos. Mater 49 (2015) 1439–1447.
[25] P.C. Ma, N.A. Siddiqui, G. Marom, J.K. Kim, Dispersion and functionalization of carbon nanotubes for polymer-based nanocomposites: a review, Compos. Part A 41 (2010) 1345–1367.
[26] J.R. Potts, D.R. Dreyer, C.W. Bielawski, R.S. Ruoffet, Graphene-based polymer nanocomposites, Polymer 52 (2011) 5–25.
[27] K.S. Song, Y.Y. Zhang, J.S. Meng, E.C. Green, N. Tajaddod, H. Li, M.L. Minus, Structural polymer-based carbon nanotube composite fibers: understanding the processing-structure- performance relationship, Materials 6 (2013) 2543–2577.
[28] H. Qian, E.S. Greenhalgh, M.S.P. Shaffer, A. Bismarck, Carbon nanotube-based hierarchical composites: a review, J. Mater. Chem. 20 (2010) 4751–4762.
[29] S. Sprenger, Epoxy resins modified with elastomers and surface-modified silica nanoparticles, Polymer 54 (2013) 4790–4797.
[30] ASTM B117-11 Standard practice for operating salt spray (Fog) apparatus.
[31] W. Dong, S. Nie, A. Zhang, Tribological behaviour of PEEK filled with CF/PTFE/Graphite sliding against stainless steel surface under water lubrication, Proc. Inst. Mech. Eng. J.-J. Eng. 227 (2013) 1129–1137.
[32] G.J. Li, J. Wang, Q. Peng, C. Li, Y. Wang, B.L. Shen, Influence of salt bath nitrocarburizing and post-oxidation process on surface microstructure evolution of 17-4PH stainless steel, J. Mater. Process. Technol. 207 (2008) 187–192.
[33] S. Zeng, C. Reyes, J. Liu, P.A. Rodgers, S.H. Wentworth, L. Sun, Facile hydroxylation of halloysite nanotubes for epoxy nanocomposite applications, Polymer 55 (2014) 6519–6528.
[34] X. Shi, T.A. Nguyen, Z. Suo, Y. Liu, R. Avci, Effect of nanoparticles on the anticorrosion and mechanical properties of epoxy coating, Surf. Coat. Tech. 204 (2009) 237–245.
[35] Z.Z. Lazarevic, V.B. Miskovic-Stankovic, Z. Kacarevic-Popovic, D.M. Drazic, Determination of the protective properties of electrodeposited organic epoxy coatings on aluminium and modified aluminium surfaces, Corros. Sci. 47 (2005) 823–834.
[36] V.B. Miskovic-Stankovic, D.M. Drazic, Z. Kacarevic-Popovic, The sorption characteristic of epoxy coatings electrodeposited on steel during exposure to different corrosive agents, Corros. Sci. 38 (1996) 1513–1523.
[37] R. Bassani, G. Levita, M. Meozzi, G. Palla, Friction and wear of epoxy resin on inox steel remarks on the influence of velocity, load and induced thermal state, Wear 247 (2001) 125–132.
[38] W. Bonfield, B.C. Edwards, A.J. Markham, J.R. White, Wear transfer films formed by carbon fibre reinforced epoxy resin sliding on stainless steel, Wear 37 (1976) 113–121.
[39] N.P. Suh, The delamination theory of wear, Wear 25 (1973) 111–124.
[40] M.Q. Zhang, M.Z. Rong, S.L. Yu, B. Wetzel, K. Friedrich, Effect of particle surface treatment on the tribological performance of epoxy based nanocomposites, Wear 253 (2002) 1086–1093.
[41] J. Zhang, L. Chang, S. Deng, L. Ye, Z. Zhang, Some insights into effect of nanoparticles on sliding wear performance of epoxy nanocomposites, Wear 304 (2013) 138–143.
[42] R. Bassni, G. Levita, M. Meozzi, G. Palla, Friction and wear of epoxy resin on inox steel: remarks on the influence of velocity, load and induced thermal state, Wear 247 (2001) 125–132.
[43] C.J. Schwartz, S. Bahadur, Studies on the tribological behaviour and transfer film-counter face bond strength for polyphenylene sulphide filled with nanoscale alumina particles, Wear 237 (2000) 261–273.
[44] Q. Wang, J. Xu, W. Shen, W. Liu, An investigation of friction and wear properties of nanometer Si_3N_4 filled PEEK, Wear 196 (1996) 82–86.

Chapter 6: Polydopamine as sizing on carbon fibre surfaces for enhancement of epoxy laminated composites

6.1 Introduction and significance

In this chapter, we reported that dopamine polymerization on carbon fibre (CF) surface can be a new sizing method to increase the adhesion ability of carbon fibre and epoxy. So, significantly reinforced interfacial fracture toughness and impact strength was reported for the CFRP laminates. The highlights in this work include:

1. We reported that polydopamine (PDA) can increase the stability of crack growth as sizing on CF surfaces. The crack propagation behaviour changed from a saw-tooth-shaped curve in neat CFRP laminates to a relative smooth trending curve in PDA-CFRP laminates.
2. We found that the fracture micro-mechanism in neat CFRP was primarily interfacial debonding, however, in PDA-CFRP, it was the combination of fibre/epoxy debonding, epoxy/epoxy debonding and fibre pull-out.
3. We found that the PDA sizing enhanced the interfacial layer by single fibre pull-out test, which improved the load transfer ability between epoxy and CF surfaces.

This section is included as it appears as a journal paper published by **Wei Han**, Hongping Zhang, Javad Tavakoli, Jonathan Campbell and Youhong Tang. Polydopamine as sizing on carbon fibre surfaces for enhancement of epoxy laminated composites. ***Compos Part A*** 2018; 107:626-632.

6.2 Polydopamine as sizing on carbon fibre surfaces for enhancement of epoxy laminated composites

Composites Part A 107 (2018) 626–632

Contents lists available at ScienceDirect

Composites Part A

journal homepage: www.elsevier.com/locate/compositesa

Polydopamine as sizing on carbon fiber surfaces for enhancement of epoxy laminated composites

Wei Han[a], Hong-Ping Zhang[a,b], Javad Tavakoli[a], Jonathan Campbell[a], Youhong Tang[a,*]

[a] College of Science and Engineering, Flinders University, South Australia 5042, Australia
[b] School of Materials Science and Engineering, Southwest University of Science and Technology, Mianyang, Sichuan 621010, China

ARTICLE INFO

Keywords:
A. Carbon fibres
B. Delamination
Fibre/matrix bond
Surface properties

ABSTRACT

Carbon fiber reinforced polymer (CFRP) laminate normally has plastic dominant crack propagation behavior, inducing potential insecurity in the safety and reliability of structures in practical applications. In this study, we report a simple process to increase the stability of crack growth by using polydopamine (PDA) as sizing on the surface of carbon fiber (CF) fabric. The crack propagation behavior changes from a saw-tooth-shaped curve in neat CFRP laminate to a relatively smooth trending curve in PDA coated CFRP laminate with increased Mode I interlaminar fracture toughness. Enhanced impact strength and interlaminar shear strength of PDA coated CFRP laminates is also observed. A single fiber pull-out experiment and morphological study reveal that, with PDA coating on CF fabrics, cracks tend to fracture through the epoxy matrix rather than between fiber and matrix interfaces. The use of PDA as sizing on the CF contributes to improving the load transfer between the CF and the polymer matrix by enhancing the interfaces between the epoxy and the CF, increasing the friction of the fractured interface, reducing unstable crack growth, and thereby enhancing interfacial fracture toughness and impact performance.

1. Introduction

Carbon fiber reinforced polymer (CFRP) is an extremely strong and light material that is now widely used in high value-added commodities wherever high strength-to-weight ratio and rigidity are required, such as in aerospace, automotive, civil engineering, and sports goods applications. For example, the Airbus A350 XWB was built of 52% CFRP including wing spars and fuselage components. One of the major problems that limits the stability and application range of CFRP is that the binding polymer is often a thermoset resin such as epoxy, but epoxy is a brittle material, so that the mechanical properties of the epoxy resin, especially the strength and toughness, still need to be further enhanced [1–8]. Engineers face unique challenges in failure detection of CFRP because failure occurs catastrophically due to the brittle fracture mechanics. Meanwhile, CFRP tends to be strengthened in the fiber horizontal direction when load-bearing occurs in that direction, but is weak in the vertical direction so that little load could be placed in that direction. Study of the mechanisms of the fracture toughness of CFRP is mainly governed by the subsequent debonding appearance, i.e., debonding between the carbon fiber (CF) and polymer matrix, fiber pull-out, and delamination between the CFRP sheets. Therefore, many researchers have studied how to toughen the epoxy resins using nanoparticles such as nanosilica, nanohalloysite, carbonaceous nanoparticles like graphene nanoplatelets, and graphene oxide [9–15]. However, large scale CFRP production using nanofillers has been a challenge due to many unsolved problems such as nanoparticle agglomeration or achieving homogeneous dispersion of nanoparticles of a high weight/volume portion in resins while maintaining relatively low viscosity. Viscous resin systems cannot easily impregnate continuous fibers or fiber fabrics using fabrication methods based on resin infusion, and filtering of dense fiber bundles against agglomerated nanofillers can lead to severe segregation and depletion of nanofillers in matrices [16,17].

Alternatively, the use of sizing to improve the poor adhesions between fiber and matrix is a promising approach. Such methods include wet chemical or electrochemical oxidation, plasma treatment, gas phase oxidation, etc. Bubert et al. used oxygen plasma treatment of fibers and changed the surfaces by forming a 1 nm thickness functional group layer to improve the wetting properties of CF [18]. Xu et al. demonstrated that both γ-ray co-irradiation grafting and pro-irradiation grafting were effective methods to improve the interfacial adhesion of composites [19]. But these methods had drawbacks of high energy consumption and could eventually impair the fiber strength.

Polydopamine (PDA) has been reported to have significant

* Corresponding author.
E-mail address: youhong.tang@flinders.edu.au (Y. Tang).

https://doi.org/10.1016/j.compositesa.2018.02.003
Received 15 November 2017; Received in revised form 17 January 2018; Accepted 2 February 2018
Available online 03 February 2018

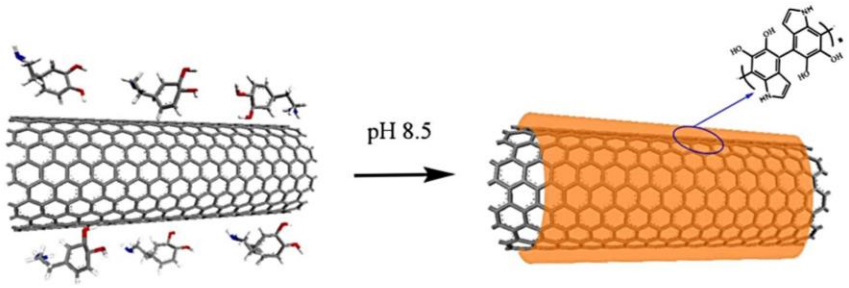

Fig. 1. Schematic diagram of polydopamine coating on a CF surface and acting as sizing. (For interpretation of the references to colour in this figure legend, the reader is referred to the web version of this article.)

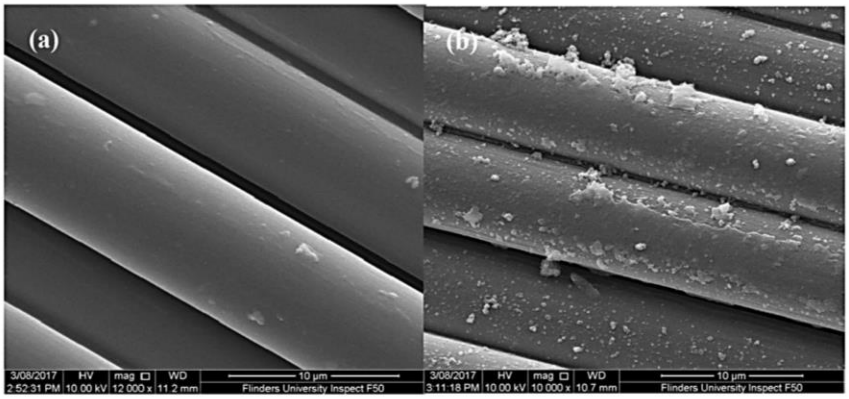

Fig. 2. SEM images of (a) CF and (b) PDA -CF surfaces.

applications in numerous biomedical and mechanical areas, due to its superior adhesion to various material surfaces including metals, oxides, polymers, and ceramics [20]. Researchers have reported that PDA could also be applied to modify the surface of nanofillers such as carbon nanotubes [21], graphene [22], and clay [23], revealing its excellent ability to improve the mechanical, thermal, and electromagnetic interference shielding performance of polymer matrices. PDA has also been used to modify the surface of short CFs; the resulting epoxy composites showed distinct improvement in tensile strength and Young's modulus [21]. Recently, much research has been focused on enhancing the interface of CFRP composites, but the effects of PDA sizing modifications of CF surfaces on the crack propagation mechanisms of CFRP have seldom been reported.

In this study, a feasible method of fabricating CFRP by simply using PDA as sizing on carbon fabric has been reported. With 3.2 wt% PDA acting as sizing of CF, the modified CFRP composites can significantly improve energy transfer between CFs and epoxy resin, increasing the friction of fractured interfaces, reducing unstable crack growth, and thereby enhancing interfacial fracture toughness and dynamic impact performance.

2. Experiments

2.1. PDA sizing on carbon fiber fabrics

To prepare PDA coated CF fabrics, first 4 g of dopamine (Sigma, Australia) was dissolved in a mixed solution of deionized water (4000 mL) and aqueous solution of TRIS (3.6 g, 1000 mL) with magnetic stirring for 30 min. Meanwhile, CF fabrics (200 gm plain-weave, Hexcel, USA) were placed in a container. Then, the mixed solution was transferred to the container. The container was shaken by a benchtop orbital shaker (Labec, Australia) at 100 rpm for 24 h at ambient temperature. The modified CF fabrics were collected and washed several times with deionized water to remove the residual dopamine, until the scrubbing filtrate became colorless. Finally, the modified CF fabrics were dried in a vacuum oven at 40 °C for 24 h. Fig. 1 shows a schematic drawing of the use of PDA as sizing on the CF surface.

2.2. Preparation of PDA-CFRP composites

A vacuum bagging method was used to fabricate the CFRP composites. First, a release film was placed on a plate and the PDA modified CF fabrics were laid upon it. A release-agent coated release film 10 um in thickness was inserted in the middle layer of the fabrics to induce the initial delamination. After that, a peel cloth and a diversion mesh were placed on the fabrics and all were sealed in a vacuum bag. Raw resin with the major ingredients of a bisphenol A epoxy (Kinetix R246 epoxy resin, ATL Composites Pty. Ltd., Australia) and a hardener (Kinetix H126, ATL Composites Pty Ltd, Australia) were added at the ratio of 100:25 by weight percent. After layup, epoxy resin was pumped into the vacuum bag. The final panel was cured in a vacuum bag and placed in a hot press machine (Carver Inc. USA) at the pressure of 15 KN/m^2 in room temperature for 24 h. The measured cured panel thickness was approximately 3 mm for all plates and the fiber volume was nearly 32 vol.%. Test specimens were cut from the cured panels by bandsaw cutting and polished by a polisher. As controls for evaluation, pure CFRP panels were prepared separately.

2.3. Characterizations

Thermal stability analysis was performed using a thermogravimetric analysis apparatus (Hi-Res TGA 2950, TA instruments, USA). The tests

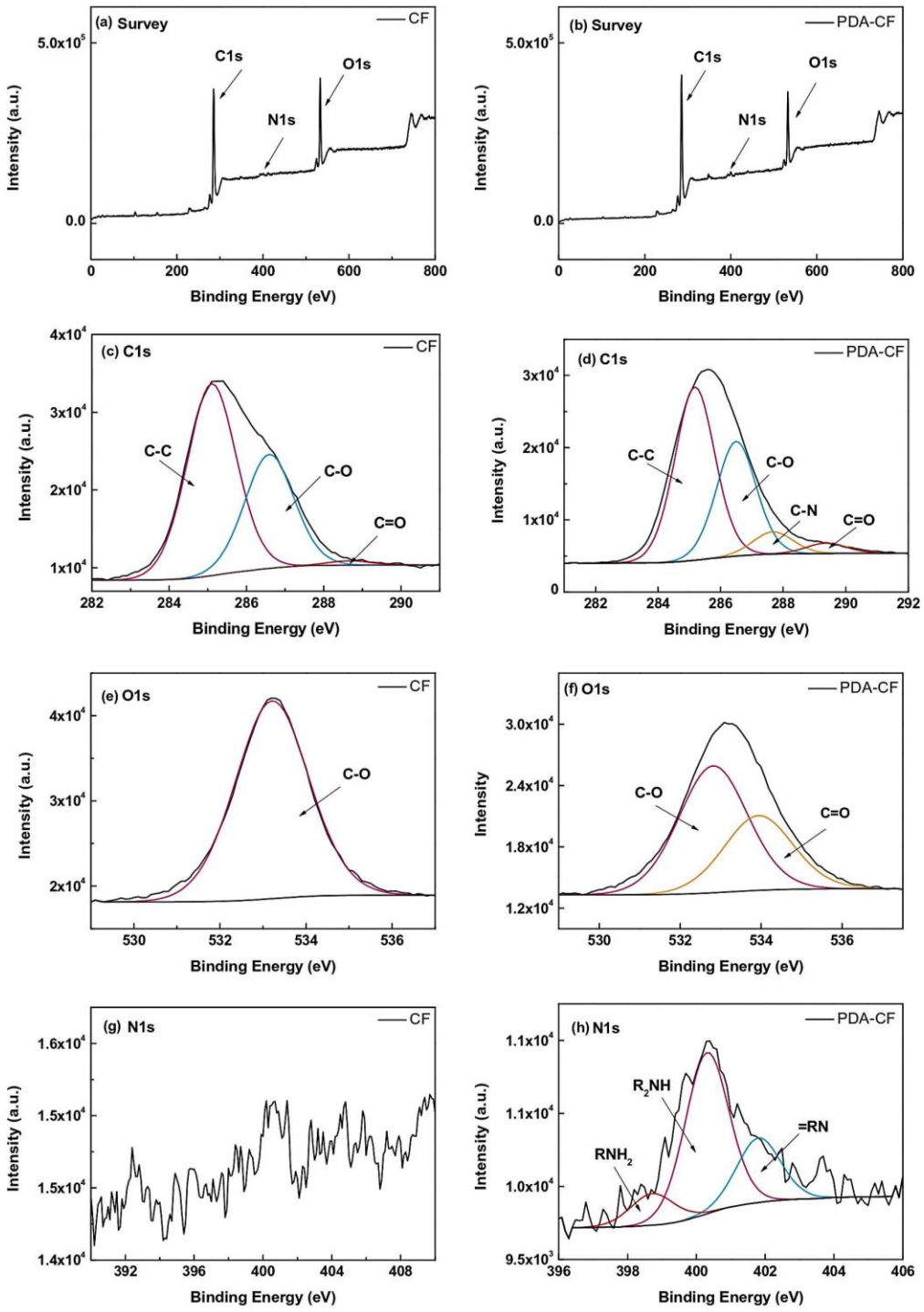

Fig. 3. The XPS spectra of CF and PDA-CF. (For interpretation of the references to colour in this figure legend, the reader is referred to the web version of this article.)

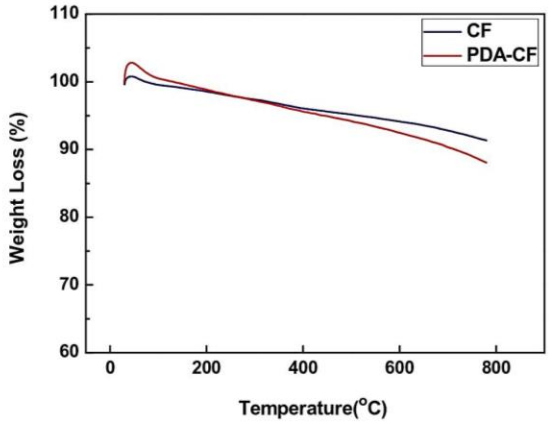

Fig. 4. Thermogravimetric analysis shows the PDA concentration on the CF surfaces. (For interpretation of the references to colour in this figure legend, the reader is referred to the web version of this article.)

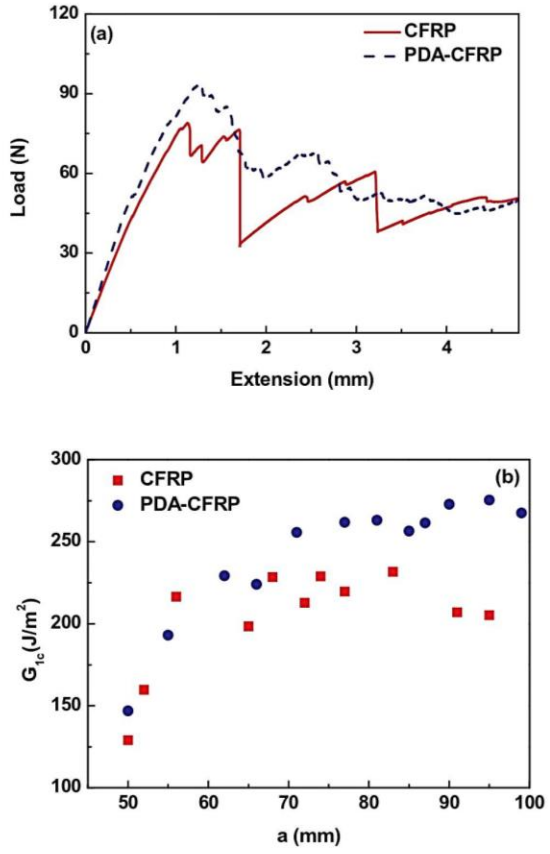

Fig. 5. (a) Load-crack opening displacement (COD) curves and (b) mode I delamination crack growth resistance curves (R-curves) of CFRP and PDA-CFRP laminates. (For interpretation of the references to colour in this figure legend, the reader is referred to the web version of this article.)

were carried out under N_2 atmosphere at the heating rate of 10.0 °C/min from room temperature to 780.0 °C. The specimens were vacuum-dried for 2 days at room temperature before TGA characterization. The XPS was performed in an ultrahigh vacuum (UHV) apparatus (SPECS, Germany) with a nonmonochromatic X-ray source for Mg Kα (1253.6 eV) radiation. High-resolution XPS spectra were fitted using combined Gaussian–Lorentzian peaks with background correction using the Shirley method.

The Mode I interlaminar fracture toughness was measured using double cantilever beam (DCB) tests performed by an Instron (U.S.) test machine fitted with a 500 N load cell in accordance with the ASTM D 5528 standard. The dimensions of the DCB specimen were 125 × 25 × 3 mm. Specimens were clamped in the jaws of the test machine via the block hinges, and specimens were loaded at the rate of 1 mm/min while the load–displacement data was recorded. Fracture surfaces of the test specimens were examined and imaged using scanning electron microscopes (Inspect F50, FEI, U.S.). The SEM samples are selected from the pre-crack tip area and all samples were sputter-coated with a ~200 Å layer of gold to minimize charging.

The interlaminar shear strength (ILSS) was measured using a 3-point short beam strength test following the ASTM D-2344 standard. The samples were loaded in a 3-point bending configuration as a simply supported beam using cylindrical supports with the diameter of 3 mm and a loading nose with the diameter of 6 mm. The sample length was 6 times the sample thickness and the span width was set at 4 times the sample thickness. ILSS was calculated from the equation: $\mathrm{ILSS} = 0.75 * \frac{P}{b * d}$, where P represents the breaking load, b is the width, and d is the thickness of the specimen. At least 8 specimens per batch were tested.

The experiments for the single fiber pull-out test were performed on a Bio Tester 5000 (Cellscale biomaterials testing, Canada) with an optical microscope and two adjustable lights to make *in situ* observations. A constant test speed of 0.05 mm/min was applied.

Impact tests were performed using a 75 J impact hammer on a pendulum impact testing machine (Australian Calibrating Services, Model AC-PIT501J-2, Australia) at room temperature following the ISO-179 standard.

3. Results and discussion

3.1. Effects of polydopamine on carbon fiber

Polydopamine modified CF was prepared using a well-established method based on catecholic chemistry, as shown in Fig. 1. The polymerization mechanism of dopamine has been well studied in previous research [21]. The polymerization of PDA on CF surface was examined by SEM (Fig. 2). As shown, the raw CF surface is quite smooth, but the PDA-CF surface is fairly coarse, indicating that the dopamine successfully polymerized on the CF surfaces. Similar morphology was reported by Wang et al. [22].

The surface chemical composition of CF and PDA-CF was investigated by XPS. Fig. 3a and b show the survey scan XPS spectra of CF and PDA-CF, respectively. The elemental concentrations demonstrate clearly that carbon and oxygen are the main surface constituents on both CF and PDA-CF surfaces. Nitrogen is found in small concentrations on CF surfaces, possibly deriving from the incomplete carbonization of the PAN-based precursor. Correspondingly, the carbon and nitrogen concentrations are increased on the surfaces of PDA-CF, indicating the sizing of the PDA on the CF surfaces. Fig. 3c–h are the spectra of C1s, O1s, and N1s on the CF and PDA-CF surfaces, respectively. The high-resolution spectra of PDA are similar with reported XPS results [24]. Compared with CF, it can be seen that the carbon peak at 287.7 eV is contributed from C—N and the peak at 289.4 eV is contributed from C—O—C. As shown in Fig. 3h, the XPS spectrum of the N 1s of PDA-CF is composed of 3 subpeaks centered at 398.5 eV (—NH_2), 400.1 eV (—NH—), and 401.8 eV (—N=), respectively. These migrations of N1s binding energy indicate that *in situ* spontaneous oxidative polymerization of dopamine on the CF surface was successfully carried out. Thermogravimetric curves of CF and PDA-CF are shown in Fig. 4. The

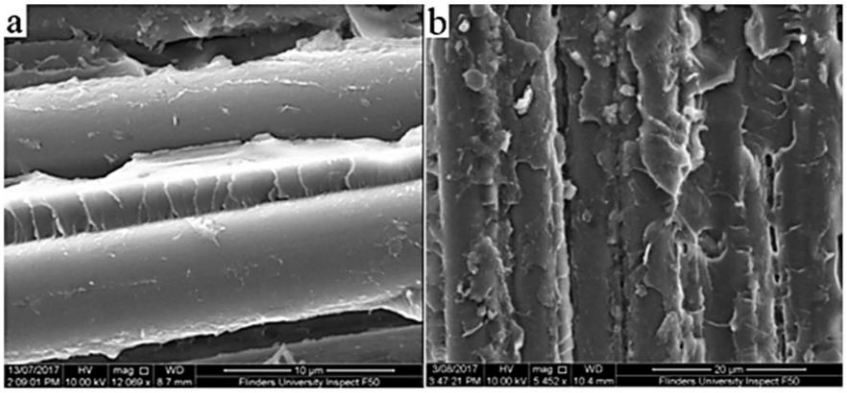

Fig. 6. SEM images of the fracture surfaces after Mode I interlaminar fracture testing of (a) CFRP and (b) PDA-CFRP.

Table 1
Improvement of ILSS by different sizing methods.

Sizing material		Epoxy	ILSS (MPa)	Improvement (%)	Ref.
PDA		Kinetix R246	67.7	25.1	Current study
Polyacrylate emulsion		Epoxy 616	92.7	14.2	[27]
Aqueous epoxy resin emulsion	E-1	Epoxy 616	82	1	[28]
	E-2		88	8.4	
	E-3		93	14.5	
J1 sizing		Epoxy 616	84	17.8	[29]
Hit sizing			85.7	20.2	
Oxidized Epoxy sizing		Epikote Rimr 935	40 58	17.6 70.6	[30]

weight loss of CF fabric is 8.7 wt% which comes from the original functional groups on the CF surface. In contrast, the PDA-CF fabric loses about 11.9 wt% of the total weight at 800 °C, the 3.2% weight loses confirming the successful coating of PDA.

3.2. Mechanical property evaluation in CFRP

To evaluate the effectiveness of this surface modification strategy, Mode I interlaminar fracture toughness was studied in both neat CFRP and PDA-CFRP laminates. Fig. 5(a) shows exemplary load-crack opening displacement (COD) curves obtained from Mode 1 fracture toughness tests at room temperature. The CFRP laminate shows a saw-tooth shaped curve formed as the force alternately increases and decreases, demonstrating unstable energy release during crack propagations. In the PDA-CFRP laminate, however, the force increases regularly to the peak level and then declines in a relatively smooth movement. The COD curves indicate that the PDA-CFRP laminate has the ability to provide an equivalent peak load while eliminating the saw-tooth effect in comparison with the behavior of the pure CFRP laminate. These curves also give evidence that the PDA sizing on the CF is an effective functional method for improving the interfacial load [22]. Fig. 5(b) shows typical Mode I delamination crack growth resistance curves (R-curves) for the CFRP laminates calculated from the load–displacement curves. Generally, the R-curves increase over about the first 10 mm of crack growth, probably as a result of the gradual formation of a fiber bridging zone behind the crack front, that is the main toughening process in these CF composites [25]. The R-curve of the CFRP shows

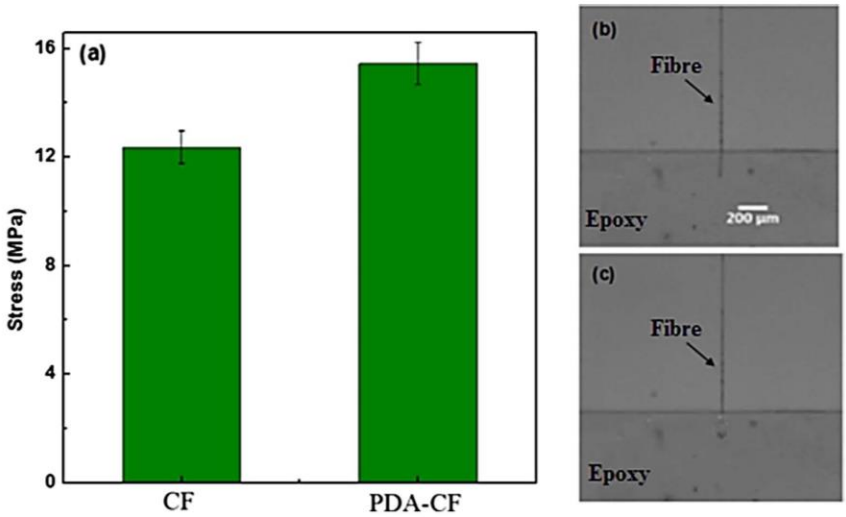

Fig. 7. (a) Interfacial stress for CF and PDA-CF by single fiber pull-out testing, and images of a single fiber (b) before and (c) after pull-out. (For interpretation of the references to colour in this figure legend, the reader is referred to the web version of this article.)

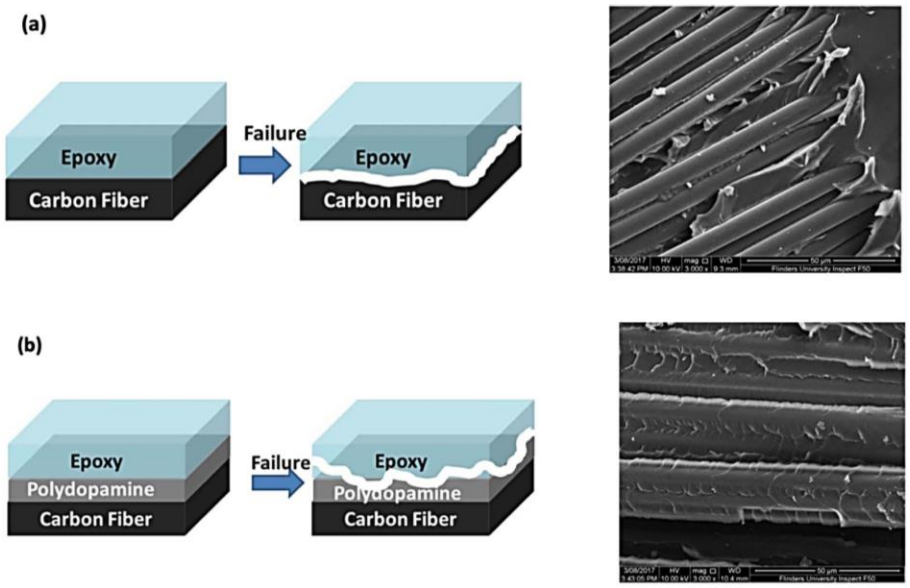

Fig. 8. Schematic diagrams and micro-morphologies of interface failure in (a) CFRP and (b) PDA-CFRP laminates. (For interpretation of the references to colour in this figure legend, the reader is referred to the web version of this article.)

that the interlaminar fracture toughness values (G_{IC}) remain stable in the range of 200–250 J/m^2 beyond the 10 mm of delamination length. Meanwhile, during the DCB test, it was observed that the delamination propagation progressed at a random rate and in an unstable manner in the neat CFRP laminate. However, the G_{IC} values in the R-curve of the PDA-CFRP laminate are different, with a slight increase in the range of 225–275 J/m^2 beyond 10 mm of delamination length, and during the DCB test the delamination increases at a reasonably consistent speed and in a stable manner. The calculated average value of G_{1c} propagation is 216.34 J/m^2 and 261.25 J/m^2 for the neat CFRP and PDA-CFRP laminates, respectively, showing a 21% increment for the laminate with PDA sizing on fiber surfaces.

The energy translation under the impact test damage mechanisms of the CFRP mainly involve 3 forms: (a) matrix powdering: the brittle epoxy matrix is crushed and forms into debris and powder. Meanwhile, microcrack propagation represents further efforts to convert the impact energy into surface free energy; (b) delamination: the impact energy continues, and delamination occurs around the interface between the CF and epoxy or between the epoxy matrix. Because the delamination transitional zone is very narrow, only small part of the impact energy can be consumed; (c) fiber fracture: at the end of the impact process, when the impact strain is greater than the fiber strain, the CF fails [26]. Fiber/matrix debonding or sliding and fiber pull-out occurs, that consumes a large proportion of the impact energy. The impact strength of the CFRP and PDA-CFRP laminates is 99.89 and 120.12 kJ/m^2 respectively, with about 20% increment with PDA added into the CFRP laminate. The PDA introduced as sizing on the fiber surfaces to enhance the interfacial strength between fiber and epoxy (as shown in the SEM images in Fig. 6) mainly contributes to the energy conversion form of delamination with the aforementioned damage mechanisms of CFRP, hence increasing the impact strength of the laminate.

The interlaminar shear strength (ILSS) under three-point bending load was found to vary significantly by virtue of the sizing. Composite samples made from PDA-CF had an ILSS of 67.7 Mpa, 25% higher than that of neat CFRP with an ILSS of 54.1 MPa. Table 1 summarizes recent reports of different sizing methods used to improve the ILSS of CFRP. Yuan et al. reported that using the polyacrylate emulsion sizing method increased the ILSS of CFRP by 14.2% [27]. Zhang et al. reported that the use of aqueous epoxy emulsion with different epoxy concentrations of 10%, 15%, and 20%. The best ILSS result came from sizing with 20% epoxy concentration aqueous emulsion with 14.5% increment [28]. Similarly, Kafi et al. reported that electrolytic oxidation and epoxy sizing enhanced the ILSS of CFRP by 17.6% and 70.6% respectively [29]. Zhang et al. reported that with a commercial sizing agent J1 purchased from Japan, the aqueous epoxy emulsion Hit sizing enhanced the ILSS of CFRP from 17.8% to 20.2% [30]. However, the epoxy sizing method, that included three stages of production, namely carbonization, electrolytic oxidation, and epoxy sizing, was environmentally unfriendly compared with our PDA sizing method.

3.3. Enhancement mechanism

To help understand the interface behavior and enhancement mechanism of the PDA-CFRP laminate, the fracture surfaces after the Mode I interlaminar fracture testing were observed by SEM. As evidenced by the clean, smooth surfaces of the fibers shown in Fig. 6(a), the fracture micromechanism in the neat CFRP laminate is primarily interfacial debonding. The epoxy resin completely detaches from the CF surfaces because of the weak bond in the interfaces. This finding indicates that CF/epoxy debonding is the dominant mechanism of shear failure, and the most likely failure site of the laminates is still the interface. Meanwhile, smooth crazes on the matrix indicate poor resistance to crack propagation. In contrast, in the SEM micrographs as shown in Fig. 6(b), a significantly different interface microstructure appears in the PDA-CFRP fracture surfaces. The fiber/epoxy debonding is combined with resin/resin debonding and fiber pull-out. Significant plastic deformation is shown clearly and an amount of epoxy still adheres to the PDA-CF surface. The development of these microstructures would be related to the enhanced interactions between PDA and epoxy that are responsible for the improvement in interlaminar strength.

Micromechanical tests using single fiber pull-out experiments can simply evaluate interface strength directly [31]. Fig. 7 shows the interfacial stress of CF and PDA-CF from single fiber pull-out testing. The interfacial stress τ was obtained using the equation:

$$\tau = \frac{F}{\pi DL} \quad (1)$$

where F is the measured maximum test load from the test and πDL signifies the fiber-embedded area, which is the product of the fiber-embedded length in epoxy and the circumferential length. The interfacial stress of the CF/epoxy and PDA-CF/epoxy is 12.36 MPa and 15.44 MPa respectively, demonstrating a 25% increment for the PDA/CF epoxy. The PDA enhancement of interfacial strength may results from the PDA attached on the CF surface that increases the friction of the fractured interface. Schematic diagrams and micro-morphologies of interface debonding in the neat CFRP are displayed in Fig. 8(a), where the epoxy resin tends to wholly detach from the CF and retain a comparatively clean surface. This response is due to the weak binding energy between the epoxy and CF surfaces. In the DPA-CFRP on the other hand, the crack propagates through the interfaces of PDA /epoxy with non-straight crack paths and the leftover fiber is captured by the abundant epoxy, as shown in Fig. 8(b). This response indicates that the PDA sizing enhances the interface layer by improving the load transfer between epoxy and CF surfaces.

4. Conclusions

In this study, 3.2 wt% polydopamine was used as sizing on CF fabrics. The results showed that the modified CF fabrics significantly enhanced the mechanical properties of the CFRP laminates, with a 20–25% increment obtained for Mode I interlaminar fracture toughness, impact strength, interlaminar shear strength, and interfacial stress compared with pure CFRP. More importantly, the crack propagation behavior during the Mode I interlaminar fracture toughness evaluation changed from saw-tooth-shaped curves for neat CFRP to relatively smooth curves. The enhanced mechanism was mainly due to significantly increased interfacial bonding between epoxy resin and CF by the PDA sizing. The PDA layer also improved the load transfer between CFs and polymer matrix, increasing the fractured interface friction and reducing unstable crack growth, and thereby enhancing interfacial fracture toughness and impact performance.

Acknowledgement

W Han is grateful for the research training program scholarship during his PhD study.

References

[1] Maugis D. Subcritical crack growth, surface energy, fracture toughness, stick-slip and embrittlement. J Mater Sci 1985;20(9):3041–73.
[2] Ghasemnejad H, Hadavinia H, Aboutorabi A. Effect of delamination failure in crashworthiness analysis of hybrid composite box structures. Mater Des 2010;31(3):1105–16.
[3] Maksimov IL. Thermomechanical fracture instability and stick-slip crack propagation. Appl Phys Lett 1989;55(1):42–4.
[4] Kinloch AJ, Williams JG. Crack blunting mechanisms in polymers. J Mater Sci 1980;15:987–96.
[5] Lee C, Wei X, Kysar JW, Hone J. Measurement of the elastic properties and intrinsic strength of monolayer graphene. Science 2008;321(5887):385–8.
[6] Qin W, Vautard F, Drzal LT, Yu J. Mechanical and electrical properties of carbon fiber composites with incorporation of graphene nanoplatelets at the fiber-matrix interphase. Compos Part B 2015;69:335–41.
[7] Hamer S, Leibovich H, Green A, Avrahami R, Zussman E, et al. Mode I and mode II fracture energy of MWCNT reinforced nanofibril mats interleaved carbon/epoxy laminates. Compos Sci Techno 2014;90:48–56.
[8] Lee SH, Kim H, Hang S, Cheong SK. Interlaminar fracture toughness of composite laminates with CNT-enhanced nonwoven carbon tissue interleave. Compos Sci Technol 2012;73(1):1–8.
[9] Wicks SS, Villoria RG, Wardle BL. Interlaminar and intralaminar reinforcement of composite laminates with aligned carbon nanotubes. Compos Sci Technol 2010;70(1):20–8.
[10] Chi Y, Chu J, Chen M, Li C, Mao W, et al. Directly deposited graphene nanowalls on carbon fiber for improving the interface strength in composites. Appl Phys Lett 2016;108(21):211601.
[11] Ning H, Li J, Hu N, Yan C, Liu Y, et al. Interlaminar mechanical properties of carbon fiber reinforced plastic laminates modified with graphene oxide interleaf. Carbon 2015;91:224–33.
[12] Irshidat MR, Al-Saleh MH, Almashagbeh H. Effect of carbon nanotubes on strengthening of RC beams retrofitted with carbon fiber/epoxy composites. Mater Des 2016;89:225–34.
[13] Zhang RL, Gao B, Du WT, Zhang J, Cui HZ, et al. Enhanced mechanical properties of multiscale carbon fiber/epoxy composites by fiber surface treatment with graphene oxide/polyhedral oligomeric silsesquioxane. Compos A: Appl Sci Manuf 2016;84:455–63.
[14] Zhang P, Ma L, Fan F, Zeng Z, Peng C, et al. Fracture toughness of graphene. Nat Commun 2014;5:3782. http://dx.doi.org/10.1038/ncomms4782.
[15] Zhang X, Fan X, Yan C, Li H, Zhu Y, Li X, et al. Interfacial microstructure and properties of carbon fiber composites modified with graphene oxide. ACS Appl Mater Interfaces 2012;4(3):1543–52.
[16] Yu B, Jiang Z, Tang XZ, Yue CY, Yang J. Enhanced interphase between epoxy matrix and carbon fiber with carbon nanotube-modified silane coating. Compos Sci Technol 2014;9:131–40.
[17] Han W, Tang YH, Ye L. Chapter 8: carbon fiber-reinforced polymer laminates with nanofiller-enhanced multifunctionality. In: Beaumont PWR, editor. Struct Integrity Carbon Fiber Composit. Switzerland: Springer; 2017. p. 171–89.
[18] Bubert H, Ai X, Haiber S, Heintze M, Brüser V, Pasch E, et al. Basic analytical investigation of plasma-chemically modified carbon fibres. Spectrochim Acta B 2002;57:1601–10.
[19] Xu ZW, Huang YD, Zhang CH, Liu L, Zhang YH, Wang L. Effect of c-ray irradiation grafting on the carbon fibres and interfacial adhesion of epoxy composites. Compos Sci Technol 2007;67:3261–70.
[20] Lynge ME, Westen R, Postma A, Stadler B. Polydopamine- a nature-inspired polymer coating for biomedical science. Nanoscale 2011;3(12):4916–28.
[21] Liu X, Wang G, Liang R, Shi L, Qiu J. Environment-friendly facile synthesis of Pt nanoparticles supported on polydopamine modified carbon materials. J Mater Chem A 2013;1:3945–53.
[22] Wang PF, Yang JL, Liu WS, Tang XZ, Zhao K, Lu XH, et al. Tunable crack propagation behavior in carbon fiber reinforced plastic laminates with polydopamine and graphene oxide treated fibers. Mater Des 2017;113:68–75.
[23] Liaqat F, Tahir MN, Huesmann H, Daniel P, Kappl M, et al. Ultrastrong composites from dopamine modified-polymer-infiltrated colloidal crystals. Mater Horiz 2015;2:434–41.
[24] Qu KG, Zheng Y, Jiao Y, Zhang XX, Dai S, Qiao SZ, et al. dual heteroatom-doped carbon nanotubes for highly efficient overall water splitting. Adv Energy Mater. 2017:1602068.
[25] Mouritz AP, Baini C, Herszberg I. Mode I interlaminar fracture toughness properties of advanced textile fiberglass composites. Compos part A 1999;30:859–70.
[26] Yang Y, Xu F, Zhang YQ, Liu GW. Experimental study on the impact resistance of 2D plain-woven C/SiC composite. Ceram Int 2014;10(40):15551–9.
[27] Yuan X, Zhu B, Cai X, Liu J, Qiao K, Yu J. Optimization of interfacial properties of carbon fiber/epoxy composites via a modified polyacrylate emulsion sizing. Appl Surf Sci 2017;401:414–23.
[28] Zhang R, Huang Y, Liu L, Tang Y, Su D, Xu L. Influence of sizing emulsifier content on the properties of carbon fibers and its composites. Mater Des 2012;33:367–71.
[29] Kafi A, Huson M, Creighton C, Khoo J, Mazzola L, et al. Effect of surface functionality of PAN-based carbon fibres on the mechanical performance of carbon/epoxy composites. Compos Sci Technol 2014;94:89–95.
[30] Zhang RL, Zhang JS, Zhao LH, Sun YL. Sizing agent on the carbon fibers surface and interface properties of its composites. Fiber Polym 2015;16:657–63.
[31] Sethi S, Ray BC. Environmental effects on fibre reinforced polymeric composites: evolving reasons and remarks on interfacial strength and stability. Adv Colloid Interface Sci 2015;217:43–67.

Chapter 7: Synergistic effects of coupling agent and nanoparticle on enhancing glass fibre/ polystyrene laminates for harsh environment applications

7.1 Introduction and significance

In this chapter, we reported the synergistic effects of halloysite nanotubes (HNTs) and industrial-used coupling agent (APTES) enhanced mechanical properties of the glass fibre/polystyrene laminates. It was found that impact, interlaminar shear strength and interlaminar fracture toughness of the reinforced laminates significantly decreased under marine environments. The highlights in this work include:

1. We have studied different concentration of HNTs and APTES reinforced polystyrene composites and found the best concentration was 1 wt% HNTs combination 1 wt% APTES in polystyrene laminate in this study.

2. We found that in the optimised concentrations of HNTs and APTES, the interlaminar shear strength and mode 1 interlaminar fracture toughness increased by 26.5% and 11.5%.

3. We found that APTES acted as a barrier that reduced the permeability of the laminates and significantly decreased deterioration effects under marine environment. With the synergistic effects of HNTs and APTES in the laminates, the interlaminar shear strength and mode 1 interlaminar fracture toughness decreased by 13.9% and 6.4% after 3 weeks salt water immersion. However, 24.8% and 12.3% decreasing was reported in the same time for the unmodified laminates.

This section is included as it submitted and under review as a journal paper by **Wei Han**, Nazila Dehbari, Sheng Chen, Tom Jung, Karl Sammut and Youhong Tang. Synergistic effects of coupling agent and nanoparticle on enhancing glass fibre/ polystyrene laminates for harsh environment applications**,** ***Appl Compos Mater*** 2017 (Under review).

7.2 Synergistic effects of coupling agent and nanoparticle on enhancing glass fibre/ polystyrene laminates for harsh environment applications

Applied Composite Materials

Synergistic effects of coupling agent and nanoparticle on enhancing glass fiber/ polystyrene laminates for harsh environment applications

--Manuscript Draft--

Manuscript Number:	
Full Title:	Synergistic effects of coupling agent and nanoparticle on enhancing glass fiber/ polystyrene laminates for harsh environment applications
Article Type:	Original Research
Keywords:	nanoparticles; coupling agent; interlaminar fracture toughness; interlaminar shear strength; marine environment; laminate
Corresponding Author:	Youhong Tang Flinders University Adelaide, SA AUSTRALIA
Corresponding Author Secondary Information:	
Corresponding Author's Institution:	Flinders University
Corresponding Author's Secondary Institution:	
First Author:	Wei Han
First Author Secondary Information:	
Order of Authors:	Wei Han
	Nazila Dehbari
	Sheng Chen
	Tom Jung
	Karl Sammut
	Youhong Tang
Order of Authors Secondary Information:	
Funding Information:	Premier's Research and Industry Fund with a Catalyst Research Grant (CRG 65) — A/Prof Youhong Tang
Abstract:	Polymeric laminate materials have been favored for use in harsh environments. Due to the structural differences between polymers and crystalline solids, polymers in general can dissolve molecules such as water and gas, this attribute implies that the permeability of the polymer affects some properties such as interface shear strength and interface fracture strength. In this study, a small amount of commercially-available halloysite nanotubes (HNTs) and an industrial-used coupling agent (APTES) were mechanically mixed with modified glass fiber (GF)/polystyrene (PS) laminates. HNTs and APTES synergistically enhanced the mechanical properties of the PS matrix. When the modified PS composite was incorporated with GF to form a laminate, the interlaminate shear strength and model I interlaminar fracture toughness also clearly increased. The synergistic effects of HNTs and APTES in the GF/PS laminate significantly decreased the deterioration of the mechanical properties of the laminate under marine environments. Due to commercial availability, the low cost of the raw material, and the simple fabrication method, this modified laminate has the potential for large-scale applications in such harsh environments.

Synergistic effects of coupling agent and nanoparticle on enhancing glass fiber/ polystyrene laminates for harsh environment applications

Wei Han [1, 2], Nazila Dehbari [1, 2], Sheng Chen [3], Tom Jung [4], Karl Sammut [2], Youhong Tang [1, 2 *]

[1] Centre for NanoScale Science and Technology, College of Science and Engineering, Flinders University, South Australia 5042, Australia

[2] Centre for Maritime Engineering, Control and Imaging, College of Science and Engineering, Flinders University, South Australia 5042, Australia

[3] School of Chemistry, The University of New South Wales, NSW 2052, Australia

[4] RPC Pipe Systems, South Australia 5160, Australia

[*] Corresponding author. Tel.: +61-8-820 12138; Email: youhong.tang@flinders.edu.au (Y Tang)

Abstract

Polymeric laminate materials have been favored for use in harsh environments. Due to the structural differences between polymers and crystalline solids, polymers in general can dissolve molecules such as water and gas, this attribute implies that the permeability of the polymer affects some properties such as interface shear strength and interface fracture strength. In this study, a small amount of commercially-available halloysite nanotubes (HNTs) and an industrial-used coupling agent (APTES) were mechanically mixed with modified glass fiber (GF)/polystyrene (PS) laminates. HNTs and APTES synergistically enhanced the mechanical properties of the PS matrix. When the modified PS composite was incorporated with GF to form a laminate, the interlaminate shear strength and model I interlaminar fracture toughness also clearly increased. The synergistic effects of HNTs and APTES in the GF/PS laminate significantly decreased the deterioration of the mechanical properties of the laminate under marine environments. Due to commercial availability, the low cost of the raw material, and the simple fabrication method, this modified laminate has the potential for large-scale applications in such harsh environments.

Keywords: nanoparticles; coupling agent; interlaminar fracture toughness; interlaminar shear strength; marine environment; laminate

1. Introduction

Glass fiber reinforced plastic (GRP) has been widely used in water pipe infrastructure, irrigation, and environmental management applications, particularly where performance, strength, and endurance are essential. GRP pipes offer superior corrosion resistance, durability, and hydraulic flow characteristics. They also present a cost-effective upfront and lifelong solution with low installation, maintenance, and operating costs. GRP pipes are sandwich-type composites using polymer mortar with relatively high rigidity at the core of pipe walls and GRP with a high tensile strength at the inner and outer surfaces of pipe walls. Their weight per unit length is 20-25% of that of cast iron pipes and 10% of that of centrifugally reinforced concrete pipes [1]. Moreover, GRP pipes have good on-site applicability due to their superior impact resistance. Their flat inner surface allows smooth flow of water and their improved corrosion resistance provides a semi-permanent life span. In a life cycle cost analysis, GRP pipes have reportedly shown good economic efficiency that is comparable to that of cast iron pipes. However, laminated composites exhibit poor matrix-dominated and interlaminar properties [2-6] and are often susceptible to various cutting and polishing process. The major problem is that the binding polymer is often a thermoset resin such as polystyrene (PS), polyether ether ketone, polyimide, polyphenylene sulfide, polyether ketone, polyamide, etc. Of the industry grade, PS is the most commonly used resin in GRP pipe manufacturing due to it is an inexpensive resin per unit weight. However, PS is a rather poor barrier to oxygen and water vapor, and it is hard and rather brittle, which means the mechanical properties of resin, especially the strength and toughness, still needs to be further enhanced in order to increase the stability and application range of the composites. Meanwhile, GRP pipes have been promoted for use in harsh environment such as the marine environment. Their great advantage over metals is their low density and the fact that they are not susceptible to corrosion. In the marine environment, however, sea water has other chemical properties, such as oxidizing or reducing abilities, and these properties must be properly considered [7-9].

The incorporation of nanofillers such as halloysite nanotubes (HNTs), carbon nanotubes (CNTs), and nanosilica has successfully improved interlaminar properties of polymeric materials [10, 11]. HNTs exhibit unique structural properties such as high specific stiffness and specific strength. Yet the addition of HNTs to GRP composites brings its

own challenges. The main challenge is to uniformly disperse them in the polymer matrix in order to obtain high interfacial areas through which stress can be transferred from the weak matrix to the strong HNTs. Effective stress transfer through the HNTs/polymer interface is the key to obtain superior mechanical properties in HNT modified laminated composites [12, 13]. The large surface area of these composites due to their nanosized dimension and very high aspect ratios of the fillers are desirable for efficient load transfer, but are undesirable for providing high attraction forces between the HNTs themselves, leading to the formation of agglomerates when they come close to each other in the polymer matrix. Various methods for dispersing HNTs in polymer resins have been reported in the literature, such as stirring, sonication, and calendaring. 3-aminopropyltriethoxysilane (APTES) has been widely utilized industrially as a coupling agent to enhance adhesion between organic materials and inorganic substrates [12, 13]. Three ethoxy groups in each APTES molecule can be hydrolyzed and react not only with active groups (e.g.–OH) on the inorganic substrate, but also with those of other APTES molecules, resulting in a polymerized network [14].

The present investigation focuses on the development of a very economical and efficient fabrication method for a structural PS based GRP laminate modified with HNTs and APTES. The results show synergistic enhanced interlaminate shear strength of the GRP laminate with HNTs and APTES added together. Due to the commercial availability and low-cost of the raw material and the simple fabrication method, these modified laminates have the potential for large-scale applications, especially under marine environments.

2. Experimental

2. 1 Composite preparation

The raw resin, polyplex EPS-1 (Nuplex Industries Pty Ltd, Australia), is a mixture with the major ingredient of styrene monomer. HNTs (Sigma-Aldrich, Australia) and APTES (Sigma-Aldrich, Australia) were added into the resin and the mixture was stirred with a fast and stable mixing laboratory homogenizer (Laboratory equipment, Australia) at 3000 r/m for 30 minutes to obtain a uniform distribution resin mixture. Then, Curox A-390 (Nuplex Industries Pty Ltd, Australia) hardener was added at a ratio of 100:1 by weight percent (wt%) while being stirred well. The mixture was then cast into the specimen

cavities of silicon rubber molds and cured at room temperature for 24 hrs. As controls for evaluation, pure resin and resins modified with HNTs or APTES were prepared. Table 1 shows the components of the prepared composite samples.

Table 1. Components of composite samples (wt%)

	PS	PS1H	PS3H	PS5H	PS1A	PS2A	PS1A1H	PS1A2H	PS2A3H
PS	100	99	97	95	99	98	98	97	95
HNT	0	1	3	5	0	0	1	1	3
APTES	0	0	0	0	1	2	1	2	2

2. 2 Laminate preparation

Laminate panels were prepared using the vacuum bag laminating method [15]. First, hand-stacking random direction of short cut ECR-glass fiber (length =~ 10 cm, RPC Australia) was used to obtain the desired weight, and then a release-agent coated release film was inserted (10 um thickness) into the middle of the layer to induce the initial delamination. After layup, PS resin was pumped into the glass fiber. Four groups of resin were selected to fabricate the laminates: pure polystyrene (GF/PS), 1% APTES modified PS (GF/PS1A), 1% HNTs modified polystyrene (GF/PS1H), and 1% APTES with 1% HNTs modified polystyrene resin (GF/PS1A1H). The panels were cured in a vacuum bag and placed in a hot press machine (Carver Inc. USA) at the pressure of 15 KN/m^2 at room temperature for 24 hrs. The cured panel thickness was found to be approximately 3 mm for all panels and the fiber volume ratio was about 32%. Test specimens were cut from the cured panels by a bandsaw.

2. 3 Characterizations

Rheological dynamic strain sweep measurements of the uncured PS, HNTs/PS, and APTES/PS were performed on a rheometer (Anton Paar Physica MCR301, USA) at room temperature, with the frequency set to 10 rad/s for each test to evaluate the fillers' effects on the viscosity of the PS resin. Mechanical tensile tests were performed on a universal material testing machine (Instron, Model 5969, USA) at room temperature with a 50 KN load cell, in accordance with ASTM D638. The samples were stretched at a crosshead

speed rate of 5.0 mm/min until failure; at least 5 specimens were tested for each sample. Impact tests were conducted using a 25 J impact hammer and performed on a pendulum impact testing machine (Australian Calibrating Services, Model AC-PIT501J-2, Australia) at room temperature following the ISO-179 standard.

Mode I interlaminar fracture toughness was measured by double cantilever beam (DCB) tests in accordance with the ASTM D 5528 standard. The dimensions of a DCB specimen were 125 mm×25 mm×3 mm. Specimens were clamped in the jaws of the test machine via the block hinges and were loaded at a rate of 1 mm/min while load-displacement data was recorded. Each specimen was initially loaded to the point of failure, at which time the crack could propagate a short distance (generally around 3-5 mm) before the specimen was unloaded.

The interlaminar shear strength (ILSS) was measured using a 3-point short beam strength test following the ASTM D-2344 standard. The samples were loaded in a 3-point bending configuration as a simply supported beam using cylindrical supports with the diameter of 3 mm and a loading nose with the diameter of 6 mm. The sample length was 6 times the sample thickness, the width was twice the thickness, and the span length was set to 4 times the sample thickness. The maximum observed load for each sample was used for calculating the ILSS values. The dynamic properties of the GRP laminates with various HNTs/APTES loadings were evaluated using the dual cantilever bending fixture in a dynamic mechanical analyzer (DMA) (TA Q800, USA). The temperature was increased from 40 °C to 160 °C at a heating rate of 5 °C/min using a 10 μm amplitude with a frequency of 1 Hz for all samples.

Environmental tests were performed to simulate the marine environment. 5 wt% NaCl solvent was used to simulate marine water. Samples were put under salt spray for periods of 0, 1, and 3 weeks in accordance with the ASTM b117 standard. Then, the samples were washed by running water and oven dried for 24 hrs at 60 °C. Mode I interlaminar fracture toughness in the dried samples was measured by DCB tests in accordance with the ASTM D 5528 standard and interlaminar shear strength was tested following the ASTM D-2344 standard. Scanning electron microscopes (SEM, Inspect F50, FEI, USA) were employed to study the fracture surfaces of the specimens.

3. Results and discussion

3. 1 Processability of HNTs/APTES modified PS composites

The viscosity of the uncured neat PS and HNTs/APTES modified PS at room temperature is shown in Fig. 1. The neat PS has a viscosity of about 1.27 Pa·s. With 1 wt% HNTs or APTES added in PS, the viscosity increases slightly to 1.51 Pa.s (PS1H) and 1.60 Pa·s (PS1A), respectively. Combined with 1 wt% HNTs and 1 wt% APTES, the viscosity is 1.33 Pa s (PS1A1H). With such low values, HNTs modified PS resin would easily impregnate glass fiber layers as the neat PS does in the vacuum bagging process.

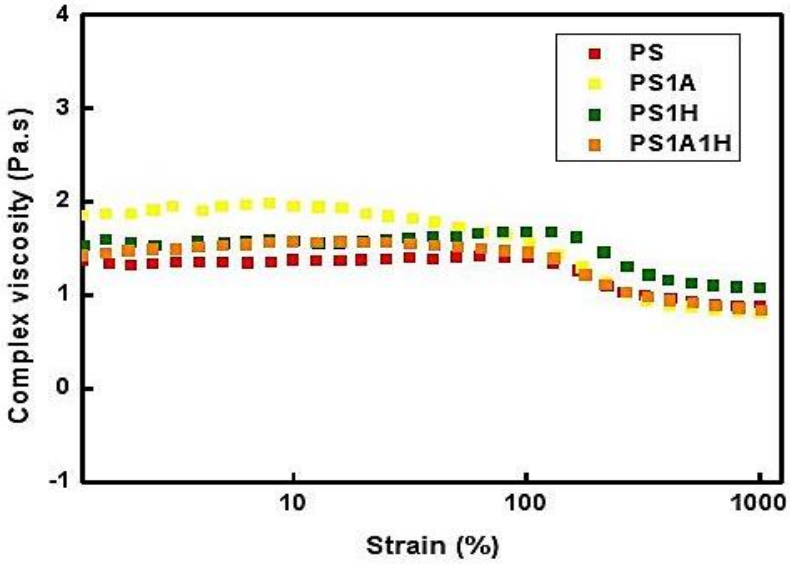

Fig. 1. Dynamic strain sweep of neat PS and PS composites before curing at room temperature.

3. 2 HNTs and APTES synergistically toughening polystyrene

The impact strengths of neat PS and the PS composites are shown in Fig. 2(a). The impact strengths of PS1H and PS3H are 6.6 and 13.2 kJ/m^2, respectively, higher than that of the neat PS (5.7 kJ/m^2). With the combination of HNTs and APTES, the impact strengths are 17.3, 14.6, and 16.0 kJ/m^2 for PS1A1H, PS2A1H and PS2A3H, increases of 204%, 156%, and 180% respectively compared with that of the neat PS. Fig. 2(b) shows a SEM image of an impact surface of PS1A1H. With HNTs added into the matrix,

dimple-like structures in the fracture surface reveal that a few individual HNTs located at their centers and crazes were formed at the interfaces between the HNTs and PS [15]. Plastic deformation in the PS ligaments among neighboring HNTs was found, resulting in a large number of dimples on the fracture surfaces. In each of the fracture events, a substantial amount of energy was dissipated because the events involved a massive number of localized energy dissipating processes [12].

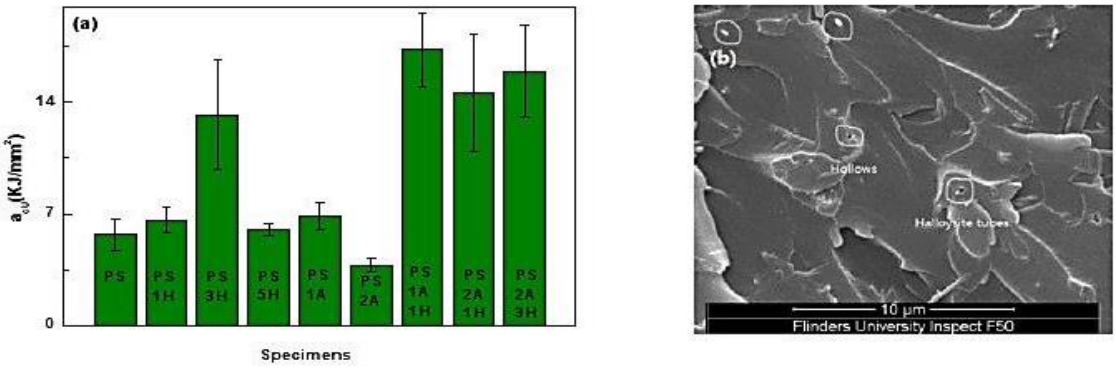

Fig. 2. (a) Impact strength of neat PS and PS composites and (b) SEM image of a fracture surface of PS1A1H composite.

3. 3 Mode I interlaminar fracture toughness of the laminates

Typical mode I delamination crack growth resistance curves (R-curves) for the GRP composites calculated from the load-displacement curves are shown in Fig. 3. Generally, the R-curve increases over about the first 10 mm of crack growth, probably caused by the gradual formation of a fiber bridging zone behind the crack front that is the main toughening process in these fiber glass composites [16]. The R-curves of the GF/PS1H and GF/PS1A laminates show that the interlaminar fracture toughness values (G_{IC}) drop off beyond 10 mm at a range of 0.5-0.7 kJ/m^2. During the DCB test, it was observed that the delamination increased at a random rate and in an unstable manner. The G_{IC} values in the R-curve of GF/PS1A1H are different, with reasonable consistency beyond 10 mm in the range of 0.7-0.8 kJ/m^2, and during the DCB test the delamination grew at a reasonably consistent speed and in a stable manner.

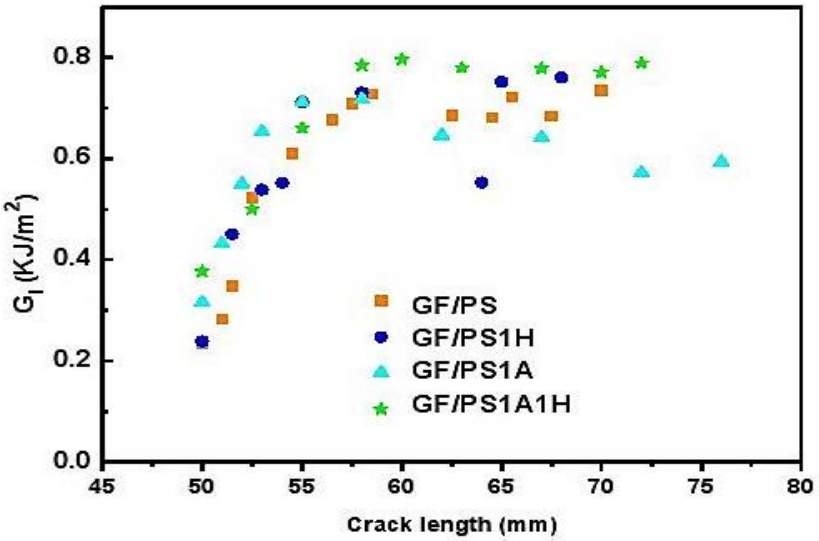

Fig. 3. Typical R-curves for mode I interlaminar fracture measurement of PS laminates.

3. 4 Interlaminar shear strength of the laminates

Interlaminar shear strength (ILSS) is used for quality control and process specification purposes. It also can be used for comparative testing of composite materials, provided that failures occur consistently in the same mode. Fig. 4 clearly demonstrates that the presence of HNT dispersed into the resin contributes to the improvement in ILSS. The GF/PS1H1A laminate was found to have maximum interlaminar shear strength of 38.2 MPa, with an increase of 26.5% over that of the GF/PS composite, The GF/PS1H laminate had a value of 35.1 MPa, with an increase of 16.2% over that of the GF/PS. However, the ILSS value of the GF/PS1A decreased by 18.9% compared to that of the GF/PS. The mechanism of improvement in ILSS might be related to the increase in wettability between fiber and matrix, the different interfacial microstructures, and chemical bonding between nanofillers and matrix resin after the introduction of HNTs into the interfacial region [17]. Some researchers have considered that nanoparticle improvement in lamination shear strength may be highly dependent on the quantity and distribution of particles in the interfacial region, being well-dispersed in the sizing and homogeneously surrounding the fiber surfaces [16].

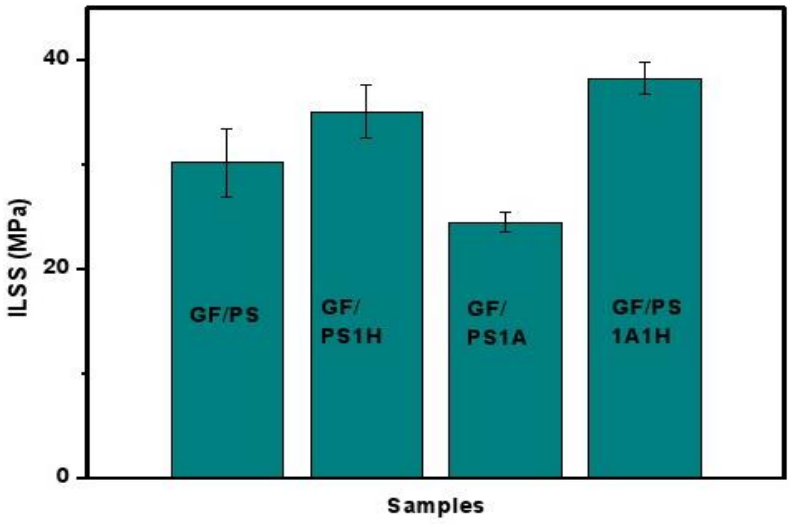

Fig. 4. Interlaminar shear strength (ILSS) of GF/PS and GF/PS composites laminates.

3. 5 Dynamic mechanical analysis of the laminates

The variations in dynamic mechanical properties, such as storage modulus (E′), loss modulus (E″), and loss tangent (tanδ) within the temperature range of 40-140 °C (T) for the GF/PS composites are shown in Fig. 5. From Fig. 5(a), it is evident that during the earlier glassy state of the composites, E′ increases with the addition of HNTs into the matrix. However, E′ of the APTES modified GF/PS is similar to that of GF/PS. Fig. 5(b) shows that the peak position of E″ shifts a little to the left with the addition of APTES into the GF/PS composite. However, with 1 wt% HNTs added into the GF/PS composite, the peak height is higher than that of GF/PS composite, suggesting that the presence of HNTs dissipates some energy because of the viscoelastic deformation of polymer at the HNTs/PS interface [18]. The Tg value drops 3.7 °C with the addition of 1 wt% APTES in GF/PS1A and GF/PS1A1H. The APTES molecules penetrated into the inter-chain spaces of the PS chains, restricting the formation of crosslinks and in turn resulting in a lower Tg value [19].

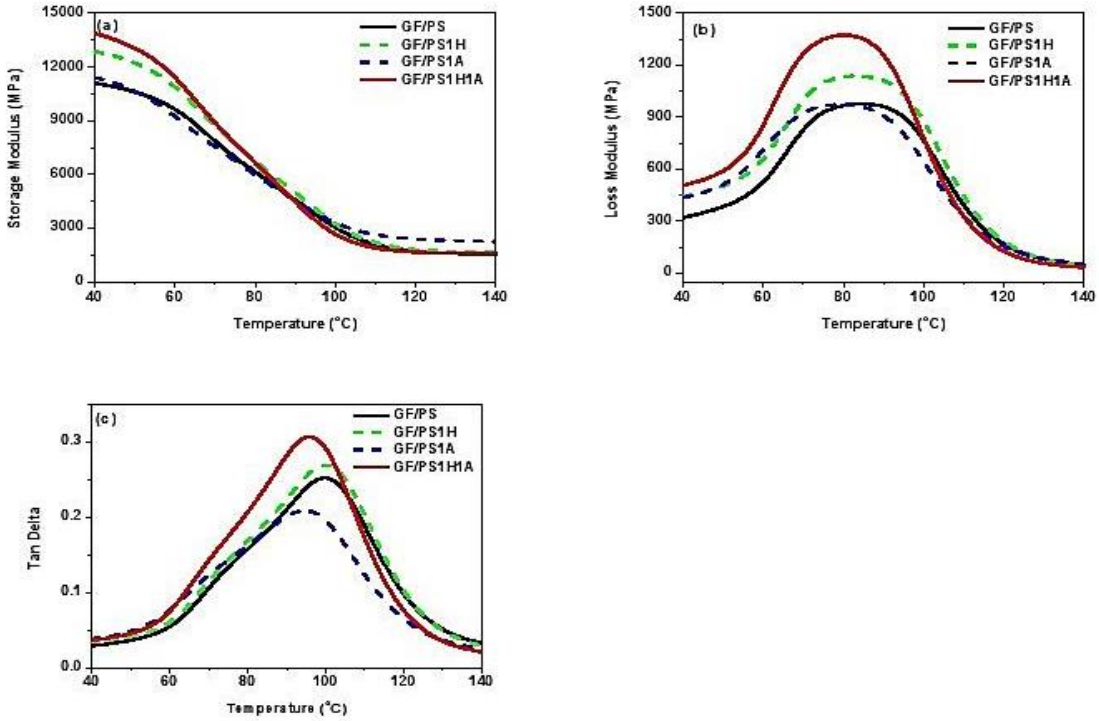

Fig. 5. Dynamic mechanical properties of GF/PS and GF/PS composite laminates.

3. 6 Morphological study of fractured surfaces

To help understand the interface behavior and enhancement mechanism of HNTs/APTES modified GF/PS laminates, the fracture surfaces after the mode I interlaminar fracture test were observed by SEM. As evidenced by the smooth, clean surfaces of the fibers shown in Fig. 6(a) and 6(b), the fracture micro-mechanism in the GF/PS and GF/PS1A laminates is primarily interfacial debonding. The matrix completely detaches from the fiber surfaces because of weak adhesion. This finding indicated that fiber/matrix debonding was the dominant mechanism of shear failure, and the weakest part of such laminates was still the interfaces. Meanwhile, smooth crazes on the matrix indicate poor crack propagation resistance. In comparison, in the PS/GF1H and PS/GF1A1H laminates, a significantly different interface microstructure appears in the SEM micrographs in Fig. 6(c) and 6(d) respectively. These images do not display complete matrix debonding from the fiber surfaces. The fiber/resin debonding is combined with resin/resin fracture. Considerable plastic deformation and amount of resin adhering to the glass fiber surfaces

can be seen. In the GF/PS1A1H laminate, dimple-like structures appear on the fracture surfaces, facilitating the increase in the fractured surface area and degree of micro-cracking preceding the fracture. The development of these microstructures should be related to the interactions between the HNTs/APTES and PS, which seems to be responsible for the improvement in the interlaminar shear strength.

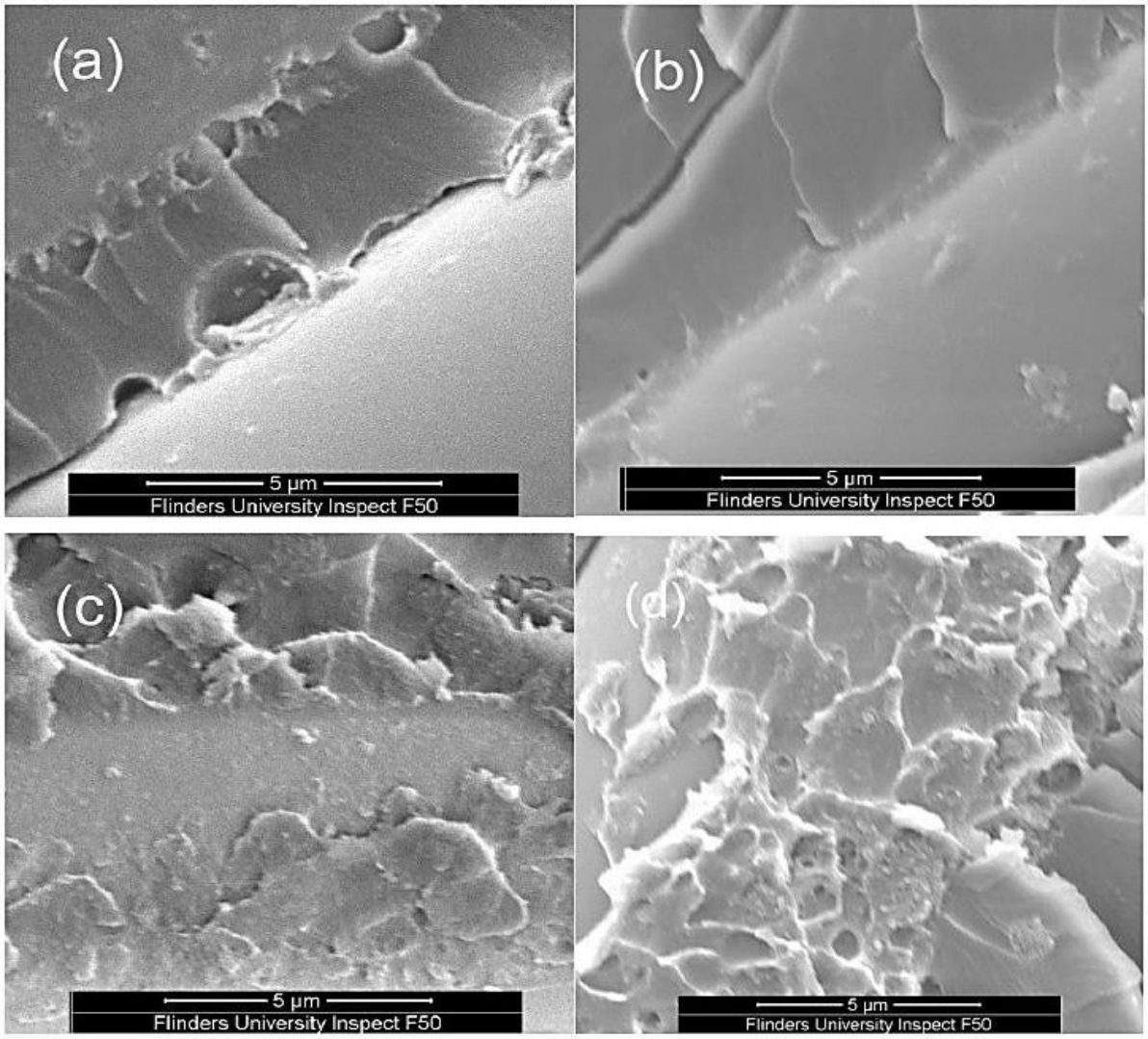

Fig. 6. SEM images of fractured surfaces of (a) GF/PS, (b) GF/PS1A, (c) PS/GF1H and (d) PS/GF1A1H composites laminates.

3. 7. Deterioration of GF/PS laminates in harsh environment

Polymeric materials have been used for many years in marine environments. However, they are weak and may be susceptible to other degradation processes. Polymers lack the microstructure as found in metals and the mechanical properties normally determined by the basis of molecular structure and molecular interaction. PS suffers from environmentally-caused deterioration such as swelling or dissolution in marine environment, and the molecular structure of PS may be attacked by chemical reactions such as oxidation or by heat that can, for example, cause partial reversal of polymerization reactions [20].

Generally, polymers are able to dissolve molecules and, therefore, the permeability of polymers is very important in influencing their mechanical properties under harsh environments such as salt water. A polymer's moisture uptake content (M_t) is calculated by its weight before exposure (ω_0) and after exposure (ω_t) as follows:

$$M_t = \left(\frac{\omega_t - \omega_0}{\omega_0}\right) \times 100$$

Fig. 7 depicts the M_t results from 1 and 3 weeks of salt spray ageing tests. In the first week, the M_t of GF/PS is 0.16%. The lowest moisture uptake occurs in the GF/PS1A1H laminates, reduced by 69% compared with that of the GF/PS. The GF/PS1A has the second lowest moisture uptake laminate, reduced by 31% compared with that of the GF/PS. The GF/PS1H has the same moisture uptake content as the GF/PS. In the third week, the M_t of the GF/PS increases to 0.67%, over 300% more than that in the first week. The lowest moisture uptake laminate is still in the GF/PS1A1H, 57% less than that of the GF/PS. The moisture uptake of the GF/PS1A is 34% less than that of the GF/PS and the GF/PS1H has similar moisture uptake content to the GF/PS in both the first and third weeks. These findings indicated that HNTs acting as rigid particles had negligible effect on moisture permeability in the GF/PS laminate, however, APTES had a barrier effect in reducing the amount of moisture permeating into the GF/PS laminates. Moreover, with the synergistic effect of HNTs with APTES, the better barrier appeared to significantly reduce the laminate's permeability.

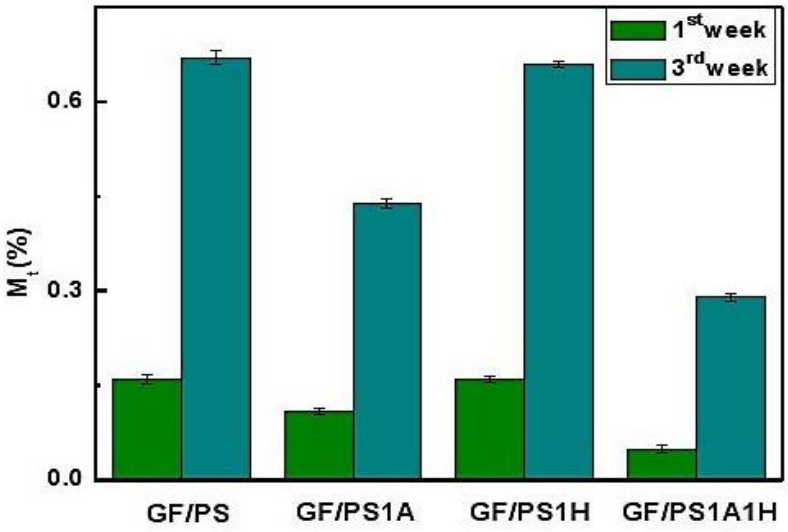

Fig. 7. Moisture uptake content (M_t) for GF/PS and GF/PS composite laminates during salt spray test.

Fig. 8 shows that the ILSS values of laminates decrease with time during the salt spray ageing test. The highest ILSS results after the salt spray ageing test still come from the GF/PS1A1H laminate, but drop 3.7% in the 1st week and 13.9% in the 3rd week compared with the original ILSS result. However, the ILSS results for the GF/PS laminate drop 7.6% and 24.8% in the 1st and 3rd weeks, respectively. Fig. 9 shows the mode I interlaminar fracture toughness G_{IC} values measured after 0, 1, and 3 weeks of salt spray testing and the results of G_{IC} values are listed in Table 4. After a week's salt spray ageing test, all G_{IC} values decrease in the range of 4.1-6.8%. Moreover, the G_{IC} values continuously decrease over the range of 6.4%-15.4% by the 3rd week. These results indicated that both ILSS and G_{IC} decreased with duration of immersion. After a period of salt water permeation, the laminates began to swell and the moisture sorption caused by the swelling volume gradually increased. As well, physical or chemical degradation such as hydrolysis of the polymer, chain breakage, creation of small molecules, and extraction of these molecules from the composite began and mass loss of composite took place. Meanwhile, micro-cracks (voids) appeared in the interfaces between fiber and polymer or interlaminate due

to chemical degradation and water pressure, leading to a sharp increase in moisture sorption [21]. It was noteworthy, however, that the APTES presented as films in the GF surface, GF/PS interfaces, and within the PS resin, that could reduce the permeability of the GF/PS laminate. Meanwhile, the synergistic effects of APTES and HNTs also greatly improved the performance of the GF/PS laminates under the marine environment.

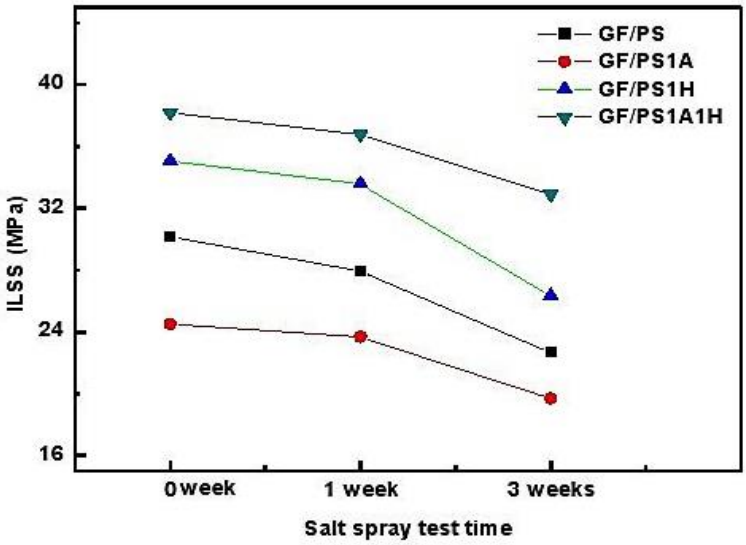

Fig. 8. ILSS values of GF/PS and GF/PS composite laminates after different salt spray test durations

Table 4. Model I interlaminar fracture toughness of GF/PS and GF/PS composite laminate after different durations of salt spray testing.

Samples	G_{IC-0} (J/m^2)	G_{IC-1} (J/m^2)	Difference (%)	G_{IC-3} (J/m^2)	Difference (%)
GF/PS	683±43	644±46	-5.7	599±34	-12.3
GF/PS1H	732±32	682±48	-6.8	619±35	-15.4
GF/PS1A	666±32	634±34	-4.8	611±33	-8.3
GF/PS1A1H	749±20	718±34	-4.1	701±42	-6.4

Note: G_{IC-0}, G_{IC-1} and G_{IC-3} is the model I interlaminar fracture toughness of the laminate before, after 1 week and after 3 weeks salt spray test, respectively.

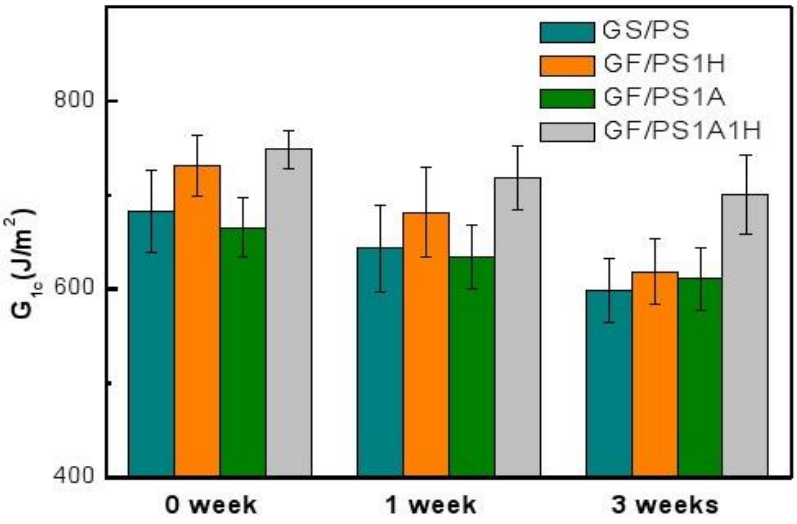

Fig. 9. Mode 1 interlaminar fracture toughness of GF/PS and GF/PS composite laminates after different salt spray test periods.

4. Conclusion

The present study demonstrates an economical and promising processing technique for GF/PS composite laminates. With the present processing parameters, the addition of 1 wt% of commercially available nanoparticles (HNTs) and 1 wt% of an industrially used coupling agent (APTES) resulted in the best dispersion in the PS matrix. The incorporation of 1 wt% HNTs and 1 wt% APTES into the conventional structural GF/PS composite resulted in 26.5% and 11.5% increments in interlaminar shear strength and model interlaminar fracture toughness respectively. SEM analysis confirmed good dispersion of 1 wt% HNTs in the matrix. Fracture surface morphological analysis showed that dimple-like structures appeared on the fracture surfaces, facilitating an increase in the fractured surface area and consuming the energy of micro-cracking preceding the fracture. Meanwhile, APTES act as a barrier that reduced the permeability of the GF/PS laminates and significantly decreased their deterioration under the marine environment. The effects of salt water on the mechanical properties of the laminates, especially the synergistic effects of APTES and HNTs in the GF/PS laminates, either stopped or slowed

any decrease in interlaminar fracture toughness and interlaminar shear strength. These findings demonstrated the great potential of such laminates to be used in harsh environment.

Acknowledgements

Y Tang is grateful for the support of the Premier's Research and Industry Fund with a Catalyst Research Grant (Grant No.: CRG 65) for the research work.

Reference

1. Jin, N.J., Hwang, H.G., Yeon, J.H.: Structural analysis and optimum design of GRP pipes based on properties of materials. Constr Build Mater. 38, 316-326 (2013).

2. Yoshimura, A., Nakao, T., Yashiro, S., Takeda, N.: Improvement on out of plane impact resistance of CFRP laminates due to through the thickness stitching. Compos Part A: Appl Sci Manuf. 39, 1370-1379 (2008).

3. Ray, B.C., Rathore, D.: Durability and integrity studies of environmentally conditioned interfaces in fibrous polymeric composites: Critical concepts and comments. Adv Colloid Interface Sci. 209, 68-83 (2014).

4. Wicks, S.S., de Villoria, R.G., Wardle, B.L.: Interlaminar and intralaminar reinforcement of composite laminates with aligned carbon nanotubes. Compos Sci Technol. 70, 20-28 (2010).

5. Lee, S.W., Youn, J.R.: Characterization of short glass fiber filled polystyrene by fiber orientation and mechanical properties. Macromol. Symp. 148, 211-227 (1999).

6. Li, Y., Lin, Q., Chen, L., Zhou, X.: Assembly of triblock copolymer brush at glass fiber/polystyrene interface and its effect on interfacial shear strength. Compos Sci Technol 69, 1919-1924 (2009).

7. Elley-Bristow, D.M., Bellinger, M.A., Sauer, J.A., Hara, M.: Interfacial bonding of silica glass fiber to polystyrene ionomers. J Polym Sci Part B 37, 2705-2710 (1999).

8. Haneefa, A., Bindu, P., Aravind, I., Thomas, S.: Studies on tensile and flexural properties of short banana/glass hybrid fiber reinforced polystyrene composites. J Compos Mater 42, 1471-1489 (2008).

9. lancau H, Bere P, Borzan M, Hancu L, Crai A. The influence of reinforced materials and manufacturing procedures on the mechanical characteristics of polymeric composite materials. Mater Plast 2008; 4: 251-256.

10. Tang, Y., Ye, L., Deng, S., Yang, C., Yuan, W.: Influences of processing methods and chemical treatments on fracture toughness of halloysite-epoxy composites. Mater. Des. 42, 471-477 (2012).

11. Tang, Y., Ye, L., Zhang, Z., Friedrich, K.: Interlaminar fracture toughness and CAI strength of fibre-reinforced composites with nanoparticles-A review. Compos. Sci. Technol. 86, 26-37 (2013).

12. Lin, Y., Ng, K.M., Chan, C.M., Sun, G.X., Wu, J.S.: High-impact polystyrene/halloysite nanocomposites prepared by emulsion Polymerization using sodium dodecyl sulfate as surfactant. J. Colloid Interface Sci. 358, 423-429 (2011).

13. Liu, H., Wang, C., Zou, S., Wei, Z., Tong, Z.: Facile fabrication of polystyrene/halloysite nanotube microspheres with core–shell structure via Pickering suspension polymerization. Polym. Bull. 69, 765-777 (2012).

14. Ma, P.C., Zheng, Q.B., Mäder, E., Kim, J.K.: Behavior of load transfer in functionalized carbon nanotube/epoxy nanocomposites. Polymer 53, 6081-6088 (2012).

15. Han, W., Yu, Y., Tang, Y., Sammut, K.: Nano-halloysite concentration effects on fracture toughness of diverse epoxy nanocomposites. ASTM Mater. Performance Charact. 3, 1-13 (2014).

16. Huang, X.N., Hull, D.: Effects of fiber bridging on GIC of a unidirectional glass/epoxy composite. Comp. Sci. Technol. 35, 283-299 (1989).

17. Zhang, X., Fan, X., Yan, C., Li, H., Zhu, Y., Li, X., Yu, L.: Interfacial microstructure and properties of carbon fiber composites modified with graphene oxide. ACS Appl. Mater. Interfaces 4, 1543-1552 (2012).

18. Zhu, Q.Y., Wu, F., Yang, Q., Wang, J., Chen, W.: Dynamic mechanical and thermal properties of cross-linked polystyrene/glass fiber composites. J. Wuhan Uni. Technol. – Mater. Sci. Ed. 25, 780-784 (2010).

19. Chen, C.H., Wang, W.S.: The development of glass fiber reinforced polystyrene for pultrusion: Process feasibility, dynamic mechanical properties, and postformabiIity. Polym. Compos. 19, 415-422 (1998).

20. Reuben, R.L.: Materials in Marine Technology, Springer-Verlag, London (1994).

21. Yu, Y., Yang, X., Wang, L., Liu, H.: Hygrothermal aging on pultruded carbon fiber/vinyl ester resin composite for sucker rod application. J. Reinf. Plast. Compos. 25, 149-160 (2006).

Chapter 8: Hybrid enhancements by polydopamine and nanosilica on carbon fibre reinforced polymer laminates under marine environment

8.1 Introduction and significance

In this chapter, we reported a new method of hybrid enhancement with nanosilica (Nanopox F400) for matrix toughening and PDA sizing for laminate interface enhancement. The Mode 1 interlaminar fracture toughness and interlaminar shear strength were significantly increased in modified CFRP laminates and the enhancement mechanism was proposed here. Meanwhile, we found that the nanosilica and PDA enhanced laminates successfully offset the deterioration by salt water in the simulated marine environment. The highlights in this work include:

1. We studied that with 2 wt% nanosilica modified CFRP, the Mode 1 fracture toughness increased by 17% and interlaminar shear strength increased by 8%, compared with the neat CFRP. With 2 wt% nanosilica and 3 wt% PDA, the Mode 1 fracture toughness increased by 39% and interlaminar shear strength increased by 22%, compares to the neat CFRP.
2. The salt spray test results indicated that the salt water weakened the ability of rigid silica particles to deflect cracking paths, but salt water did not show significant damage on the PDA layer in this study.

This section is included as it submitted and under review as a journal paper by **Wei Han**, Hongping Zhang, Xin Xu and Youhong Tang. Hybrid enhancement by polydomamine and nanosilica on carbon fibre reinforced polymer laminates under marine environment, ***Compos Part A*** 2018; 112: 283-289.

8.2 Hybrid enhancements by polydopamine and nanosilica on carbon fibre reinforced polymer laminates under marine environment

Composites Part A 112 (2018) 283–289

Contents lists available at ScienceDirect

Composites Part A

journal homepage: www.elsevier.com/locate/compositesa

Hybrid enhancements by polydopamine and nanosilica on carbon fibre reinforced polymer laminates under marine environment

Wei Han[a], Hong-Ping Zhang[a,b], Xin Xu[a], Youhong Tang[a,*]

[a] College of Science and Engineering, Flinders University, South Australia 5042, Australia
[b] School of Materials Science and Engineering, Southwest University of Science and Technology, Sichuan 621010, China

ARTICLE INFO

Keywords:
A. Laminates
B. Fracture toughness
B. Environmental degradation
B. Interface/interphase

ABSTRACT

In this study, two enhancement methods, i.e., toughen the epoxy matrix by commercially available nanosilica and enhance the interfaces of fibres and matrix by autoxidation of dopamine were applied together in carbon fibre reinforced polymer laminates with potential large-scale applicability. Significant enhancements were found for Mode I interlaminar fracture toughness and interlaminar shear strength with the combined addition of nanosilica and polydopamine in the laminates. The enhancement mechanism is proposed as well. Salt spray tests were applied in this study to simulate a marine environment for the laminates. Model I interlaminar fracture toughness and interlaminar shear strength both decreased under the simulated marine environment with an increase in immersion time, but the deterioration was significantly mitigated when nanosilica and polydopamine were added together with still much higher mechanical properties measured after 3 weeks of salt spray immersion than in neat laminate without salt spray immersion, providing promising evidence for maritime engineering applications of such laminates.

1. Introduction

Growing demand exists for carbon fibre reinforced polymer (CFRP) composite materials with enhanced properties, which are essential for applications in engineering fields, especially in harsh environments. As CFRP is a combination of fibre and matrix, its properties are dominated by high strength and stiffness in fibres as well as low strength in the ductile polymer matrix and the interfaces between fibres and matrix. These poor polymer properties and weak interfaces between fibres and polymer significantly limit the applications of CFRP. Consequently, it is of interest to enhance the polymer resin as well as the interfaces between the resin and fibre of the CFRP composites to extend laminate applications in various fields.

Significant work has been done to enhance polymer matrix as well as interfaces in recently years, with some studies focusing on large-scale production and commercialization. The use of nanoparticles to toughen polymer matrix is one promising method, employing such particles as nanosilica, halloysite nanotubes, and carbonaceous nanoparticles such as graphene nanoplatelets and graphene oxide. Improvements in Young's modulus, fracture toughness and tensile strength have been reported [1–6]. However, one of the challenges in using nanoparticles is the achievement of homogeneous dispersion of high weight/volume ratio nanoparticles in matrix while maintaining comparatively low viscosity. The difficulty is that viscous resin systems cannot easily impregnate continuous fibres or fibre fabric during CFRP production. Meanwhile, based on a resin infusion process, the filtering of dense fibre bundles against agglomerated nanofillers can lead to severe segregation and depletion of nanofillers in matrices [7,8], also significantly offsetting the enhancement effects of nanoparticles in laminates. One of the solutions is the use of *in situ* synthesized methods such as the sol-gel manufacturing process, whereby particle size and excellent distribution are unaffected during any further processes. Several commercially produced nanosilica-modified epoxies are available, such as Nanopox F400, a concentration of 40 wt% nanosilica in diglycidyl ether of bisphenol A (DGEBA) epoxy resin [9], with an average particle size of 20 nm and a narrow range of particle size distribution. In our previous research, only 2 wt% nanosilica added in the epoxy improved the fracture toughness and corrosion rate under a marine environment [9]. Meanwhile Sprenger reported using nanoparticles no longer further improvement the delamination fracture value when the value reached to 500 J/m^2. Above that value, the dominated delamination fracture of laminate often changes from matrix failure to interfacial failure [10]. Therefore, the addition of a single type of nanoparticle did not further mitigate the occurrence of delamination fracture.

Sizing is a method of wetting out fibre surfaces to improve the poor interfacial adhesion of CFRP. Polydopamine (PDA) is a bionic material

* Corresponding author.
E-mail address: youhong.tang@flinders.edu.au (Y. Tang).

https://doi.org/10.1016/j.compositesa.2018.06.019
Received 19 February 2018; Received in revised form 4 June 2018; Accepted 12 June 2018
Available online 12 June 2018
1359-835X/

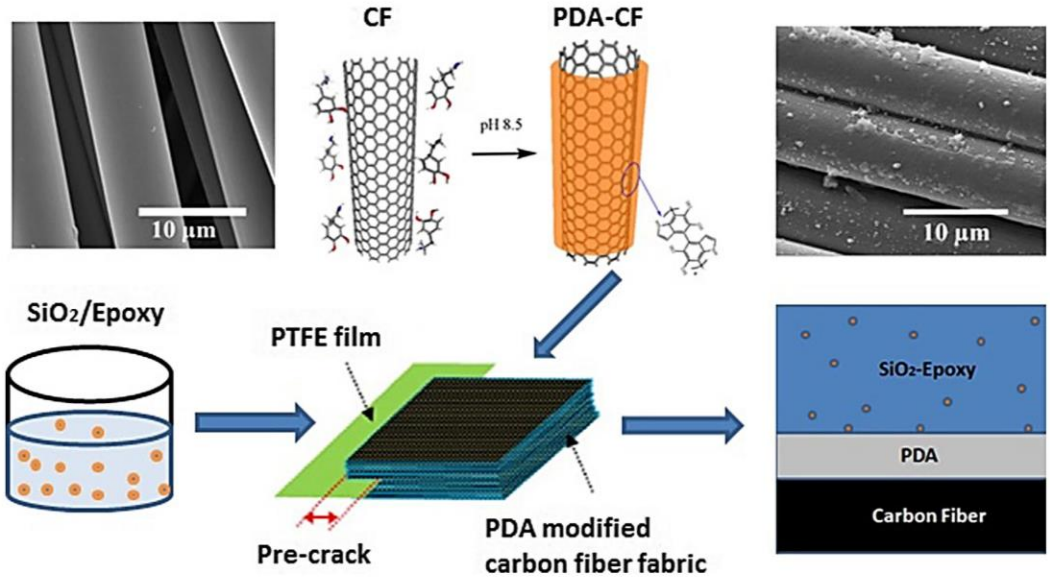

Fig. 1. Schematic drawing demonstrating the hybrid enhancement strategy by toughening epoxy matrix with nanosilica and enhancing the interface by applying polydopamine on carbon fibre surfaces. (For interpretation of the references to color in this figure legend, the reader is referred to the web version of this article.)

which has excellent adhesion to a range of solid surfaces, such as metals, oxides, polymers and ceramics by autoxidation of dopamine in basic aqueous solutions [11]. Recently, it has also been applied to modify nanoparticles such as carbon nanotubes [12], graphene [13] and clay [14], revealing excellent ability to improve the mechanical, thermal and electromagnetic interference shielding performance of polymer matrices. In addition, PDA has been used to modify short carbon fibres, revealing significant improvement in tensile strength and Young's modulus [12]. Furthermore, Yang et al. reported that the catechol groups in PDA were forming hydrogen bonds with polar groups in epoxy [15]. In addition, the interfacial covalent bonding was forming between PDA and epoxy because of the primary and secondary amine groups in PDA may react with epoxy groups and the amine hardener may react with PDA [16,17]. We reported using a simple method for surface modification to improve the load transfer between carbon fibre and epoxy matrix, increase the fractured interface friction and reduce unstable crack growth in CFRP composites [18].

The application of CFRP composites in maritime engineering was initially the demand of building lightweight, strong, corrosion-resistant durable naval vessels. CFRP can overcome corrosion problems experienced with steel or aluminium alloys and environmental degradation suffered by wood. Additionally, CFRP can significantly reduce the weight of a structure but still maintain the desired performance and structural integrity. However, under the marine environment, the mechanical properties of laminates degrade due to UV, moisture, temperature and ageing – creating the potential of accidentally creating fracture. Bastioli et al. reported water aging may strongly affect the matrix behaviour, by producing changes in its chemical and physical nature by itself or in conjunction with other chemical or physical agents such as heat and ultraviolet light [19,20]. Moreover, the fibre/matrix interface can be degraded by a hydrolysis reaction of unsaturated groups within the resin under marine conditions [21–23]. A concern is the incomplete understanding and shortage database of using fibre reinforced composites as marine structures with long-term durability. Consequently, to efficiently enhance the properties of CFRP and extend its applications in the harsh marine environment, there is interest in improving the mechanical performance at least to offset the deterioration generated by that environment.

Current enhancements to interfacial adhesion rely on sizing wet-out fibre surfaces. However, the inherent poor properties of polymer matrix render these solutions inefficient. Furthermore, polymer matrix enhancement can only toughen the matrix itself, with less enhancement of the interfaces. In this work, we demonstrate a feasible hybrid method to enhance the laminate, with potential large-scale application under marine environments. Commercially available nanosilica can provide the necessary polymer matrix toughness, while polydopamine on carbon fibre surfaces can provide significant interfacial adhesion among fibres and matrix. With those hybrid enhancements, laminates can offset deterioration under a simulated marine environment and still achieve superior mechanical performance to that displayed by neat laminate without salt water immersion.

2. Experiments

2.1. Polydopamine for CFRP interfacial enhancement

The as-received carbon fabric was submerged in acetone for 48 h to wash off the commercial sizing and impurity. For fabrication of the PDA sizing fibres, 4 g dopamine hydrochloride (Sigma, Australia) was dissolved in a mixed solution of deionized water (4000 mL) and aqueous solution of TRIS (3.6 g tris(hydroxymethyl)aminomethane, 1000 mL deionized water), with magnetic stirring for 30 min. 200 gm unidirectional carbon fibre fabrics (Hexcel, USA) were prepared into 8 layers with the size of 30 cm * 30 cm then placed in a container and the mixed solution was transferred to the container. The container was shaken by a benchtop orbital shaker (Labec, Australia) at 100 rpm for 24 h at ambient temperature. Then, the modified carbon fibre fabrics were collected, washed with deionized water several times to remove the residual dopamine, and dried in a vacuum oven at 40 °C for 24 h. Finally, the thickness of PDA layer on the carbon fabric was 50–100 nm. From our previous report, approximately 3.2 wt% of polydopamine was coated on the carbon fabric [20].

2.2. PDA-SiO_2-CFRP composites preparation

A vacuum-assisted resin transfer moulding (VARTM) process was

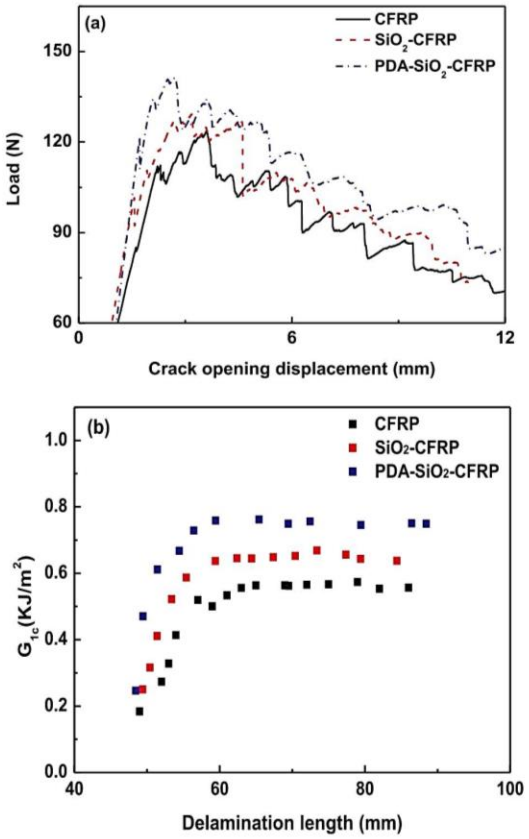

Fig. 2. (a) Typical load-crack opening displacement curves obtained from Mode 1 interlaminar fracture toughness tests and (b) typical Mode I delamination crack growth resistance curves (R-curves) for different laminates. (For interpretation of the references to color in this figure legend, the reader is referred to the web version of this article.)

used to fabricate the CFRP composites, as shown in the schematic drawing in Fig. 1. In this procedure, a flat metal plate was first treated with a releasing agent. For the PDA-SiO_2-CFRP, the raw resin was prepared by using a diglycidyl ether of bisphenol A (DGEBA) epoxy resin, Araldite-F (Ciba-Geigy, Australia) to dilute the commercialized Nanopox F400 resin (40 wt% nanosilica) to 2 wt% nanosilica epoxy resin. A piperidine (Sigma-Aldrich, Australia) hardener was added at the ratio of 100:5 by weight while being stirred slowly. A PDA-modified carbon fibre ply stack was next placed on the metal plate between two PTFE films, one above and one below the stack. A 10-μm thick non-stick film was inserted in the middle layer of the stack to create the initial delamination. The peel films were placed between two infusion meshes (above and below the peel films). Then the mixture resin was placed in a vacuum oven to preheat to 80 °C and degassed as well. After that, the resin was pumped into the vacuum bag and placed in a hot press machine (Carver Inc. USA) with a pressure at 10 KN/m^2 and curing temperature at 120 °C for 24 h. Finally, the cured panel thickness was measured to be approximately 3 mm for all plates and the fibre volume was measured at nearly 32 vol.%. Test specimens were cut from the cured panels by means of bandsaw cutting and polisher polished. As controls for evaluation, pure CFRP and 2% SiO_2-CFRP were prepared separately. Fig. 1 illustrates the hybrid enhancement strategy used in this study.

Table 1
Selected interlaminar fracture toughness and interlaminar shear strength values with simple nanosilica enhancement on matrix or with current hybrid enhancement.

	G_{IC} (KJ/m^2)	Improvement (%)	Ref.
CFRP	0.54 ± 0.02	–	
2% SiO_2-CFRP	0.63 ± 0.02	17	
3%PDA-2% SiO_2-CFRP	0.75 ± 0.01	39	
GFRP	0.83	–	[26]
10% SiO_2-GFRP	0.90	8	
20% SiO_2 GFRP	0.95	15	
CFRP	0.54	–	[27]
4% SiO_2-CFRP	0.62	15	
6% SiO_2-CFRP	0.64	19	
8% SiO_2-CFRP	0.62	15	
10% SiO_2-CFRP	0.62	15	
12% SiO_2-CFRP	0.61	13	
CFRP	1.25	–	[28]
4% SiO_2-CFRP	1.17	−6	
8% SiO_2-CFRP	1.31	5	
8% SiO_2-4%CSR-CFRP	1.52	22	
8% SiO_2-8%CSR-CFRP	1.76	41	
	ILSS (MPa)	Improvement (%)	
CFRP	55.7 ± 1.4	–	
2% SiO_2-CFRP	59.9 ± 1.6	8	
PDA-2% SiO_2-CFRP	67.8 ± 1.6	22	
CFRP	45.5	–	[29]
2.5% GO-CFRP	46.0	1	
10% GO-CFRP	50.7	11	
CFRP	44.6	–	[30]
3% CB-CFRP	31.8	−29	
3% MWCNTs-CFRP	46.7	5	
3% GnPs-CFRP	47.5	7	

2.3. Characterizations

The Mode I interlaminar fracture toughness was measured using double cantilever beam tests carried out on a universal testing machine (Instron, US) fitted with a 500 N load cell in accordance with the ASTM D 5528 standard. The dimensions of the test specimen were 125 mm × 25 mm × 3 mm. Test specimens were clamped in the jaws of the machine via the block hinges with a load rate of 1 mm/min while the load–displacement data was recorded. The fracture surfaces of test specimens were examined using a scanning electron microscope (SEM; Inspect F50, FEI, US). The SEM samples were selected around the pre-crack tip area and coated with gold to form a thin 1 nm conductive layer. The interlaminar shear strength (ILSS) was measured using a 3-point short beam strength test following the ASTM D-2344 standard. The specimens were cut to the dimensions of 50 mm × 12 mm × 3 mm. A minimum of 8 specimens per batch were tested.

Specimens were placed in a salt spray test machine for periods of 1 and 3 weeks following the ASTM b117 standard. 5 wt% NaCl solvent was used to simulate marine water and the test temperature was 42 °C. Specimens were then washed in running water and oven dried at 60 °C for 48 h. Model I interlaminar fracture toughness and interlaminar shear strength were characterized after the immersion.

3. Results and discussion

3.1. Hybrid enhancement on CRPF laminates

Fig. 2(a) shows load-crack opening displacement (COD) curves obtained from Mode 1 interlaminar fracture toughness tests for different laminates. The neat CFRP shows a saw-tooth shaped curve which forms as the load increases and decreases alternately, demonstrating unstable energy release during crack propagation. In comparison, for the SiO_2-

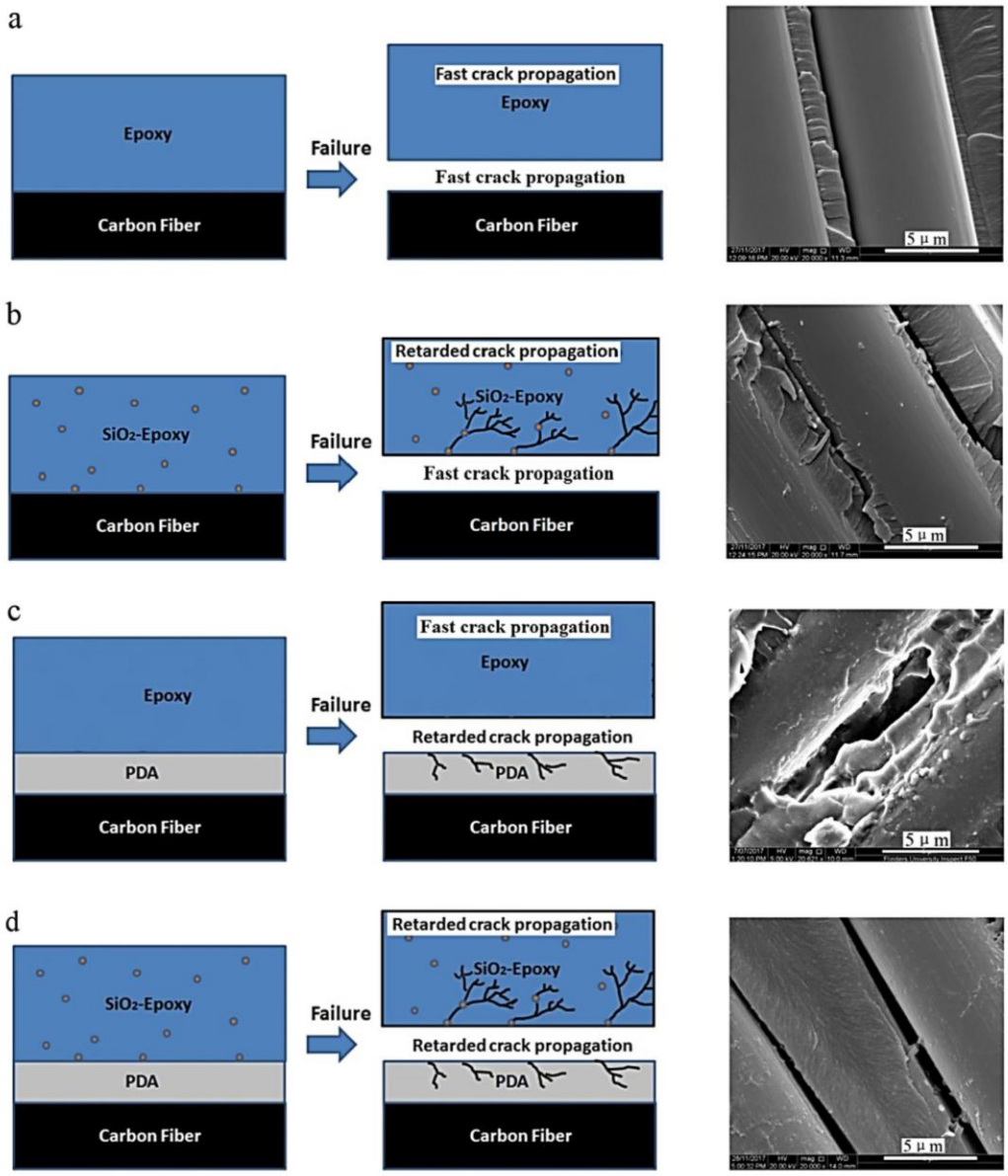

Fig. 3. Schematic drawings of failure mechanism for (a) neat CFRP; (b) SiO_2-CFRP; (c) PDA-CFRP and (d) PDA-SiO_2-CFRP, with corresponding SEM images of the fractured surfaces after model I interlaminar fracture toughness characterizations. (For interpretation of the references to color in this figure legend, the reader is referred to the web version of this article.)

CFRP sample, the COD curve shows a saw-tooth shaped curve similar to that of the neat CFRP but with higher load capacity than that of the neat CFRP. For the PDA-SiO_2-CFRP specimen, however, the force regularly increases to the peak point and then drops in a relatively smooth movement, while the load capacity increases further, as shown in Fig. 2(a). These COD curves indicate that the addition of nanosilica alone can increase the load capacity but may not improve the interface adhesion. With PDA added in the SiO_2-CFRP specimen, however, the interfacial adhesion also improves [24]. Fig. 2(b) shows typical Mode I delamination crack growth resistance curves (R-curves) calculated from the COD curves. Generally, the R-curves grow to a plateau with crack propagation.

The gradual formation of a fibre-bridging zone behind the crack front is the main toughening process in these CFRP composites [25]. The average value of G_{IC} during propagation is 540 J/m^2 for CFRP and 630 J/m^2 for SiO_2-CFRP, with about 17% improvement which is attributed to the deflection of the cracking paths because of the presence of the rigid nanosilica particles consuming more energy [9]. The average propagation G_{IC} value for PDA-SiO_2-CFRP is 750 J/m^2, which is a 39% increment compared to that of CFRP, as the PDA can further provide strong adhesions between carbon fibre and epoxy resin [11]. Table 1 shows a summary of the G_{IC} values for the nanosilica enhanced CFRP and its improvement ratios. As shown in the Table, Tsai et al. reported that compared with neat laminate, G_{IC} values increased by

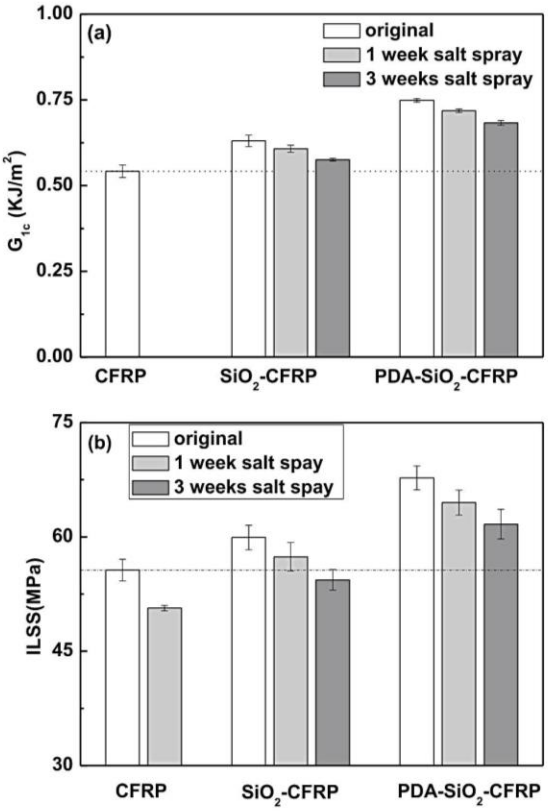

Fig. 4. (a) Model I interlaminar fracture toughness and (b) interlaminar shear strength of neat CFRP, SiO_2-CFRP and PDA-SiO_2-CFRP laminates with different salt spray durations used to simulate marine environment effects on laminate performance.

Table 2
The reduction rate of salt spray test compared to properties at 0 day of each specimen.

Salt spray test		7 days	21 days
G_{IC}	CFRP	NA	NA
	SiO_2-CFRP	−4%	−9%
	PDA-SiO_2-CFRP	−4	−9%
ILSS	CFRP	−9%	NA
	SiO_2-CFRP	−5%	−9%
	PDA-SiO2-CFRP	−5%	−9%

8.4% and 14.5% when 10 wt% and 20 wt% silica nanoparticles respectively were added in the laminate [26]. Obviously, the 2 wt% sol-gel form of nanosilica provided a greater increment of the G_{IC} than the 20 wt% unmodified nanosilica. Similarly, Zeng et al. reported that in laminates modified with 4 wt% and 6 wt% silica nanoparticles, the G_{IC} values increased by 15% and 19%, respectively [27]. However, further increasing in the concentration of nanosilica did not further increase the G_{IC} value. Meanwhile, Carolan et al. reported the use of a hybrid of nanosilica and polysiloxane core-shell rubber (CSR) to toughen the G_{IC}. They found that the use of 8 wt% SiO_2 with 8 wt% CSR significantly improved the G_{IC} value by 41% compared to that of neat CFRP [28]. In comparison, the hybrid enhancement in the PDA-SiO_2-CFRP of the current study used only 3 wt% PDA and 2 wt% nanosilica to achieve a 39% increment in the G_{IC} value. This result demonstrates a marked advantage over the use of enhancement of simple matrices by nanoparticles.

Table 1 also shows that the average ILSS value of the neat CFRP laminate is 55.7 MPa; this value increases to 59.9 MPa for SiO_2-CFRP and 67.8 MPa for PDA-SiO_2-CFRP with increments of 8% and 22%, respectively. In the report of Zhang et al. [29], the ILSS values were 46 MPa and 50.7 MPa for laminates with 2.5 wt% and 10 wt% GO nanoparticles, the values increasing by 1% and 12% respectively compared with those of the neat laminate. Srivastava et al. found that, with 3% carbon blacks (CBs), 3% multi-walled carbon nanotubes (MWCNTs) and 3% graphene nanoplatelets (GnPs) added in the laminate, the ILSS values increased by −29%, 5% and 7%, respectively [30]. Thus a significant advantage has been demonstrated of hybrid enhancement as a feasible way to enhance the interlaminar properties of laminates, compared with single nanoparticle enhancement.

Fig. 3 shows a schematic drawing of the proposed toughening mechanisms for different laminates, with SEM images of fracture surfaces. Fig. 3(a) shows a clean and smooth surface of the fibres in a CFRP fracture surface, indicating that the fracture mechanism is primarily interfacial debonding. The epoxy resin detaches completely from the carbon fibre surfaces because of weak bonding in the interfaces. This finding indicates that fibre/epoxy debonding is the dominant failure mechanism, and the most likely failure site in the laminates is still the interface. Although the SiO_2-CFRP fracture toughness surface is also clean and smooth, as observed in Fig. 3(b), the fractured resin surface is rougher than that of the neat epoxy Fig. 3(a), because the rigid nanosilica particles can deflect cracking paths, resulting in a higher G_{IC} and a rougher fracture surface, as shown in Fig. 3(b). From our previous publication [18] regarding the PDA-CFRP laminate, with the enhancement on the interfaces, a higher G_{IC} value has been reported with rough fracture surfaces been observed, as shown in Fig. 3(c). In contrast, in the PDA-SiO_2-CFRP fractured surface, a significantly different interface microstructure is shown in Fig. 3(d). A large amount of epoxy adhering to the PDA treated carbon fibre surfaces and the rough fractured epoxy surface indicate that the failure mechanism is a combination of epoxy resin fracture and interface debonding. The development of these microstructures is related to both PDA-enhanced interactions between carbon fibre and epoxy and nanosilica toughened epoxy matrix. Therefore, the overall G_{IC} value is significantly increased.

3.2. Marine environment effects on the hybrid enhancement of laminates

Fig. 4(a) shows the Mode I interlaminar fracture toughness G_{IC} values after 0, 1 and 3 weeks' salt spray testing to simulate marine environment effects on laminate mechanical properties. Generally speaking, the marine environment will deteriorate Mode I interlaminar fracture toughness. As shown in the figure, after a week's salt spray test, the G_{IC} values decrease to 0.61 KJ/m^2 for SiO_2-CFRP and 0.72 KJ/m^2 for PDA-SiO_2-CFRP, respectively. Moreover, the G_{IC} values continue to decrease, reaching 0.58 KJ/m^2 for SiO_2-CFRP and 0.68 KJ/m^2 for PDA-SiO_2-CFRP after 3 weeks' salt spray testing. Such trends of deterioration effects have also been reported previously [9]. After a period of salt water permeation, it is found that laminates began to swell, and the moisture sorption caused by the volume swelling gradually increased. Meanwhile, physical or chemical degradation, such as hydrolysis of the polymer, chain breakage, creation of small molecules and extraction of these molecules from the composite began, and mass loss of composite occurred [31]. However, the deterioration of the laminate G_{Ic} values was diminished by the addition of nanosilica, as reported by us previously [9], with further mitigation when PDA and nanosilica were added together. As a result, the G_{Ic} values of SiO_2-CFRP and PDA-SiO_2-CFRP after 3 weeks' salt spray testing were still 7% and 26% higher respectively than those of the neat CFRP (0.54 KJ/m^2) without any salt spray test. This finding shows that the hybrid enhancement significantly improved the Mode I interlaminar fracture toughness under the marine environment.

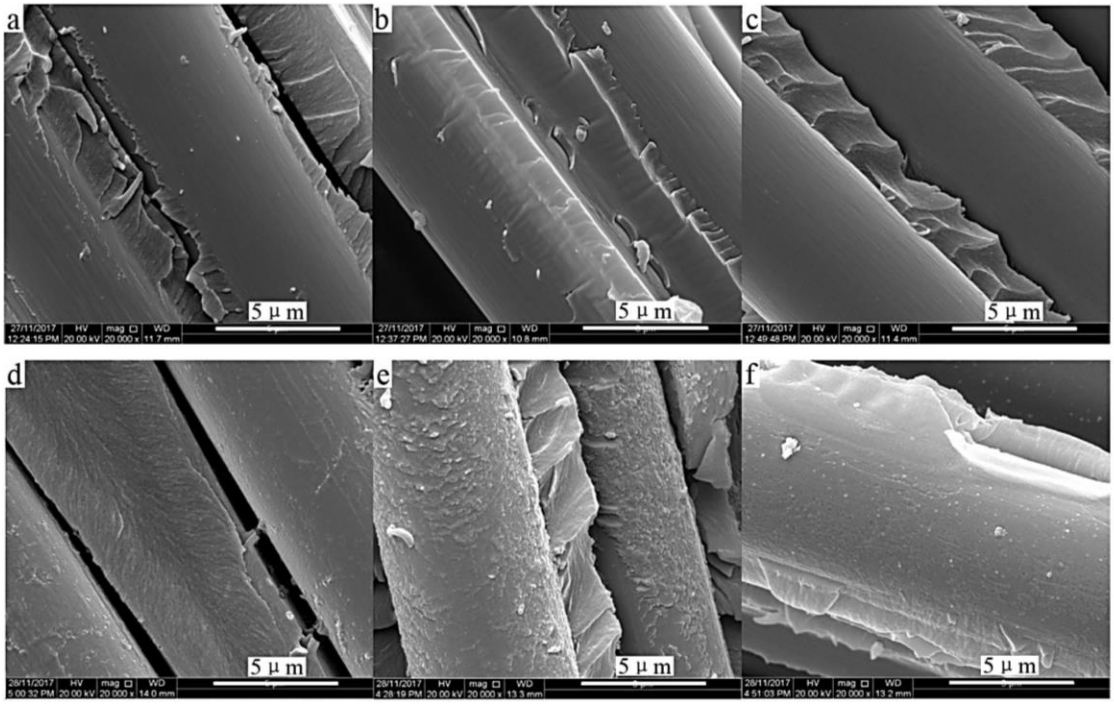

Fig. 5. SEM images of fracture surfaces of (a)–(c) SiO_2-CFRP and (d)–(f) PDA-SiO_2-CFRP laminates (a) and (d) before salt spray testing and (b) and (e) after 1 week and (c) and (f) 3 weeks of salt spray testing.

Fig. 4(b) shows that the ILSS values of all laminates decreases after the salt spray test. The highest ILSS result after the salt spray test still comes from the PDA-SiO_2-CFRP laminate, with reduction rates of 5% in 7 days and 9% in 21 days compared with that in 0 day as shown in Table 2. For the SiO_2-CFRP laminate, it has the similar reduction rates of 5% in 7 days and 9% in 21 days, respectively. However, CFRP has a reduction rate of 9% in 7 days observed indicates that SiO_2 or PDA-SiO_2 are applied in CFRP can efficiently reduce the degradation of mechanical properties under marine environment. Interestingly, the ILSS value of the SiO_2-CFRP laminate after the 3-week salt spray test decreases to a value which is even 2.3% lower than that of the neat CFRP without the salt spray test. However, the ILSS value of the PDA-SiO_2-CFRP laminate is still 11% higher than that of the unmodified CFRP. Hence, it can be concluded that in terms of mechanical properties, PDA-SiO_2-CFRP laminate is superior to SiO_2-CFRP laminate under marine environment.

Fig. 5 shows SEM images of interlaminar fracture toughness surfaces after different salt spray periods. The morphologies of the fracture surfaces changed significantly with the salt spray duration. Fig. 5(a)–(c) shows SEM images of the fracture surfaces of SiO_2-CFRP without and after 1 and 3 weeks of salt spray tests. The fracture surfaces become smoother as the salt spray duration increases. Especially in Fig. 5(c), the fracture surfaces of SiO_2-CFRP after 3 weeks' salt spray were very similar to that of the neat CFRP fracture surface shown in the SEM image of Fig. 3(a). This result indicates that, due to salt water permeation, the nanosilica/resin interfaces have been attacked by salt water, weakening the ability of rigid silica particles to deflect cracking paths. Therefore, the fracture surface of SiO_2-CFRP becomes smoother. For PDA-SiO_2-CFRP, as shown in Fig. 5(d)–(f), significant amount of resin still adheres to the PDA treated carbon fibre surfaces. Although the resin surfaces are less rough, the PDA layers do not show significant damage. Therefore, most of deboning comes from the epoxy resin fracture, indicating that the salt water on the PDA layer may serve as an effective layer to slow the deterioration effects of swelling on the interfaces.

4. Conclusion

In this study, with the use of hybrid enhancements of CFRP laminates by nanosilica and polydopamine, CFRP shows significant improvement of mechanical properties. Increments of 39% in Mode I interlaminar fracture toughness and 26% in interlaminar shear strength were obtained for the PDA-SiO_2-CFRP compared with those of the neat CFRP. The enhanced mechanism was mainly the result of the enhancement of interfacial bonding among epoxy and carbon fibres by the PDA and the toughening of the epoxy matrix by rigid nanosilica particles. In the marine environment, the mechanical properties deteriorated with an increase in time. However, that deterioration could be effectively offset by the combined enhancements from nanosilica and PDA, an outcome that successfully demonstrates a promising use of CFRP laminates under marine environments.

Acknowledgements

We acknowledge the use of South Australian nodes of the Australian Microscopy & Microanalysis Research Facility (AMMRF) and Australian National Fabrication Facility (ANFF) at Flinders University. W Han is grateful for the research training program scholarship during his PhD study.

References

[1] Maugis D. Subcritical crack growth, surface energy, fracture toughness, stick-slip and embrittlement. J Mater Sci 1985;20(9):3041–73.
[2] Ghasemnejad H, Hadavinia H, Aboutorabi A. Effect of delamination failure in crashworthiness analysis of hybrid composite box structures. Mater Des 2010;31(3):1105–16.
[3] Maksimov IL. Thermomechanical fracture instability and stick-slip crack

propagation. Appl Phys Lett 1989;55(1):42–4.
[4] Kinloch AJ, Williams JG. Crack blunting mechanisms in polymers. J Mater Sci 1980;15:987–96.
[5] Lee C, Wei X, Kysar JW, Hone J. Measurement of the elastic properties and intrinsic strength of monolayer graphene. Science 2008;321(5887):385–8.
[6] Qin W, Vautard F, Drzal LT, Yu J. Mechanical and electrical properties of carbon fiber composites with incorporation of graphene nanoplatelets at the fiber-matrix interphase. Compos Part B 2015;69:335–41.
[7] Wicks SS, Villoria RG, Wardle BL. Interlaminar and intralaminar reinforcement of composite laminates with aligned carbon nanotubes. Compos Sci Technol 2010;70(1):20–8.
[8] Chi Y, Chu J, Chen M, Li C, Mao W, et al. Directly deposited graphene nanowalls on carbon fiber for improving the interface strength in composites. Appl Phys Lett 2016;108(21):211601.
[9] Han W, Chen S, Campbell J, Zhang XJ, Tang Y. Nanosilica enhanced fracture toughness and wear properties of epoxy under marine environment. Mater Chem Phys 2016;177:147–55.
[10] Sprenger S. Fiber-reinforced composites based on epoxy resins modified with elastomers and surface-modified silica nanoparticles. J Mater Sci 2014;49:2391–402.
[11] Irshidat MR, Al-Saleh MH, Almashagbeh H. Effect of carbon nanotubes on strengthening of RC beams retrofitted with carbon fiber/epoxy composites. Mater Des 2016;89:225–34.
[12] Zhang RL, Gao B, Du WT, Zhang J, Cui HZ, et al. Enhanced mechanical properties of multiscale carbon fiber/epoxy composites by fiber surface treatment with graphene oxide/polyhedral oligomeric silsesquioxane. Compos Part A 2016;84:455–63.
[13] Zhang P, Ma L, Fan F, Zeng Z, Peng C, et al. Fracture toughness of graphene. Nat Commun 2014;5:3782.
[14] Zhang X, Fan X, Yan C, Li H, Zhu Y, Li X, et al. Interfacial microstructure and properties of carbon fiber composites modified with graphene oxide. ACS Appl Mater Interfaces 2012;4(3):1543–52.
[15] Yang L, Phua SL, Teo JKH, Toh CL, Lau SK, Ma J, et al. A biomimetic approach to enhancing interfacial interactions: polydopamine-coated clay as reinforcement for epoxy resin. ACS Appl Mater. Interfaces 2011;3:3026–32.
[16] Hu X, Qi R, Zhu J, Lu J, Luo Y, Jin J, et al. Preparation and properties of dopamine reduced graphene oxide and its composites of epoxy. J Appl Polym Sci 2014;131:39754.
[17] Chen S, Cao Y, Feng J. Polydopamine as an efficient and robust platform to functionalize carbon fiber for high-performance polymer composites. ACS Appl Mater. Interfaces 2014;6:349–56.
[18] Han W, Zhang H, Tavakoli J, Campbell J, Tang Y. Polydopamine as sizing on carbon fiber surfaces for enhancement of epoxy laminated composites. Compos Part A 2018;107:626–32.
[19] Bastioli C, Casciola M, Romano G. Role of the interface in composite materials during water ageing. In: Proceedings of the third international conference oncomposite interfaces, Cleveland, OH, 21–24 May 1990. p. 569–81.
[20] Blaga A. Water sorption characteristics of GRP composite: effect of outdoor weathering. Polym Compos 1981;2(1):13–7.
[21] Alvarez VA, Analia V. Effect of water sorption on the flexural properties of fully biodegradable composites. J Compos Mater 2004;38:1165–81.
[22] Csaba S, Hiroyuki H, Kiyohito K. Blister appearance in thermoplastic composites. Adv Compos Mater 2001;10:63–75.
[23] Kootsooks A, Maritz AP. Seawater durability of glass- and carbon-polymer composites. Compos Sci Technol 2004;64:1503–11.
[24] Qu KG, Zheng Y, Jiao Y, Zhang XX, Dai S, Qiao SZ. Polydopamine-inspired, dual heteroatom-doped carbon nanotubes for highly efficient overall water splitting. Adv Energy Mater 2017:1602068.
[25] Mouritz AP, Baini C, Herszberg I. Mode I interlaminar fracture toughness properties of advanced textile fiberglass composites. Compos Part A 1999;30:859–70.
[26] Tsai JL, Huang BH, Cheng YL. Enhancing fracture toughness of glass/epoxy composites by using rubber particles together with silica nanoparticles. J Compos Mater 2009;43(25):3107–23.
[27] Zeng Y, Liu HY, Mai YW, Du XS. Improving interlaminar fracture toughness of carbon fibre/epoxy laminates by incorporation of nano-particles. Compos Part B 2012;43:90–4.
[28] Carolan D, Kinloch AJ, Ivankovic A, Sprenger S, Taylor AC. Mechanical and fracture performance of carbon fibre reinforced composites with nanoparticle modified matrices. Procedia Struct Integrity 2016;1:96–103.
[29] Zhang XQ, Fan XY, Yan C, Li HZ, Zhu YD, Li XT, et al. Interfacial microstructure and properties of carbon fiber composites modified with graphene oxide. ACS Appl Mater Interfaces 2012;4:1543–52.
[30] Srivastava VK, Gries T, Veit D, Quadflieg T, Mohr B, Kolloch M. Effect of nanomaterial on mode I and mode II interlaminar fracture toughness of woven carbon fabric reinforced polymer composites. Eng Fract Mech 2017;180:73–86.
[31] Yu Y, Yang X, Wang L, Liu H. Hygrothermal aging on pultruded carbon fiber/vinyl ester resin composite for sucker rod application. J Reinf Plast Compos 2006;25:149–60.

Chapter 9: Conclusions and perspectives

9.1 Conclusions

Mechanical properties of marine composites have been significantly deteriorated in marine environment, therefore, reinforcing mechanical properties of marine composites is necessary and urgent. This thesis is devoted to study a variety of nanoparticles and sizing enhanced FRP composites to offset the marine environment deterioration effects, especial salt spray effects. This study commences with discovering concentration and functional groups of nanoparticles (HNTs and nanosilica) effects on the mechanical and thermal properties of polymer matrix. Following by a discussion about mechanisms of salt water effect on composites, meanwhile it is found that nanosilica enhancement can complement the loss due to the salt water immersion. Then, a study of synergistic effects of HNTs and APTES on toughening the mechanical properties of glass fibre reinforced polystyrene has been conducted along with studying effect of reinforcement in the marine environment. At last, a study of a feasible method by using polydopamine to enhance the interface of epoxy resin and carbon fibre surfaces, and then hybrid enhancements with nanosilica to fabricate a low-cost, large-scale and durable nanoparticle reinforced composite has been explored to provide an alternative choice for maritime engineering applications. Based on the research in this thesis, the following conclusions can be drawn:

1) The morphology of (PPA)-treated HNTs changed from nanotubes to nanoplatelets, therefore increased the contact surface between the HNTs and epoxy resin. Fracture toughness of epoxy matrices increased with HNTs concentration going up in the composites. However, there was an optimised concentration (5 wt% in this study), the addition of further HNTs achieves only marginal fracture toughness enhancement and more negative effects appeared, such as HNTs concentration gradient in cured epoxy composites, potentially significant decrease in glass transition temperature (Tg) and potential immature tensile failure.

2) Amino and epoxide functional groups modified nanosilica significant enhanced the fracture toughness of epoxy composites at a low concentration. The interface between the nanosilica and the epoxy became stronger due to the chemical bonding. Meanwhile, the epoxide modified nanosilica has more specific surface area compared to amino modified nanosilica.

3) Synergistic effects of HNTs and 3-aminopropyltriethoxysilane (APTES) on glass fibre reinforced composite has been studied. The interlaminate shear strength and Model I interlaminar fracture toughness of modified composite increased as well as significantly decreased the deterioration of the mechanical properties of the composite under marine environments.

4) A new method was developed using polydopamine (PDA) as sizing on the surface of carbon fibre (CF) fabric. The crack propagation behaviour changed from a saw-tooth shaped curve in neat CFRP laminate to a relatively smooth trending curve in a PDA modified CFRP laminate. Moreover, the Mode I interlaminar fracture toughness, impact strength and interlaminar shear strength of PDA coated CFRP laminates was also increased.

5) A hybrid toughening method by using nanosilica to toughen the matrix and polydopamine sizing to enhance the fibre and matrix interfaces was studied. The Mode I interlaminar fracture toughness, impact strength and interlaminar shear strength of modified CFRP laminates was significantly enhanced. Meanwhile, the deterioration of the mechanical properties of the modified CFRP laminates under marine environments was offset by the improvement of the hybrid matrix and interface toughened effects.

9.2 Perspectives

Although significant progress for nanoparticles enhanced fibre reinforced polymer composites used in the marine environment has been made in this thesis, there are still some challenges in the future research.

1) The enhanced properties by nanoparticles can complement the loss of deterioration of composite due to salt water immersion, other facts such as temperature, biodeterioration and ultraviolet also great affect the various degradation for marine composites. It is highly desirable to combine those effects to find out whether nanoparticles enhancement still can complement the loss of deterioration of those effects.

2) Multifunctional is very valued property for advanced materials. Nanoparticles can provide such as electrical conductivity, thermal conductivity, magnetic and UV block characters which are not original owned in normal marine composite materials. However, introducing such characters may affect the mechanical property or machinability of the composite. Therefore, it is

a big challenge to make multifunctional composite which still maintain their original performances.

3) The purpose of this thesis is to fabricate a durable nanoparticle reinforced composite to provide an alternative option for maritime engineering. Although the material has been made in the laboratory, it is necessary to develop the composite structures which can be large-scale production and commercialization.

We believe that further explorations in nanoparticle enhanced fiber reinforced composite area will contribute to maritime engineering with all the above problems solved.

Appendix: Publications during Ph.D

Refereed book chapter publication

(1) **W. Han**, Y. H. Tang, L. Ye. (2016) Carbon fiber-reinforced polymer laminates with nanofiller-enhanced multifunctionality in the structural integrity of carbon fiber composites: In: Fifty years of progress and achievement of the science, development, and applications 1st ed., PP. 171-198, Springer, UK.

Refereed journal publications

(1) **W. Han**, Y. Tang. Water-swelling rubber containing small amount of nanofillers with enhanced water swelling durability. Adv Mater Res 2013; 774-776: 544-547.

(2) S. Chen, J. J. Duan, **W. Han**, S. Z. Qiao. Graphene-MnO_2 framework as a new generation of three-dimensional oxygen evolution promoter. Chem Commun 2013; 50: 207-209.

(3) **W. Han**, Y. Yu, Y. Tang, K. Sammut. Nano-halloysite concentration effects on fracture toughness of diverse epoxy nanocomposites. ASTM Mater Performance Charact 2014; 3: 1-13.

(4) H.Wu, S. Chiang, **W. Han**, Y. Tang, F. Kang, C. Yang. A simple and efficient protocol to improve the isotropic thermal conductivity of silver-epoxy pastes. Compos Sci Technol 2014; 99: 109-116.

(5) **W. Han**, Y. Yu, L. M. Fang, M. R. Johnston, Y. Tang. Functionalized silica/epoxy nanocomposites with enhanced fracture toughness for large-scale applications. J Compos Mater 2015; 49(12):1439-1447.

(6) J. C. Zhao, N. Dehbari, **W. Han**, L. P. Huang, Y. Tang. Electrospun multi-scale hybrid nanofiber/net with enhanced water swelling ability in rubber composites. Mater Des 2015; 86:14-21.

(7) **W. Han**, S. Chen, J. Campbell, X. J. Zhang, Y. Tang. Nanosilica enhanced fracture toughness and wear properties of epoxy under marine environment. Mater Chem Phy 2016; 177:147-155.

(8) **W. Han**, N. Dehbari, S. Chen, T. Jung, K. Sammut, Y. Tang. Synergistic effects of coupling agent and nanoparticle on enhancing glass fiber/polystyrene laminates for harsh environment applications. Appl Compos Mater 2017 (under review).

(9) **W. Han**, H. P. Zhang, J. Tavakoli, J. Campbell, Y. Tang. Polydopamine as sizing on carbon fibre surfaces for enhancement of epoxy laminated composites. Compos Part A 2018; 107:626-632.

(10) H. P. Zhang, **W. Han**, J. Tavakoli, Y. Zhang, X. Lin, X. Lu, Y. Tang. Understanding interfacial interactions of polydopamine and glass fiber and their enhancement mechanisms in epoxy based laminates. Compos Sci Technol 2017 (under review).

(11) **W. Han**, H. P. Zhang, X. Xu, Y. Tang. Hybrid enhancement by polydomamine and nanosilica on carbon fibre reinforced polymer laminates under marine environment. Compos Part B 2018; 112: 283-289.

Refereed conference publications

(1) **W. Han**, J. C. Zhang, C. B. Zhao, Y. Tang. Small amount of functionalized nanosilica with dramatic enhanced fracture toughness of epoxy matrix for large-scale applications. In: Proceeding of the 6th Asia-Europe symposium on Processing and Properties of Reinforced Polymers, 2nd -6th June 2013, Wuhan, China.

(2) **W. Han**, S. Cheng, Y. Tang. Graphene/superabsorbent composites for potential environmental sensor applications, In: Proceeding of 2014 International Conference Nanoscience and Nanotechnology (ICONN), 2014, 46-49. DOI: 10.1109 / ICONN.2014.6965258.

(3) **W. Han**, Y. Tang, T. Jung. Synergistic effects of HNTs and APTES on polystyrene enhancement. 10th International Conference on Structural Integrity and Failure (SIF-2016).12th-15th July 2016, Adelaide, Australia.

Bibliography

[1]. Alamri H and Low IM. Microstructural, mechanical, and thermal characteristics of recycled cellulose fiber-halloysite-epoxy hybrid nanocomposites. Polym Compos 2012; 33: 589–600.

[2]. Alamri H and Low IM. Effect of Water Absorption on the Mechanical properties of nano-filler reinforced epoxy nanocomposites. Mater Des 2012; 42: 214–222.

[3]. Akbarinezhada E, Ebrahimib M, Sharifb F and Ghanbarzadeha A. Evaluating protection performance of zinc rich epoxy paints modified with polyaniline and polyaniline-clay nanocomposite. Prog Org Coat 2014; 77:1299-1308.

[4]. Akangah P, Lingaiah S and Shivakumar K. Effect of Nylon-66 nano-fiber interleaving on impact damage resistance of epoxy/carbon fiber composite laminates. Compos Struct 2010; 92: 1432–39.

[5] Andre RS, Pavinatto A, Mercante LA, Paris EC, Mattoso LHC and Correa DS. Improving the electrochemical properties of polyamide 6/polyaniline electrospun nanofibers by surface modification with ZnO nanoparticles. RSC Adv 2015; 5:73875-81.

[6]. Arai M, Hirokawa J, Hanamura Y, Ito H, Hojo M and Quaresimin M. Characteristic of mode I fatigue crack propagation of CFRP laminates toughened with interlayer. Compos Part B 2014; 65: 26–33.

[7]. Ashrafi B, Guan J, Mirjalili V, Zhang Y, Chun L, et al. Enhancement of mechanical performance of epoxy/cabob fibre laminate composites using single-walled carbon nanotubes. Compos Sci Technol 2011; 71: 1569–78.

[8] Balakrishnan H, Hassan A, Wahit MU, Yussuf AA and Razak SBA. Novel Toughened Polylactic Acid Nanocomposite: Mechanical, Thermal and Morphological Properties. Mater Des 2010; 31: 3289–98.

[9] Barbero EJ. Introduction to composite materials design. Taylor and Francis, 2011; London.

[10]. Becker O, Varley RJ and Simon GP. Use of layered silicates to supplementarily toughen high performance epoxy-carbon fiber composites. J Mater Sci Lett 2003; 22: 1411–14.

[11]. Bekyarova E, Thostenson ET, Yu A, Kim H, et al. Multiscale carbon nanotube carbon fibre reinforcement for advanced epoxy composites. Langmuir 2007; 23: 3970–74.

[12]. Blackman BRK, Kinloch AJ, Sohn Lee J, et al. The fracture and fatigue behaviour of nano-modified epoxy Polymers. J Mater Sci 2007; 42: 7049–51.

[13]. Boger L, Wichmann MHG, Meyer LO and Schulte K. Load and health monitoring in glass fibre reinforced composites with an electrically conductive nanocomposites epoxy matrix. Compos Sci Technol 2008; 68, 1886–94.

[14]. Bouhofer W and Kovacs JZ. A review and analysis of electrical percolation in carbon nanotube polymer composites. Compos Sci Technol 2009; 69: 1486.

[15]. Bowles KJ and Frimpong S, Void effects on the interlaminar shear strength of unidirectional graphite-fibre-reinforced composites. J Compos Mater 1992; 26: 1487–1509.

[16] Choi SH, Kim DH, Raghu AV, . Reddy KR et al. Properties of graphene/waterborne polyurethane nanocomposites cast from colloidal dispersion mixtures. J Macromol Sci Part B 2012; 51: 197–207.

[17]. Chronakis IS. Novel nanocomposites and nanoceramics based on polymer nanofibers using electrospinning process—a review. J Mater Process Technol 2005; 167:283–293.

[18]. Chou TW, Gao L, Thostenson ET, Zhang Z and Byun JH. An assessment of the science and technology of carbon nanotube-based fibers and composites. Compos Sci Technol 2010; 70:1–19.

[19]. Compton BG and Lewis JA. 3D printing: 3D-printing of lightweight cellular composites. Adv Mater 2014; 26: 5930–35.

[20] Cousin P and Smith P. Dynamic Mechanical Properties of Sulfonated Polystyrene/ Alumina Composites. J Polym Sci Polym Phys 1994; 32: 459–468.

[21]. Diez-Pascual AM, Naffakh M, Marco C, Gomez-Fatou MA and Ellis GJ. Multiscale fiberreinforced thermoplastic composites incorporating carbon nanotubes: a review. Curr Opin Solid State Mater Sci 2014; 18:62–80.

[22]. Dalina WADW, Mariatti M, Ramlee R, Ishak ZAM and Mohamed AR. Comparison on the properties of glass fiber/MWCNT/epoxy and carbon fiber/MWCNT/epoxy composites Adv Mater Res 2014; 858: 32–39.

[23]. Dean D, Obore AM, Richmond S and Nyairo E. Multiscale fibre-reinforced nanocomposites: synthesis, processing and properties. Compos Sci Technol 2006; 66: 2135–42.

[24]. Deng SQ, Ye L, Friedrich K. Fracture behaviours of epoxy nanocomposites with nano-silica at low and elevated temperatures. J Mater Sci 2007; 42: 2766–74.

[25] Deng SQ, Zhang JN, Ye L and Wu JS. Toughening epoxies with halloysite nanotubes. Polymer 2008, 49: 5119–27.

[26] Deng SQ, Zhang JN and Ye L. Halloysite-epoxy nanocomposites with improved particle dispersion through ball mill homegenisation and chemical tTreatments. Compos Sci Technol 2009; 69: 2497–505.

[27]. Dzenis YA and Reneker DH. Delamination resistant composites prepared by small diameter fiber reinforcement at ply interfaces. U.S. Patent 6265333, 2001, USA.

[28]. Fiedler B, Gojny FH, Wichmann MHG, Nolte MCM and Schulte K. Fundamental aspects of nano-reinforced composites. Compos Sci Technol 2006; 66: 3115–25.

[29]. Fukushima Y and Inagaki S. Synthesis of an intercalated compound of montmorillonite and 6-polyamide. J Incl Phenom 1987; 5: 473–482.

[30]. Garcia EJ, Wardle Bl and Hart AJ. Joining prepreg composite interfaces with aligned carbon nanotubes. Compos Part A 2008; 39: 1065–70.

[31]. Gellert EP and Turley DM. Seawater immersion ageing of glass-fibre reinforced polymer laminates for marine applications. Compos Part A 1999; 30: 1259–65.

[32]. Godara A, Mezzo L, Luizi F, Warrier A, Lomov SV, et al. Influence of carbon nanotube reinforcement on the processing and the mechanical behaviour of carbon fibre/epoxy composites. Carbon 2009; 47: 2914–23.

[33]. Gaier JR, YoderVandenberg Y, Berkebile S, Stueben H and Balagadde F. The electrical and thermal conductivity of woven pristine and intercalated graphite fibre-polymer composites. Carbon 2003; 41: 2187–93.

[34]. Gkikas G, Douka DD, Barkoula NM and Paipetis AS. Nano-enhanced composite materials under thermal shock and environmental degradation: a durability study. Compos Part B 2015; 70: 206–214.

[35]. Han SJ, Lee H, Jeong HM, Kim BK, et al. Graphene modified lipophilically by stearic acid and its composite with low density polyethylene. J Macromol Sci Part B 2014; 53: 1193-1204.

[36]. Hassan M, Reddy KR, Haque E, Minett AI and Gomes VG. High-yield aqueous phase exfoliation of graphene for facile nanocomposite synthesis via emulsion polymerization. J Colloid Interface Sci 2013; 410: 43–51.

[37]. Hassan M, Reddy KR, Haque E,. Faisal SN et al. Hierarchical assembly of graphene /polyaniline nanostructures to synthesize free-standing supercapacitor electrode. Compos Sci Technol 2014; 98: 1–8.

[38]. Hida S, Hori T, Shiga T, Elliott J and Shiomi J. Thermal resistance and phonon scattering at the interface between carbon nanotube and amorphous polyethylene. Int J Heat Mass Transf 2013; 67: 1024–29.

[39] Horvath E, Kristof J, Frost RL, Redey A et al. Hydrazine-hydrate intercalated halloysite under controlled-rate thermal analysis conditions. J Therm Anal Calorim 2003; 71: 707–714.

[40]. Hsieh TH, Kinloch AJ, Masania K, Lee JS, Taylor AC and Sprenger S. The toughness of epoxy polymers and fibre composites modified with rubber microparticles and silica nanoparticles. J Mater Sci 2010; 45: 1193–1210.

[41]. Hsieh TH, Kinloch AJ, Masania K, Taylor AC and Sprenger S. The mechanisms and mechanics of the toughening of epoxy polymers modified with silica nanoparticles. Polymer 2010; 51: 6284–94.

[42]. Hull D. Fractography. Cambridge University Press 1999; London.

[43]. Iqbal K, Khan SU, Munir A and Kim JK. Impact damage resistance of CFRP with nanoclayfilled epoxy matrix. Compos Sci Technol 2009; 69: 1949–57.

[44]. Le Gac PY, Le Saux V, Paris M, Marco Y. Ageing mechanism and mechanical degradation behavior of polychloroprene rubber in a marine environment: Comparison of accelerated ageing and long term exposure. Polym Degrad Stabil 2012; 97: 288–96.

[45]. Lan T and Pinnavaia TJ. Clay-reinforced epoxy nanocomposites. Chem Mater 1994; 6: 2216–19.

[46]. Lee CL and Wei KH. Resin transfer molding (RTM) process of a high performance epoxy resin. II: effects of process variables on the physical, static and dynamic mechanical behaviour. Polym Eng Sci 2000; 40: 935–943.

[47]. Lee YR, Kim SC, Lee H, Jeong HM, Raghu AV, et al. Graphite oxides as effective fire retardants of epoxy resin. Macromol Res 2011; 19 66–71.

[48]. Lin Y, Gigliotti M, Lafarie-Frenot MC, Bai J, et al. Experimental study to assess the effect of carbon nanotube addition on the through-thickness electrical conductivity of CFRP laminates for aircraft applications. Compos Part B 2015; 76: 31–37.

[49]. Liu HY, Wang GT, Mai YW, et al. On fracture toughness of nano-particle modified epoxy. Compos Part B 2011; 42: 2170–75.

[50]. Liu HY, Wang GT and Mai YW. Cyclic fatigue crack propagation of nanoparticle modified epoxy. Compos Sci Technol 2012; 72: 1530–38.

[51] Joussein E, Petit S, Churchman J, Theng B, et al. Halloysite Clay Minerals—A Review," Clay Miner 2005; 40: 383–426.

[52]. Joshi SC and Dikshit V. Enhancing interlaminar fracture characteristics of woven CFRP prepreg composites through CNT dispersion. J Compos Mater 2011; 46: 665–675.

[53]. Jopek H and Strek T. Optimization of the effective thermal conductivity of a composite, in Convection and Conduction Heat Transfer. ed. by Ahsan A, Intech 2011, pp. 197–214. Croatia.

[54]. Kang S, Hong SII, Choe CR, et al. Preparation and characterization of epoxy composites filled with functionalized nanosilica particles obtained via sol-gel process. Polymer 2001; 42: 879–887.

[55]. Kepple KL, Sanborn GP, Lacasse PA, Gruenberg KM and Ready WJ. Improved fracture toughness of carbon fibre composite functionalized with multi walled carbon nanotubes. Carbon 2008; 46: 2026–33.

[56]. Kinloch AJ, Mohammed RD, Taylor AC, Sprenger S and Egan D. The interlaminar toughness of carbon-fibre reinforced plastic composites using "hybrid-toughened" matrices. J Mater Sci 2006; 41: 5043–46.

[57]. Knoll JB, Riecken BT, N. Kosmann, S. Chandrasekaran, K. Schulte, B. Fiedler, The effect of carbon nanoparticles on the fatigue performance of carbon fibre reinforced epoxy. Compos. Part A 2014; 67:233–240.

[58]. Koecher MC, Pande JH, Merkley S. Henderson DT, et al. Piezoresistive in-situ stain sensing of composite laminate S structures. Compos Part B 2015; 69: 534–541.

[59]. Kostopoulos V, Karapappas P, Loutas T, Vavouliotis A, et al. Interlaminar fracture toughness of carbon fibre-reinforced polymer laminates with nano- and micro-fillers. Strain 2011; 47:269–282.

[60]. Kostopoulos V, Karapappas P, Karapappas S, Tsantzalis A, et al. Model I interlaminar fracture of CNF or/and PZT doped CFRPs via acoustic emission monitoring. Compos Sci Technol 2007; 67: 822–828.

[61]. Ma PC, Siddiquia NA, Maromb G, Kima JK. Dispersion and functionalization of carbon nanotubes for polymer-based nanocomposites: a review. Compos Part A 2010; 41 (10): 1345–67.

[62]. Ma J, Mo MS, Du XS, et al. Effect of inorganic nanoparticles on mechanical property, fracture toughness and toughening mechanism of two epoxy systems. Polymer 2008; 49: 3510–23.

[63]. Manjunatha CM, Taylor AC, Kinloch AJ, Sprenger S. The effect of rubber micro-particles and silica nano-particles on the tensile fatigue behaviour of a glass-fibre epoxy composite. J Mater Sci 2009; 44: 342–345.

[64]. Molnar K, Kostakova E, Meszaros L. The effect of needleless electrospun nanofibrous interleaves on mechanical properties of carbon fabrics/epoxy laminates. Express Polym Lett 2014; 8: 62–72.

[65]. Mouritz AP, Gellert E, Burchill P, Challis K. Review of advanced composite structures for naval ships and submarines. Compos Struct 2001; 53: 21–41.

[66]. Neser G. Polymer based composites in marine use: history and future trends： 10th International Conference on Marine Technology. Procedia Engineering 2017; 194: 19–24.

[67]. Pimenta S and Pinho ST. Recycling carbon fibre reinforced polymers for structural applications: technology review and market outlook. Waste Manag 2011; 31; 378–392.

[68]. Prusty RK, Rathore DK and Ray BC. Assessment and modification strategies for improved interlaminar properties of advanced FRP composites: a review. J Adv Res Manufac Mate Sci Metallurg Eng 2014; 1: 1–25.

[69] Qian H, Greenhalgh ES, Shaffer MSP, Bismarck A. Carbon nanotube-based hierarchical composites: a review. J Mater Chem 2010; 20: 4751–62.

[70]. Quaresimin M and Varley RJ. Understanding the effect of nano-modifier addition upon the properties of fibre reinforced laminates. Compos Sci Technol 2008; 68: 718–726.

[71]. Radcliffe DJ and Rosenberg HM. The thermal conductivity of glass-fibre and carbonfibre/ epoxy composites from 2 to 80 K. Cryogenics 1982; 22(5): 245–249.

[72]. Rahman IA, Padavettan V. Synthesis of silica nanoparticles by sol-gel: size-dependent properties, surface modification and applications in silica-polymer nanocomposites-a review. J Nano Mat 2012; 2012: 132424.

[73]. Rahman MM, Hosur M, Hsiao KT, Wallace L and Jeelani S. Low velocity impact properties of carbon nanofibers integrated carbon fiber/epoxy hybrid composites manufactured by OOAVBO process. Compos Struct 2015; 120: 32–40.

[74]. Rahmanian S, Thean KS, Suraya AR, Shazed MA, et al. Carbon and glass hierarchical fibers: influence of carbon nanotubes on tensile, flexural and impact properties of short fiber reinforced composites. Mater Des 2013; 43: 10–16.

[75]. Reia da Costa EF, Skordos AA, Partidge IK and Rezai A. RTM processing and electrical performance of carbon nanotube modified epoxy/fibre composites. Compos Part A 2012; 43: 593–602.

[76]. Reddy KR, Hassan M and Gomes VG. Hybrid nanostructures based on titanium dioxide for enhanced photocatalysis. Appl Catal A Gen 2015; 489: 1–16.

[77]. Reddy KR, Sin BC, Ryu KS, Kim JC, et al. Conducting polymer functionalized multi-walled carbon nanotubes with noble metal nanoparticles: synthesis, morphological characteristics and electrical properties. Synth Met 2009; 159: 595–603.

[78]. Reddy] KR, Sin BC, Yoo CH, Sohn D and Lee Y. Coating of multiwalled carbon nanotubes with polymer nanospheres through microemulsion polymerization. J Colloid Interface Sci 2009; 340: 160–165.

[79]. Reddy KR, Lee KP and Iyenger GA. Self-assembly directed synthesis of poly (ortho-toluidine)-metal (gold and palladium) composite nanospheres. J Nanosci Nanotechnol 2007; 7: 3117–25.

[80]. Romhany G and Szebenyi G. Interlaminar crack propagation in MWCNT/fiber reinforced hybrid composites. Express Polym Lett 2009; 3: 145–151.

[81]. Sager RJ, Klein PJ, Davis DC, Lagoudas DC, et al. Interlaminar fracture toughness of woven fabric composite laminates with carbon nanotube/epoxy interleaf films. J Appl Polym Sci 2011; 121: 2394–405.

[82]. Siddiqui NA, Woo RSC, Kim JK, Leung CCK and Munir A. Model I interlaminar fracture behaviour and mechanical properties of CFRPs with nanoclay-filled epoxy matrix. Compos Part A 2007; 38: 449–460.

[83]. Shao Y, Yashiro T, Okubo K and Fujii T. Effect of cellulose nano fiber (CNF) on fatigue performance of carbon fiber fabric composites. Compos Part A 2015; 76: 244–254.

[84]. Shen Z, Simon GP and Cheng YB. Comparison of solution intercalation and melt intercalation of polymereclay nanocomposites. Polymer 2002; 43: 4251–60.

[85]. Sprenger S. Epoxy resins modified with elastomers and surface-modified silica nanoparticles. Polymer 2013; 54: 4790–97.

[86]. Sprenger S. Fiber-reinforced composites based on epoxy resins modified with elastomers and surface-modified silica nanoparticles. J Mater Sci 2014; 49: 2391–402.

[87]. Shen Z, Simon GP, Cheng YB. Comparison of solution intercalation and melt intercalation of polymer–clay nanocomposites. Polymer 2002; 43: 4251–60.

[88] Srivastava VK, Gries T, Veit D, Quadflieg T, et al. Effect of nanomaterial on mode I and mode II interlaminar fracture toughness of woven carbon fabric reinforced polymer composites. Eng Fract Mech 2017; 180: 73–86.

[89]. Tang Y, Ye L, Deng S, Yang C, Yuan W. Influences of processing methods and chemical treatments on fracture toughness of halloysite-epoxy composites. Mater Des 2012; 42: 471–77.

[90]. Tang Y, Ye L, Zhang Z, Friedrich K. Interlaminar fracture toughness and CAI strength of fibre-reinforced composites with nanoparticles-A review. Compos Sci Technol 2013; 86: 26–37.

[91]. Tang Y, Ye L, Zhang D and Deng S, Characterisation of transverse tensile, interlaminar shear and interlaminate fracture in CF/EP laminates with 10 wt% and 20 wt% silica nanoparticles in matrix resins. Compos Part A 2011; 42, 1943–50.

[92] Tang Y, Deng S, Ye L, Yang C, Yuan Q, et al. Effects of unfolded and intercalated halloysites on mechanical properties of halloysite–epoxy nanocomposites. Compos Part A 2011; 42: 345–354.

[93] Tang Y, Ye L., Deng S, Yang C and Yuan W. Influences of processing methods and chemical treatments on fracture toughness of halloysite–epoxy composites. Mater Des 2012; 42: 471–477.

[94]. Tumbleston JR, Shirvanyants D, et al., Continuous liquid interface production of 3D objects. Science 2015; 347:1349–52.

[95]. Thostenson ET and Chou TW. Carbon nanotube networks: sensing of distributed strain and damage for life prediction and self-healing. Adv Mater 1996; 18: 2837–41.

[96]. Timmerman JF, Hayes BS and Seferis JC. Nanoclay reinforcement effects on the cryogenic microcracking of carbon fiber/epoxy composites. Compos Sci Techno 2002; 62: 1249–58.

[97]. Thaker PR. Processing and characterisation of carbon nanotubes reinforced epoxy resin based multi-scale multi-functional composites. Ph.D. Thesis, Texas A&M University, 2009.

[98]. Wang K, Chen L, Wu JS, et al. Epoxy nanocomposites with highly exfoliated clay: mechanical properties and fracture mechanisms. Macromolecules 2005; 38: 788–800.

[99] Xiao KQ, Ye L and Kwok YS. Effects of pre-cracking methods on fracture behaviour of an araldite-F epoxy and its rubber-modified systems. J Mater Sci 1998; 33: 2831–36.

[100]. Xie XL, Mai YW and Zhou XP. Dispersion and alignment of carbon nanotubes in polymer matrix: a review. Mater Sci Eng 2005; 49: 89–112.

[101]. Xu SA, Wang GT and Mai YW. Effect of hybridization of liquid rubber and nanosilica particles on the morphology, mechanical properties and fracture toughness of epoxy composites. J Mater Sci 2013; 48: 3546–56.

[102]. Xu X, Zhou Z, Hei Y, Zhang B, et al. Improving compression-after-impact performance of carbon-fiber composites by CNTs/thermoplastic hybrid film interlayer. Compos Sci Technol 2014; 95: 75–81.

[103]. Xu Y and Hoa SV. Mechanical properties of carbon fiber reinforced epoxy/clay nanocomposites. Compos Sci Technol 2008; 68: 854–861.

[104]. Xie XL, Mai YW and Zhou XP. Dispersion and alignment of carbon nanotubes in polymer matrix: a review. Mater Sci Eng R-Rep 2005; 49: 89–112.

[105] Wang PF, Yang JL, Liu WS, Tang XZ, Zhao K, et al. Tunable crack propagation behavior in carbon fiber reinforced plastic laminates with polydopamine and graphene oxide treated fibers. Mater Des 2017; 113: 68–75.

[106] Wicks SS, Villoria RG, Wardle BL. Interlaminar and intralaminar reinforcement of composite laminates with aligned carbon nanotubes. Compos Sci Technol 2010; 70 (1): 20–28.

[107] Yang Y, Xu F, Zhang YQ, Liu GW. Experimental study on the impact resistance of 2D plain-woven C/SiC composite. Ceram Int 2014; 10(40): 15551-59.

[108] Ye, YP, Chen HB, Wu JS and Ye L. High impact strength epoxy nanocomposites with natural nanotubes. Polymer 2007; 48: 6426–33.

[109]. Yokozeki T, Iwahori Y, Ishibashi M, Yanagisawa T, et al. Fracture toughness improvement of CFRP laminates by dispersion of cup-stacked carbon nanotubes. Compos Sci Technol 2009; 69: 2268–73.

[110] Yu B, Jiang Z, Tang XZ, Yue CY, Yang J. Enhanced interphase between epoxy matrix and carbon fiber with carbon nanotube-modified silane coating. Compos Sci Technol 2014; 9: 131–140.

[111] Yu Y, Yang X, Wang L, Liu H. Hygrothermal aging on pultruded carbon fiber/vinyl ester resin composite for sucker rod application. J Reinf Plast Compos 2006; 25:149–160.

[112]. Yu Y, Shapter JG, Popelka-Filcoff R, et al. Copper removal using bio-inspired polydopamine coated natural zeolites. J Hazard Mater 2014; 273: 174–182.

[113]. Zeng Y, Liu HY, Mai YW and Du XS. Improving interlaminar fracture toughness of carbon fibre/epoxy laminates by incorporation of nano-particles. Compos Part B 2012; 43: 90–94.

[114]. Zhang GJ. The effect of carbon fibres and carbon nanotubes on the mechanical properties of polyimide composites. Mech Compos Mater 2011; 47: 447–450.

[115]. Zhang H, Tang LC, Zhang Z, et al. Fracture behaviours of in situ silica nanoparticle-filled epoxy at different temperatures. Polymer 2008; 49: 3816–25.

[116]. Zhang H, Liu Y, Kuwata M, Bilotti E, Peijs T. Improved fracture toughness and integrated damage sensing capability by spray coated CNTs on carbon fibre prepreg. Compos Part A 2015; 70: 102–110.

[117]. Zhang J, Lin T and Wang X. Electrospun nanofiber toughened carbon/epoxy composites: effects of polyetherketone cardo (PEK-C) nanofiber diameter and interlayer thickness. Compos Sci Technol 2010; 70: 1660–66.

[118] Zhang P, Ma L, Fan F, Zeng Z, Peng C, et al. Fracture toughness of graphene, Nat Commun 2014; 5:3782.

[119].Zhang R, Huang Y, Liu L, Tang Y, Su D, Xu L. Influence of sizing emulsifier content on the properties of carbon fibers and its composites. Mater Des 2012; 33: 367–371.

[120] Zhang RL, Zhang JS, Zhao LH, Sun YL. Sizing Agent on the Carbon Fibers Surface and Interface Properties of Its Composites. Fiber Polym 2015; 16: 657–663.

[121] Zhang RL, Gao B, Du WT, Zhang J, Cui HZ, et al. Enhanced mechanical properties of multiscale carbon fiber/epoxy composites by fiber surface treatment with graphene oxide/polyhedral oligomeric silsesquioxane. Compos A: Appl Sci Manuf 2016;84: 455–463.

[122] Zhang XQ, Fan XY, Yan C, Li HZ, Zhu YD, Li XT, and Yu LP. Interfacial Microstructure and Properties of Carbon Fiber Composites Modified with Graphene Oxide. Appl. Mater. Interfaces 2012; 4: 1543−1552.